Univerzita Karlova v Praze
Matematicko-fyzikální fakulta

DIPLOMOVÁ PRÁCE

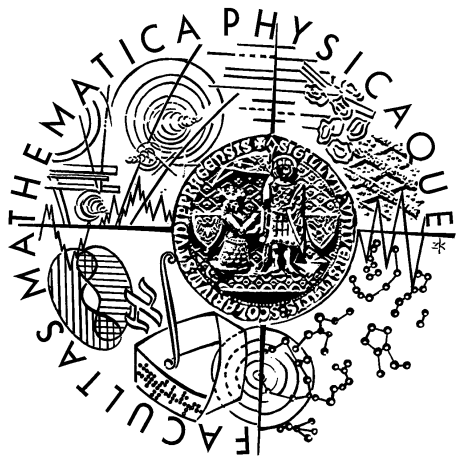

Radomír Šmída

ASTROFYZIKA VELMI VYSOKÝCH ENERGIÍ

Astronomický ústav UK

Vedoucí diplomové práce: RNDr. René Hudec, CSc.
Konzultanti: RNDr. Jiří Grygar, CSc.
prof. RNDr. Ladislav Rob, DrSc.
RNDr. Jan Řídký, CSc.

Studijní program: Fyzika

Studijní směr: Astronomie a astrofyzika

Praha 2002

Je mou milou povinností na tomto místě co nejsrdečněji poděkovat všem, kteří mi poskytli podporu při tvorbě této práce. Vedoucímu a konzultantům diplomové práce jsem vděčný za cenné připomínky a rady, kterými usnadnili vznik této práce. Poděkování patří také prof. Janu Paloušovi, který se taktéž podílel na korekturách textu.

Zároveň jsem velice vděčný Mgr. Matouši Borákovi za jeho trpělivou pomoc při mém osvojování si dovedností v oblasti potřebného software a dalším kamarádům za jejich nezištnou pomoc.

Poděkování si zaslouží i rodiče za podporu poskytovanou během celé doby mého studia.

R. Š.

Prohlašuji, že jsem svou diplomovou práci napsal samostatně a výhradně s použitím citovaných pramenů. Souhlasím se zapůjčováním práce.

V Praze dne 7. dubna 2002. Radomír Šmída

Contents

1 Introduction **1**

2 Observations of cosmic rays **3**
2.1 Extensive Air Showers 3
2.2 Atmospheric Fluorescence Detectors 6
2.3 Čerenkov Experiments 8
2.4 Scintillation Detectors 11
2.5 The experimental situation 13

3 Spectrum of cosmic rays **15**
3.1 All particle spectrum 15
3.2 Interesting features 16
3.3 Anisotropy 18
3.4 The abundances of the elements 22

4 Acceleration mechanisms **27**
4.1 Fermi's Original Theory 27
4.2 First Order Fermi Acceleration 28
4.3 Spectral index 30
4.4 Acceleration in SNRs 30
4.5 Direct acceleration 32
4.6 Hillas condition 32

5 Galactic and extragalactic CRs **34**
5.1 Origin of Galactic cosmic rays 34
5.2 Acceleration of GCRs in supernova remnants 36
5.3 Two types of supernova explosions 37
5.4 Origin of the knee 38
5.5 Beyond the knee 40
5.6 Extragalactic cosmic rays 41
5.7 Greisen-Zatsepin-Kuzmin cutoff 42

6 Possible sources **45**
6.1 Supernova remnants 45
6.2 Neutron stars 46
6.3 Radio galaxies 47

6.4 Active Galactic Nuclei and Quasars 50
6.5 Other astrophysical sources 52
6.6 Gamma ray bursts 54
6.7 The Reconnection Theory of Acceleration 56
6.8 Top-down models 57
6.9 Primordial black holes 59
6.10 New physics 60

7 Propagation in magnetic field **62**
7.1 Lorentz force 62
7.2 Numerical solution 62
7.3 Galactic magnetic field 63

8 Results of computer modelling **66**

9 Conclusions **82**

Bibliography **83**

A Shortcuts and constants **92**

Název práce: Astrofyzika velmi vysokých energií
Autor: Radomír Šmída
email autora: radomir_smida@yahoo.com
Katedra (ústav): Astronomický ústav
Vedoucí diplomové práce: RNDr. René Hudec, CSc.
Konzultanti: RNDr. Jiří Grygar, CSc.,
prof. RNDr. Ladislav Rob, DrSc.,
RNDr. Jan Řídký, CSc.
e-mail vedoucího: rhudec@asu.cas.cz

Abstrakt: V této práci se zabývám tématem astrofyziky velmi vysokých energií. Techniky pozorování spolu s výsledky experimentů jsou shrnuty v úvodu. Dále byly popsány možné urychlovací mechanismy částic kosmického záření v intervalu energií od TeV až ke konci dnes pozorovaného energetického spektra. Teoretickou část uzavírá kapitola věnovaná podrobné diskusi zdrojů částic kosmického záření.

Vlastní příspěvek předkládané práce spočívá v modelování pohybu atomových jader v magnetickém poli Galaxie. Studoval jsem vliv regulární složky i oblastí s nepravidelným magnetickým polem. Pro popis regulární složky jsem převzal bisymetrický logaritmický model se spirální konfigurací. Náhodná velikost a orientace vektoru magnetické indukce irregularních magnetických polí byla generována v předem daném počtu krychlových buňek, do nichž byla Galaxie rozdělena.

V závislosti chemického složení kosmických částic na energii byly nalezeny dva nárůsty střední hodnoty atomové hmotnosti v oblasti energií $(10 \div 500)$ TeV a pro energie vyšší než 10 PeV. Tvar závislosti je způsoben rozdílným unikáním částic z disku a z centrální výdutě. Pro energie vyšší než 10 PeV můžeme na základě výsledků modelování očekávat nárůst střední hmotnosti, pokud by zdroje v Galaxii měly vlastnosti blízké těm, jaké jsem u nich ve svém modelu předpokládal.

Klíčová slova: kosmické záření - energetické spektrum - chemické složení
- magnetické pole - zdroje - vysoké energie

Title: Very High-Energy Astrophysics
Author: Radomír Šmída
Author's email address: radomir_smida@yahoo.com
Department: Astronomical Institute of the Charles University in Prague
Supervisor: RNDr. René Hudec, CSc.
Consultants: RNDr. Jiří Grygar, CSc.,
prof. RNDr. Ladislav Rob, DrSc.,
RNDr. Jan Řídký, CSc.
Supervisor's e-mail address: rhudec@asu.cas.cz

Abstract: The topic of very high-energy astrophysics was discussed in this work. The detection techniques together with their results were summarized at first. The survey of possible acceleration mechanisms of cosmic rays in the energy range from TeV to the end of the observed energy spectra was included into the work. The possible sources of cosmic rays were in detail addressed and discussed in the last part of the general introduction.

My project consisted of modelling the trajectories of cosmic rays in the Galactic magnetic field in the energy range from 10 TeV to 10 EeV. The importance of regular and random components of the Galactic magnetic field was investigated. The bisymmetric logarithmic open-spiral configuration (BSS-A model) was used to describe the regular component. Random strength and orientation of irregular magnetic field were generated incidentally in a fraction of the cubic cells, into which the Galaxy was divided.

Two increase in relation between the mean logarithmic mass and energy of particles was found in the energy range (10÷500) TeV and above 10 PeV. This structure was caused due to the different particle's escaping energy from the Galactic disk and the bulge. We have found that for the energies above 10 PeV we can expect an increase of mean mass, if the Galactic sources will have the same characteristics which were used in our model.

Keywords: cosmic rays - energy spectrum - chemical composition - magnetic field - sources - high energy

Charles University in Prague
Faculty of Mathematics and Physics

DIPLOMA THESIS

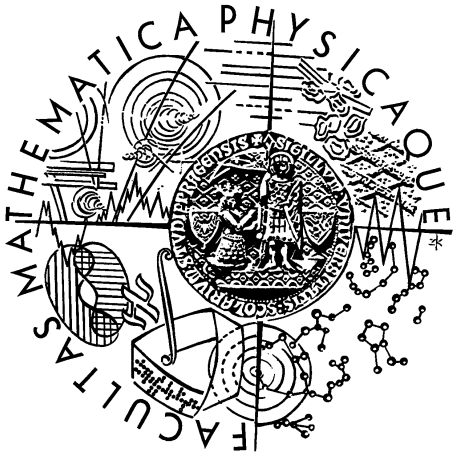

Radomír Šmída

VERY HIGH-ENERGY ASTROPHYSICS

Astronomical Institute

Supervisor: RNDr. René Hudec, CSc.
Consultants: RNDr. Jiří Grygar, CSc.
prof. RNDr. Ladislav Rob, DrSc.
RNDr. Jan Řídký, CSc.

Study Program: Physics

Specialization: Astronomy and Astrophysics

Prague 2002

Chapter 1

Introduction

The study of radioactive materials in the period from 1898 to 1912 was of widespread interest because this field offered direct insight into the nature of the atom, whose structure was still unknown. Electrometers were often used to measure the very small flux of particles coming from radioactive materials. (An electrometer consists of two thin ribbons of metal suspended in a vacuum bulb, which diverge when charge is present.) In use, electrometer readings had to be corrected for "leakage," which was dependent on the electrometer size and proportional to time, but remarkably was not dependent on the amount of charge on the electrometer foils. This leakage led to speculation about possible undiscovered radioactive contamination, or a flux of yet unknown invisible particles.

Austrian scientist Victor F. Hess studied this phenomenon by taking electrometers onto lakes where there should have been less contamination (no change in leakage) and into caves (leakage disappeared). Finally, in 1912, he solved the problem by lifting two ion chambers in balloons to altitudes of 6 km. Hess (1912) showed that there was indeed a flux of particles, and that it came from the sky with an intensity which increased with altitude (he was awarded the 1936 Nobel Prize for this work):

"The results of the present observations seem to be most readily explained by the assumption that a radiation of very high penetrating power enters our atmosphere from above, and still produces in the lower layers a part of the ionization observed in closed vessels."

His work was immediately followed by more detailed studies such as that of Kolhőrster, who showed that the particle flux increased very rapidly with altitude, with a 10 times increase at only 10 km. Cosmic rays[1] became the source of wild speculation for the next twenty years because of their exponential increase in flux with height. Finally, Pfotzer (1936) showed that the flux did not continue to increase but reached a peak at about 15 km, after which it diminished rapidly.

[1]Because of the wide speculation about the nature of cosmic rays (as they were named by Millikan in 1925), there is no single scientific definition of the phrase, only the popular description: "Things which rain down from the heaven and are not wet." The scientific literature has adopted three variations on the phrase: primary cosmic rays, the initial particle flux external to the Earth's atmosphere; cascade cosmic rays, the intermediate flux within the atmosphere; and sea-level cosmic rays, the final terrestrial flux of particles.

A new window to the Universe has been opened. Cosmic rays have been bringing the messages from events on the largest scales and information about the smallest scales of matter at the same time. During ninety years we have been obtaining many information about cosmic rays striking the atmosphere and the surface of the Earth. The measured features of cosmic rays confirmed a part of our ideas about Universe and elementary particles, however also revealed new mysteries.

The study of ultra and extremely high-energy cosmic rays is the subject of interest of two physical branches at present: astronomy-astrophysics and particle physics. Astronomically interesting is view the Universe with extremely energetic particles, astrophysically is how and where can the Universe accelerate the particles and particle-physically interesting in this topic is the study of behavior of elementary particles and interactions very close to GUT energy. Developing cooperation of two different branches is very promising and we hope that it will bring many interesting new results.

Chapter 2

Observations of cosmic rays

2.1 Extensive Air Showers

The large cascades of electrons, photons, muons and other sub-nuclear particles are produced when high-energy cosmic ray particles collide with the Earth's atmosphere (about 20 km up). On an incident cosmic ray the atmosphere acts as a calorimetr with variable density, a vertical thickness of 26 radiation lengths and about 11 interaction lengths (Bertou et al., 2000). The cosmic ray particles lose their energy by creating a shower of particles which are travelling in almost the same direction as the cosmic ray. The particles in the jet can themselves create more particles as they hit other nuclei of oxygen or nitrogen in the air. The whole cascade is called an extensive air shower (EAS) and keeps on growing until the particles in the shower run out of energy and are absorbed in the atmosphere. The incident particles are referred to as primary cosmic rays and the air shower components are referred to as cosmic ray secondaries. (For example about 3×10^{10} secondary particles initiated by a proton with the energy 10^{19} eV will reach ground level.)

A single cosmic ray can generate showers with a large number of particles depending on its energy. The smaller air showers (primaries with energies lower than 10^{13} eV) are absorbed near the top of the atmosphere and do not reach ground level. However, as the particles in the shower move through the air they emit faint flashes of blue light known as Čerenkov radiation. Although the primary cosmic particles and the secondaries produced by them in the air showers are absorbed by the atmosphere, it is possible to detect the faint Čerenkov light using large telescopes but only on dark, moonless nights (which results in an average 10% duty cycle). At even higher energies the air showers contain vast numbers of secondary particles, numbering in the billions for the most energetic cosmic rays (see below). The particles in these showers are of such high energy that they can travel all the way from the top of the atmosphere down to the ground where they can be detected directly with particle detectors (the majority of the charged particles detected by scintillator arrays are relatively low-energy electrons). The detectors are usually arranged in a grid formation (or array) on the ground allowing measurements of each shower to be made at several points. Information from the

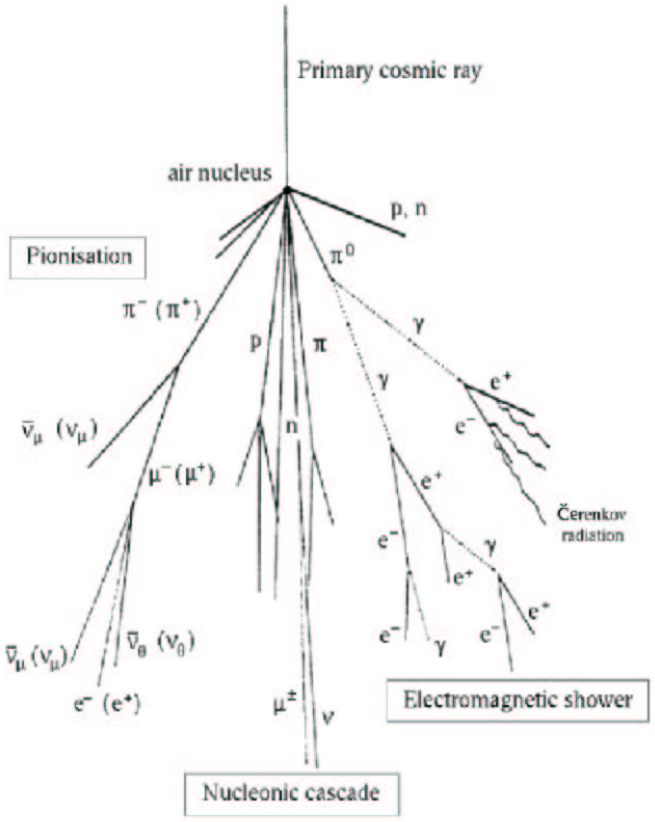

Figure 2.1: A schematic diagram showing the development of a nucleonic cascade in the atmosphere. The shower was initiated by high-energy nucleon. If the primary is gamma-ray, it will initiate only the electromagnetic shower.

detectors tells us how many particles struck the detector and the arrival time. The lateral distribution is constructed from information detected by the detectors. By adding up the number of particles recorded by each of the detectors we can estimate how many particles were in the shower and from which we can make a good guess as to the energy of the cosmic ray that started the shower. We can use the time when each detector was struck to measure the direction of the primary particle.

Knowledge of the core location and the shapes of lateral distribution are essential when estimating the shower size from air shower data. The shower size is estimated by fitting the density measurements to an assumed lateral distribution derived from Monte Carlo simulations (programs as AIRES, CORSIKA or MOCCA (see Figure (2.7))). At energy range of 10^{15} eV and higher the simulation is uncertain, because the interaction energies are several orders higher, than those attainable in man-made accelerators. VENUS, QGSJET, SIBYLL, HDPM and DPMJET are the most commonly used models for the high-energy interactions in the simulating programs. VENUS, QSJET and DPMJET model hadronic interaction of nucleons and nuclei on the basis of the Gribov-Regge theory, which

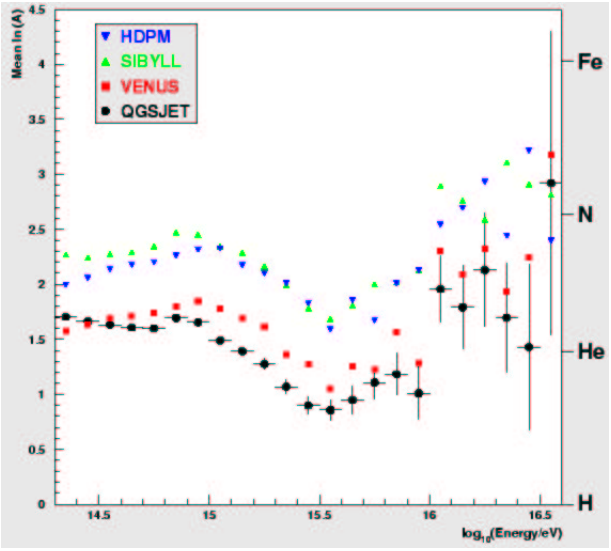

Figure 2.2: The mean logarithmic mass <ln(A)> measured by CASA-BLANCA as a function of energy. The four sets of symbols show the BLANCA data interpreted using CORSIKA with the indicated hadronic interaction model. Error bars are statistical only and shown only on the QGSJET results; errors on the other points are of similar size. Assuming a hadronic model, the systematic uncertainties in the ln(A) estimate are typically 0.2. The dominant systematic effect is clearly the difference between the hadronic models (from FOWLER ET AL. (2001)).

successfully describes scattering and the total cross-section exchange of pomerons[1]. SIBYLL is a minijet model [2]. HDPM is a purely phenomenological model which uses detailed parametrisations of the collider data for particle production.

A clear conclusion is that simulation results are never identical, even when the same theoretical models are used in different programs. The extension to reactions with nuclei and to energies, beyond the collider energy range accessible in man-made accelerator range, are somewhat arbitrary. Generally, the models are cross-checked at lower energies and then extrapolated to higher ranges. The Gribov-Regge type models have a more solid theoretical foundation than the other models and various studies seem to indicate QGSJET as being the model which best reproduces the data from the cosmic ray showers.

A ground array makes use of two main effects to separate heavy and light nuclei (and photons): the proportion of muons compared to the electromagnetic component of the shower and the shape of lateral distribution. Both parameters are due to the way the muons are produced during the shower development. The muons in a shower come from the decay of charged pions when they reach an energy low

[1]The properties of elastic and diffractive scattering of the proton and antiproton are well-described by the phenomenology of pomeron exchange (Regge theory), where the pomeron is the effective particle responsible for the growth in the hadronic cross section

[2]It simulates a hadronic reaction as a combination of an soft collision in which two strings are generated and a number of minijet pairs evolve leading to additional pairs of strings.

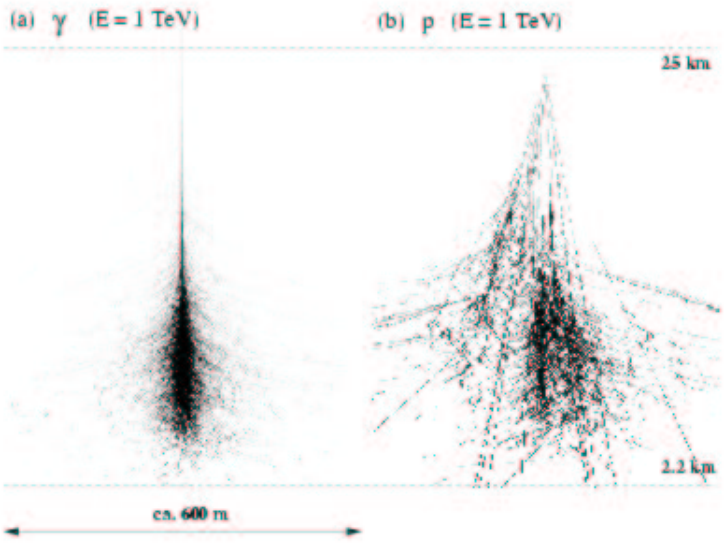

Figure 2.3: Comparison of extensive air shower initiated by gamma photon and proton (both with energy equal 10^{12} eV). Two dashed lines show an altitude from a ground. The absence of pionization and nucleonic cascade makes the differences in the shower initiated by photon. It can be seen that particle lateral distribution falls rapidly with distance from the core. From (LAMPEITL, 2000).

enough so that their decay length becomes smaller than their interaction length. Since this happens earlier in the case of a primary heavy nucleus, the resulting shower is richer in muons than a proton shower. At the same time, and since muons are produced earlier in the shower development, they reach a ground also earlier, compared to the electromagnetic component which undergoes many interactions before reaching the detector array. For a photon shower the proportion of muons will be even smaller (see Figure (2.3)) and the highest energies and another physical process will have important consequences on the EAS shower detection and characterization. This is the Landau-Pomeranchuk-Migdal (LPM) effect: the cross sections of the photon-nucleus and electron-nucleus decrease in high energies with increasing density of the medium with which they interact. Even in the upper atmosphere, the LPM effect becomes appreciable at energies in the EeV range. So that it is possible for a photon of 10^{20} eV to develop the EAS very deep in the atmosphere, yielding less than 10^9 particles at the ground level.

2.2 Atmospheric Fluorescence Detectors

The charged particles moving through the atmosphere ionize air and excite metastable energy levels in its atoms and molecules (mostly nitrogen N_2). With a very short relaxation time, electrons from those levels return to ground state emitting a characteristic isotropic fluorescence light. Some of this excitation energy

is emitted in the form of visible and UV radiation (see Figure (2.4)). The emission efficiency (ratio of the energy emitted as fluorescence light to the deposited one) is poor (less than 1%), therefore observations can only be done for the primary particle with energy $\geq 10^{19}$ eV. At higher energies, the huge number of particles in the shower produces enough light to be detected even at large distances. (At the shower maximum of the most energetic shower ever detected, 3.2×10^{20} eV, the number of particles was larger than 2×10^{11}.) The detector sees the shower as a variable light bulb (a rough estimate of the equivalent radiated power would be 3 E[eV]/10^{18} watts at the shower maximum (BERTOU ET AL., 2000)) moving at the speed of light along the shower axis.

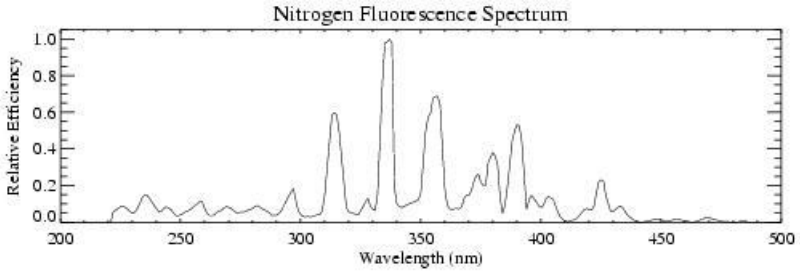

Figure 2.4: The emission spectrum of nitrogen, taken from BUNNER (1967).

The fluorescence technique is the most appropriate one for energy measurements: the emitted energy is proportional to a number of charged particles in the shower (Eq. 2.2). The longitudinal development of the shower is parameterized by the Gaisser-Hillas function (BERTOU ET AL., 2000) giving the size of shower N_e (the number of electrons in the shower) as the function of atmospheric depth x (in g/cm^2):

$$N_e(x) = N_{max} \left(\frac{x - x_0}{X_{max} - x_0} \right)^{(X_{max}-x_0)/\lambda} e^{(X_{max}-x)/\lambda}, \tag{2.1}$$

where λ is a constant equal to 70 g/cm^2, x_0 is the depth at which the first interaction occurs, and X_{max} is the depth of the shower maximum.

The total energy of the shower (or the energy E_0 of the primary particle) is then proportional to the integral of this function, knowing that the average energy loss of one created particle is 2.2×10^6 eV/(g cm^{-2}) and that the energy fraction of this electromagnetic component is $80 \div 90$ % (NAGANO & WATSON, 2000):

$$E_0[\text{eV}] = 2.65 \times 10^6 \times \int_0^\infty N_e dx. \tag{2.2}$$

The identification of the primary cosmic ray with a fluorescence telescope is based on the shower maximum in the atmosphere (X_{max}) which depends on the nature and the energy of the incident cosmic ray. On the average, at a given energy the shower generated by a heavy nucleus reaches its maximum higher in the

atmosphere than that of light nucleus or proton, respectively. Simulations show typical values of 750 and 850 g/cm^2 for iron nuclei and protons. Unfortunately, physical fluctuations of the interaction altitude and of the shower development (larger than the precision on the shower reconstruction) blur this ideal image. As an example, at 10^{19} eV the typical fluctuation on the X_{max} position is 50 g/cm^2 (WATSON, 2000). Thus, when the fluorescence technique is used alone, it is practically impossible to define the primary composition on a shower-by-shower basis. Therefore, one must look for statistical means of studying the chemical composition or use the hybrid detection method where a multi-variable analysis becomes possible.

2.3 Čerenkov Experiments

Another technique, useful for measuring cosmic rays that reach the ground, uses a phenomenon called the Čerenkov effect: charged particles moving through the atmosphere with a velocity v larger than the local speed of light c/n (the vacuum speed of light c divided by the refractive index of the air n) emit Čerenkov light.

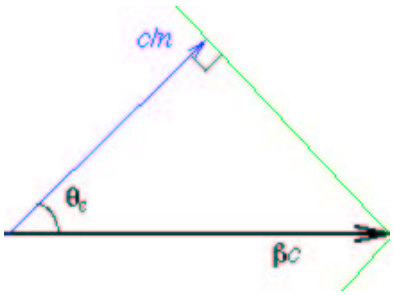

Figure 2.5: Illustrating picture for Eq. 2.3. βc is velocity of charged particle moving through a medium with the refractive index n.

While the fluorescence emission from N_2 molecules is isotropic, the Čerenkov emission is highly collimated (within $\sim 1.3°$ in the atmosphere) along the direction of motion. The angle of the wave vector with respect to the direction of motion of the particle is

$$\cos\theta = \frac{c}{nv}. \tag{2.3}$$

Čerenkov radiation is emitted only if the particle has velocity

$$v > \frac{c}{n}. \tag{2.4}$$

Therefore the process can be used in the construction of threshold detectors. If the particles pass for example through water, for which $n = 1.33$, only those with $v > 0.75c$ emit Čerenkov radiation which can be detected as an optical signal.

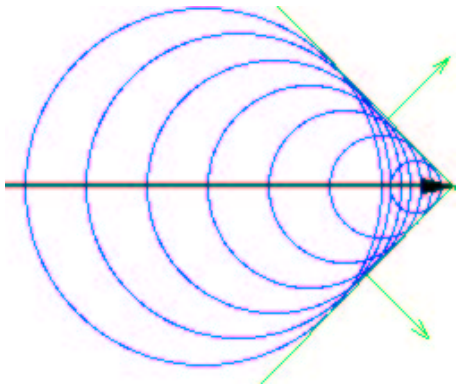

Figure 2.6: Huygens' construction for determining the direction of propagation of the Čerenkov radiation's wavefront.

It can be shown that the number of photons per unit length of track is given by:

$$N_\gamma = \frac{\alpha Z^2}{c} \int \left(1 - \frac{1}{\beta^2 n^2}\right) 2\pi\nu d\nu = \frac{\alpha z^2}{c} \int \sin^2\theta 2\pi\nu d\nu, \tag{2.5}$$

where $\alpha = \frac{e^2}{4\pi\varepsilon_0 \hbar c} = \frac{1}{137}$ is the fine structure constant, Z is the atomic number of the medium being traversed, $\beta = \frac{v}{c}$ is usual relativistic parameter and ν is the frequency of Čerenkov light. The refractive index n is a function of the frequency ν, decreasing rapidly in the ultraviolet band for most materials. Most radiation is therefore in the visible band, peaking at the blue end of the spectrum. Specially, we consider a medium with $n \sim 1$, and write $n = 1 + \delta$ (with $\delta \ll 1$). Čerenkov radiation then only occurs for β very close to 1, say $\beta = 1 - \epsilon$. The number of Čerenkov photons per centimeter of a particle track is then

$$N_\gamma \approx 500 \left(1 - \frac{1}{(1-\epsilon)^2(1+\delta)^2}\right) \approx 1000(\delta - \epsilon). \tag{2.6}$$

The condition $\beta > \frac{1}{n}$ implies $\delta > \epsilon$.

This technique is used in two ways: First, in small detector stations covering large area in the regular grid. Each detector station is filled with the pure water in CR experiments and it measures the number of particles passing through. The central computer then combines the measurements of the number of particles and their time of arrival at each station to determine the direction and energy of the original cosmic primary that set off the shower.

A second application is the detection of high-energy cosmic and gamma-rays when they enter the top of the atmosphere. The primary particle initiates cascade of the charged particles (for example electrons and positrons) emitting optical Čerenkov radiation (with very rapid emission time in nanoseconds), which can be detected by light detectors. The intensity of the radiation is given by the expression (Longair, 1992):

$$I(\omega) = \frac{\omega Q^2 v}{4\pi\varepsilon_0 c^3} \left(1 - \left[\frac{c}{nv}\right]^2\right) \sim \omega Q^2 \sin^2\theta, \tag{2.7}$$

where Q is the charge of the particle moving with velocity v, ω is a frequency of emitted Čerenkov light and ε_0 is dielectric constant[3]. The total emitted light is measured and this provides information about the charge and velocity of the particles.

There are important differences between gamma-rays and cosmic-rays. The Čerenkov light collected from a gamma-ray shower has a smaller angular distribution and tends to have an ellipsoidal shape which aligns itself with the direction of the incoming photon (orientation towards the emission source). Cosmic ray induced air showers, on the other hand, have Čerenkov light images which are much broader and less well aligned with the arrival direction.

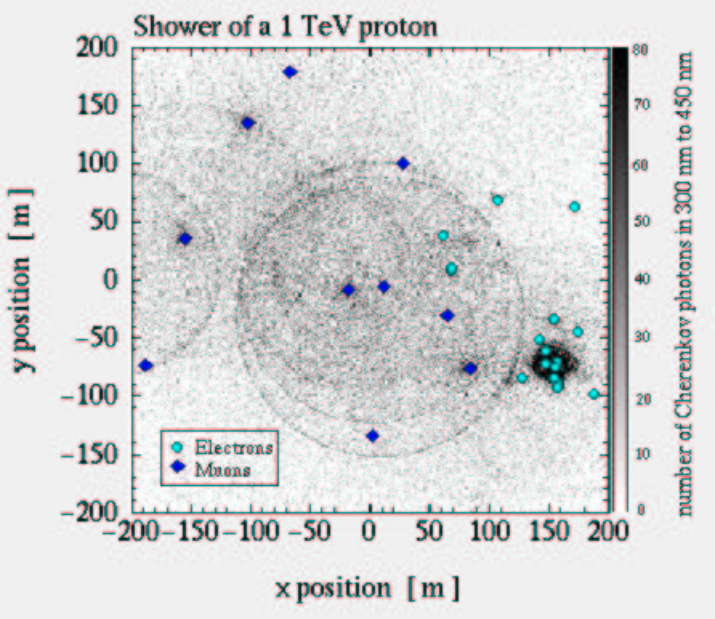

Figure 2.7: The image shows the lateral distribution of Čerenkov light of an air shower initiated by a vertical proton of 10^{12} eV energy. The area displayed covers 400×400 m^2 with the shower core at the centre. The markers denote the impact points of electrons/positrons and muons at an altitude of 2200 m. The image is result of simulation with CORSIKA 4.50 without any atmospheric extinction.(Max-Planck Institut für Kernphysik, 2001)

The atmospheric Čerenkov telescopes consist typically of one or more individual mirrors. The mirrors have a parabolic shape, vary in size from 2 to 10 m in diameter and are composed of multiple facets for ease of construction. The requirements on the mirror specifications are not as severe as for large optical telescopes. The main problem with these detectors is that the light yield is very small and photomultipliers have to be used to produce a measurable signal.

The photoelectron density induced by Čerenkov signal S is equal to

$$S = \rho_\gamma A \epsilon \,, \tag{2.8}$$

[3]The value is equal $\varepsilon_0 = 8.8542 \times 10^{-12}$ C^{-2} m^{-2} N^{-1}.

where A is the collection area of the mirror(s), ρ_γ is the density of Čerenkov photons and ϵ is the efficiency of light collector. For current Čerenkov telescopes $\epsilon \sim 0.1$ (Marsella, 1998). The noise level N can be expressed in terms of fluctuations of the night-sky background:

$$N = \sqrt{B\Omega A\epsilon t}\ , \tag{2.9}$$

where B is the night sky background photon flux, Ω is the solid angle subtended by a photomultiplier (PMT) and t is the electronic trigger formation time. The signal-to-noise ratio can be expressed as

$$S/N = \rho_\gamma \sqrt{A\epsilon/B\Omega t}. \tag{2.10}$$

The energy threshold can be defined as the minimum gamma-ray energy for which the signal-to-noise is sufficient to adequately trigger the instrument. So, the energy threshold E_{th} is proportional to (Marsella, 1998)

$$E_{th} \propto (1/\rho_\gamma)\sqrt{B\Omega t/A\epsilon} \tag{2.11}$$

It is clear that it is possible to lower energy threshold of a Čerenkov telescopes by reducing the noise contribution from night-sky light (by working at dark site or by minimizing the field of view and integration time), or by increasing the amount of collected Čerenkov signal (by maximizing the mirror size or collection efficiency).

The systematic error in the energy scale varies from telescope to telescope, but current instruments have errors in the range of $30 \div 40$ % (Marsella, 1998)

Name	Location	A (m^2)	E_{th} (GeV)
Cangaroo	Woomera, Australia	11	1000
CAT	Targasonne, France	18	250
CLUE	La Palma, Spain	2.5	1000
Durham Mark 3,5,6	Narrabri, Australia	42	250
GT-48	Crimea, Ukraine	27	900
HEGRA	LA Palma, Spain	9	500
Nooitgedacht	Potchefstroom, South Africa	7	700
Pachmari	Pachmari, India	4	
SHALON	Tien-Shan, Russia	10	1000
TACTIC	Mt. Abu, India	10	
Whipple	Mt. Hopkins, USA	75	250

Table 2.1: The list of the major atmospheric Čerenkov telescopes in operation.

2.4 Scintillation Detectors

The ionization caused by high-energy particles in the detectors can be used to measure the flux of particles and some of their other properties. The charged

particles when moving fast through the scintillation detector excite electrons in the atoms. The excited atoms then lose this energy by emitting photons. The light is detected by a sensitive detector, usually a photomultiplier tube (PMT). The photomultiplier changes a faint flash of light into a measurable electrical signal. The scintillation detector and the photomultiplier are housed in a dark box so that the only light caused by cosmic rays is detected. The resulting signal is proportional to the total energy deposited by particles in the scintillating material.

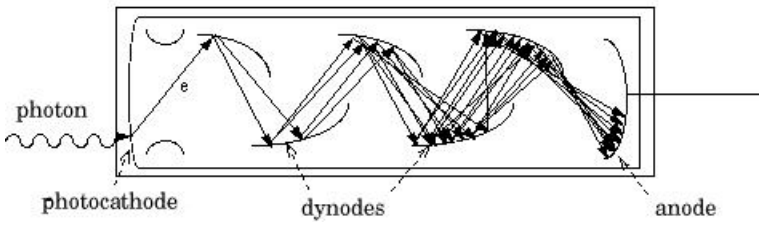

Figure 2.8: The scheme of photomultiplier: the photocathode of the PMT converts the light into photoelectrons. The photoelectrons are then accelerated by an electric field towards the dynodes of the PMT where the multiplication process takes place. The result is that photon produces a charge pulse on the anode of the PMT that can subsequently be detected by other electronic equipment.

There are two main disadvantages of this technique. First, scintillation materials convert only about 3% of the passed particles energy into the optical photons, second is that the efficiency of the conversion photons to electrons in the photocathode is only about $10 - 20\%$.

The relativistic ionization losses derived from relativistic quantum theory are described by Bethe-Bloch formula (Longair, 1992)

$$-\frac{dE}{dx} = \frac{z^2 e^4 N_e}{4\pi\varepsilon_o^2 m_e v^2}\left[ln\left(\frac{2\gamma^2 m_e v^2}{\bar{I}}\right) - \frac{v^2}{c^2}\right] = z^2 NZ f(v), \tag{2.12}$$

where $-dE$ means the energy loss of high-energy particle in length dx ($\frac{dE}{dx}$ is often referred to as the stopping power of the material), the charge of the high-energy particle is z and its velocity v, so the Lorentz factor is equal $\gamma = \frac{1}{\sqrt{1-(v/c)^2}}$, the number density of electrons is N_e. $\bar{I}$ is the ionization potential of the atom weighted mean over all states of the electrons in the atom. The value of $\bar{I}$ cannot be calculated exactly (except the simplest atoms) and has to be found experimentally.

Suppose that the atomic number of the medium through the high-energy particles passes is Z and that the number density of atoms is N, then $N_e = ZN$. The stopping power $\frac{dE}{dx}$ is conventionally expressed not in terms of length but in terms of the total mass per unit cross-section traversed by the particle. Thus, if particle travels a distance x through material of density ϱ, then

$$-\frac{dE}{d\xi} = z^2 f(v)\frac{NZ}{\varrho} = z^2 f(v)\frac{Z}{m}, \tag{2.13}$$

where $\xi = \varrho x$ and m is the mass of nucleus of the material.

There are important differences between the ionization losses of electrons and of the heavier particles. First, the interacting particles and the electrons bound in atoms are identical and second, the electrons suffer much larger scattering than the protons and nuclei, which are effectively undeviated. The formula for the ionization losses of electrons moving with velocity v is as follows:

$$-\frac{dE}{dx} = \frac{e^4 NZ}{8\pi\varepsilon_0^2 m_e v^2}\left[ln\left(\frac{\gamma^2 m_e v^2 E_{max}}{2I^2}\right) - \left(\frac{2}{\gamma} - \frac{1}{\gamma^2}\right) ln2 + \frac{1}{\gamma^2} + \frac{1}{8}\left(1 - \frac{1}{\gamma}\right)^2\right], \tag{2.14}$$

where

$$E_{max} = \frac{\gamma^2 m_e v^2}{1+\gamma} \tag{2.15}$$

is the maximum kinetic energy which can be transferred to the stationary electron.

2.5 The experimental situation

Cosmic rays and gamma-rays span an enormous range of energies, from 10^6 eV to 10^{20} eV. Given this range, a single detection technique will not suffice (see Fig. 2.9). Satellite and stratosphere balloon experiments above the Earth's atmosphere operate up to 10^{10} eV and 10^{14} eV, respectively. At higher energies, the particle flux is small (Fig. (3.3) on page 18) so that experiments become flux limited. Hence we use the Earth's atmosphere for indirect observations.

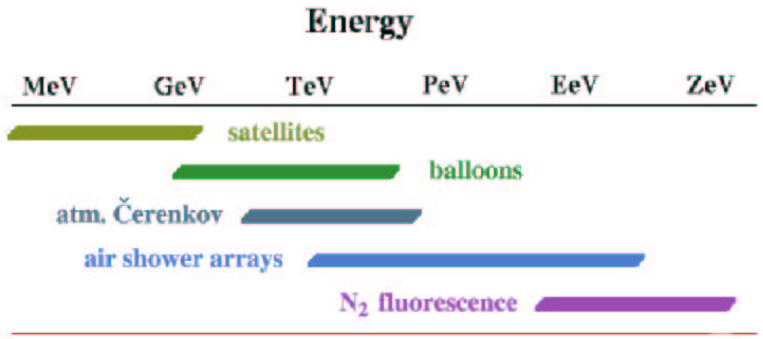

Figure 2.9: Detection techniques in the wide energy range. Satellite and balloon-borne experiments provide direct measurements of primary cosmic rays.

Name of experiment	Location	Used technique	Energy range	Time of operating
AGASA & Akeno	Akeno, Japan	muon detectors scintillation detectors	above 10^{14} eV	since 1979
AMANDA & SPASE & VULCAN	South Pole, Antarctica	Čerenkov light, muon detectors scintillation detectors	$> 5 \times 10^{13}$ eV	since 1988
ATIC	Antarctica	balloon experiments	$5 \times 10^{10} \div 10^{14}$ eV	
ARGO-YBJ	Yangbajain, Tibet, China	scintillation detectors	$10^{11} \div 2 \times 10^{13}$ eV	since 2000
BASJE	Chacaltaya, Russia		$10^{13} \div 10^{16}$ eV	
BLANCA & CASA-MIA & DICE	Dugway, Utah, USA	Čerenkov light, muon detectors scintillation detectors	$10^{14} \div 10^{16}$ eV	1990 - 1998
EAS-TOP	Gran Sasso, Italy	Čerenkov light, muon detectors scintillation detectors	$10^{13} \div 10^{16}$ eV	since 1996
Fly's Eye	Dugway, Utah, USA	air fluorescence	above 10^{17} eV	1981 - 1993
GREX & Haverah Park	Harrogate, Great Britain	scintillation detectors water Čerenkov	above 10^{17} eV	1967 -1987
HEGRA	La Palma, Spain	Čerenkov light	$5 \times 10^{11} \div 10^{16}$ eV	since 1990
HiRes	Dugway, Utah, USA	air fluorescence	above 10^{17} eV	since 1998
JACEE	Antarctica	balloon experiments	$10^{12} \div 10^{15}$ eV	
KASCADE	Karlsruhe, Germany	muon detectors scintillation detectors	$10^{14} \div 10^{17}$ eV	since 1995
Milagro	Los Alamos, New Mexico, USA	water Čerenkov	$10^{11} \div 10^{14}$ eV	since 1997
MSU	Moscow, Russia		$10^{15} \div 3 \times 10^{17}$ eV	
Norikura Observatory	Japan	scintillation detectors	$10^{14} \div 10^{16}$ eV	since 1953
Pierre Auger Project	Malargüe, Mendoza, Argentina	air fluorescence water Čerenkov	above 10^{19} eV	under construction
RUNJOB	Kamchatka, Russia	balloon experimets	$10^{12} \div 5 \times 10^{14}$ eV	
SUGAR	Narrabri, New South Wales, Australia	muon detectors	above 10^{17} eV	1968 - 1979
Tian-Shan	Kazakhstan	muon detectors scintillation detectors	$10^{13} \div 10^{18}$ eV	since 1968
Tibet	Yangbajing, Tibet, China	scintillation detectors	$10^{12} \div 10^{14}$ eV	since 1997
TUNKA-13	Lake Baikal, Russia	Čerenkov light	$10^{14} \div 10^{17}$ eV	since 1996
Volcano Ranch	New Mexico, USA	muon detectors scintillation detectors	above 10^{18} eV	1959 - 1963
Yakutsk	Yakutsk, Siberia, Russia	muon detectors scintillation detectors	above 10^{16}eV	since 1970

Table 2.2: Table of selected ground-based and balloon-borne experiments with their characteristics.

Chapter 3

Spectrum of cosmic rays

3.1 All particle spectrum

The energy spectra are not of Maxwellian form but can be represented by power-law energy distributions as ilustrated in Fig (3.1) . Let us note some features of these spectra.

1. First of all, at energies less than about 10^9 eV, the energy spectra of all species show a pronounced attenuation relative to the power-law observed at high energies. The energy and shape of the cut-off vary with the phase of the solar cycle, the fluxes decrease during periods of high solar activity. The cut-off is an artefact of the fact that the cosmic ray particles have to diffuse towards the Earth from the interstellar space through the outflowing Solar Wind. This phenomena is known as solar modulation (see Fig. (3.2)).

2. The differential energy spectra of the various cosmic ray species can be well represented by power-law distribution over energy range $> 10^9$ eV:

$$d\Phi(E)/dE = \Phi_0 E^{-\alpha}, \tag{3.1}$$

where E is energy in TeV, α is an spectral index and $d\Phi(E)/dE$ is a differential flux in particles/($m^2\,s\,sr\,TeV$). For higher energy, there are two interesting breaks in the exponent. First of them is known as a knee, second as an ankle[1].

3. At the very lowest energies below about 6×10^7 eV, there is an increase flux of helium nuclei. This component is referred to as the anomalous ^{4}He. The spectral turn up only appeared in 1972 and its intensity began to decrease again in 1981. Thus it was during period of minimum Solar activity. Apparently there was no evidence for this component in 1965 during the previous Solar minimum. The flux of these particles increases with increasing distances from the Sun. The variability of the component and the fact that it does not conform to any simple model of Solar modulation is consistent with the hypothesis that the particles are accelerated in the outer heliosphere.

[1] We will discuss them on page 17

The Sun is also a sporadic source of cosmic ray nuclei and electrons that are accelerated by shock waves traveling through the corona, and by magnetic energy released in solar flares. During such occurrences the intensity of Solar energetic particles (SEPs) in space can increase by a factor of 10^2 to 10^6 for hours to days. Such solar particle events are much more frequent during the active phase of the solar cycle. The maximum energy reached in solar particle events is typically 10^7 to 10^8 eV, occasionally reaching 10^9 eV (roughly once a year) to 10^{10} eV (roughly once a decade).

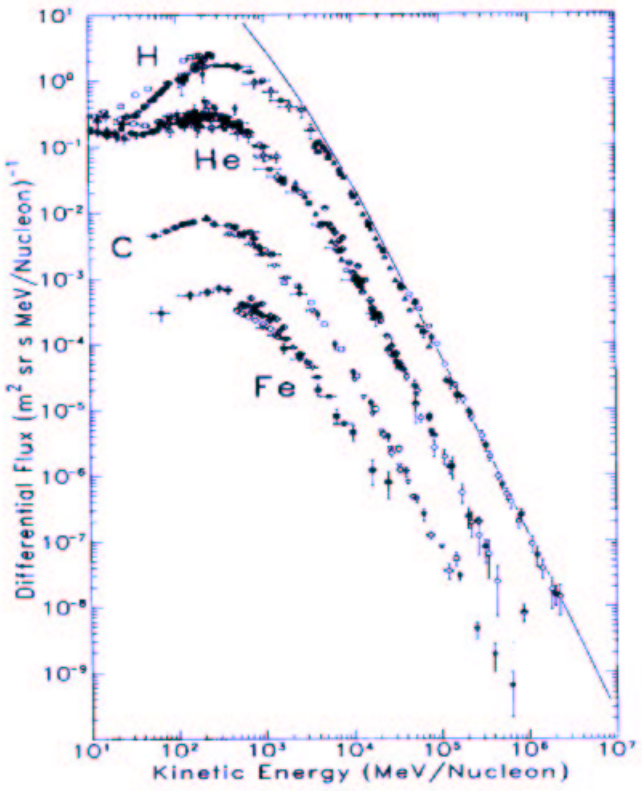

Figure 3.1: The differential energy spectra of cosmic rays at the Earth. The spectra for hydrogen, helium, carbon and iron are shown. The solid line shows the unmodulated spectrum for hydrogen, i.e. the effects of the propagation through the interplanetary medium upon the energy spectra of the particles have been eliminated using a model for the modulation process (LONGAIR, 1992).

3.2 Interesting features

Cosmic rays (CRs) from outside the Solar system show a smooth flux spectrum and are almost entirely made up from protons and fully ionized nuclei[2]. The observations of the cosmic rays themselves (mainly satellite- and balloon-borne

[2]More detailed discussion about composition of CRs is in Section 3.4

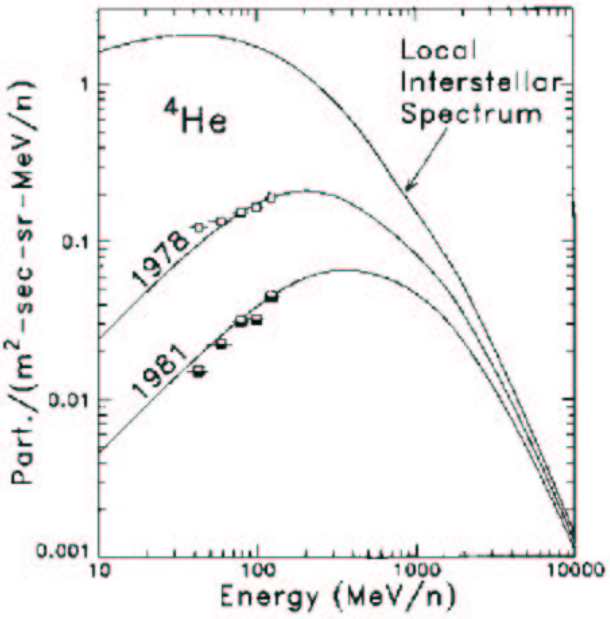

Figure 3.2: The calculated local interstellar ^{4}He spectrum with the modulated spectra fitted to observation in 1978 and 1981 (the period of minimum and maximum Solar activity). From KROEGER (1986).

experiments), and of the nonthermal radioemission from our Galaxy as well as from all other well observed galaxies (BIERMANN, 1993) suggest that the Cosmic rays, except for spalation products, have an universal spectrum of very nearly $E^{-8/3}$ from 10^{13} eV to the knee.

Only at higher energies the overall cosmic ray flux spectrum shows two distinct features (Figure (3.3)): a steepening of the slope around 3×10^{15} eV and a flattening near 6×10^{18} eV. They were named knee and ankle in the analogy with features of a human leg. The basic slope of the spectrum curve is associated with the effectivity of the most common acceleration mechanism in the variable magnetic field[3], but these changes of spectral index are puzzling. Their explanation will tell us something crucial about the origin and propagation of CRs. Hereafter we can due to knowledge of cosmic rays propagation investigate the Galactic and extragalactic magnetic field.

The slopes of the primary spectrum are $\alpha \simeq 2.7$ below the knee and $\alpha \simeq 3.0$ above the knee up to $\simeq 4 \times 10^{17}$ eV. Then it seems to steepen to about about 3.2 up to the ankle, after which it flattens to about 2.7. At the end of the energy spectra, there are many uncertainties due to big experimental errors (for example see Fig. (3.3)). The present data seem to reveal a steepening just below 10^{20} eV and no cutoff, as we expect from a theoretical prediction [4].

[3]Will be discussed in Section 4.3.

[4]Mystery of no evidence of GZK cutoff, see Section 5.7.

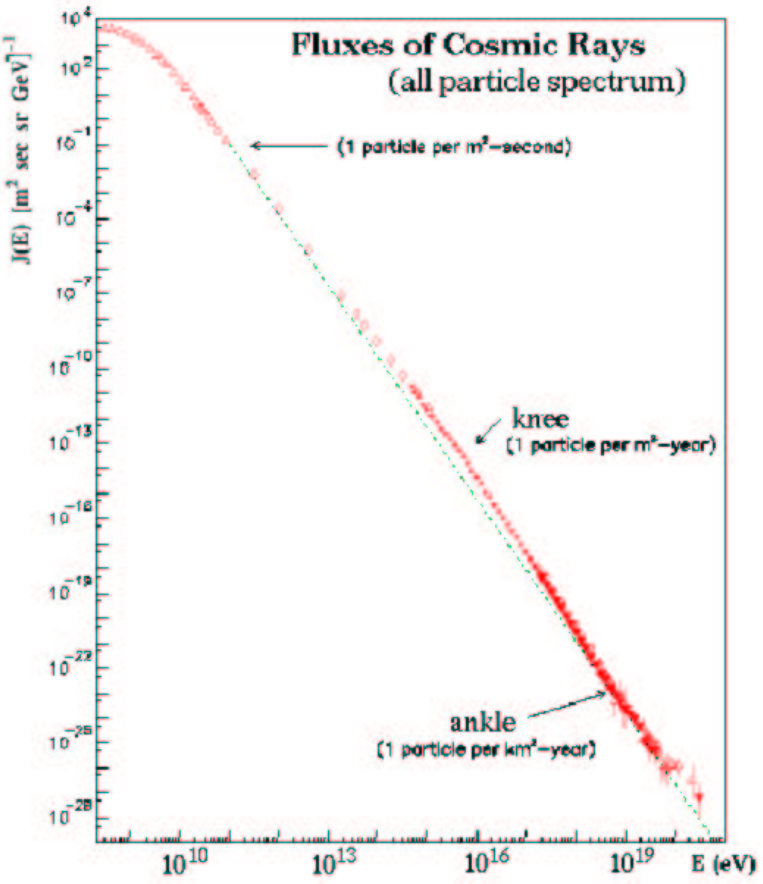

Figure 3.3: The cosmic ray all-particle spectrum. The spectrum should be expressed in the form of the power law from 10^{11} eV to 10^{20} eV. The dotted line shows E^{-3} power-law for comparison (Bhattacharjee & Sigl, 1999).

3.3 Anisotropy

It is immediately apparent from Fig. 3.1 that the flux of cosmic rays with energies less than about 10^9 eV must be significantly influenced by the process of Solar modulation and hence information about the arrival directions of these cosmic rays at the Solar System is lost. In fact, only relatively high energy protons and nuclei penetrate to the vicinity of the Earth undeflected by the magnetic field in the interplanetary medium. A measure of deflection suffered by a particle is the ratio of its Larmor radius r_g of gyration to the typical scale of a volume with given magnetic field B. For a relativistic particle the Larmor radius is

$$r_g\,[\mathrm{m}] = \left(\frac{pc}{Ze}\right)\frac{\sin\theta}{Bc} \tag{3.2}$$

or

$$r_g\,[\mathrm{pc}] \simeq \frac{E\,[10^{15}\,\mathrm{eV}]}{Z\,B\,[\mu\mathrm{G}]}\sin\theta \tag{3.3}$$

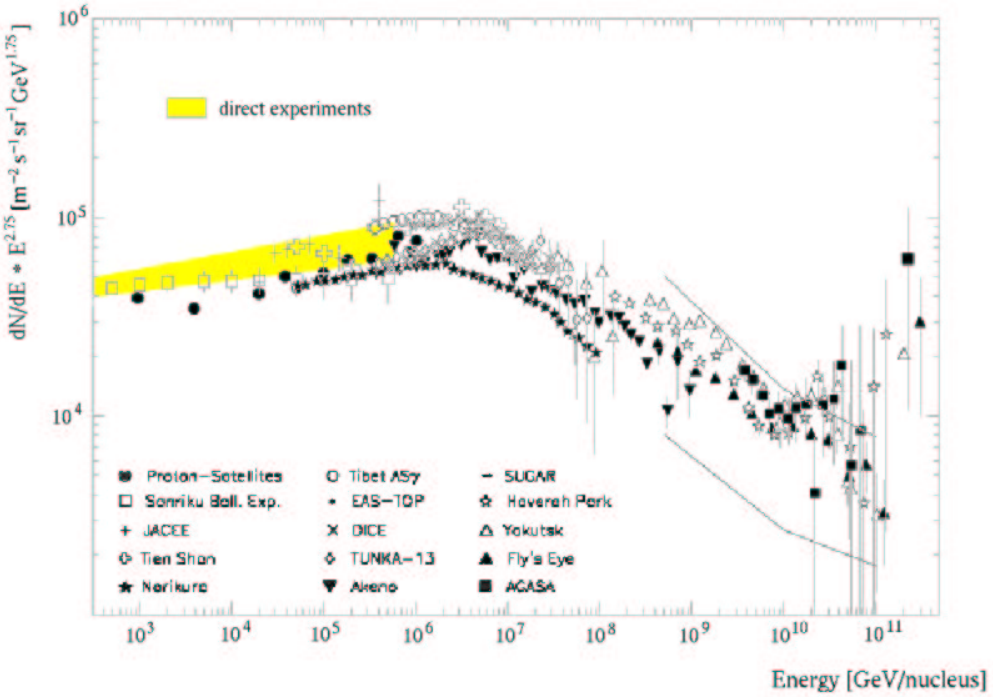

Figure 3.4: The energy spectrum from 10^{12} to 10^{20} eV multiplied by $E^{2.75}$. The resulting spectrum is composed from many experiments. From KÖHLER (1998).

for the motion of the particle with the charge $Q = Ze$ (Z is proton number) and constant energy E moving in a spiral path with constant pitch angle θ (the angle between the relativistic three-momentum $\vec{p}$ and the magnetic field $\vec{B}$ vectors).

For a relativistic proton the Larmor radius is

$$r_g[\mathrm{m}] = 3 \times 10^9 \gamma \left(\frac{B}{10^{-9}\,\mathrm{T}} \right) \tag{3.4}$$

where the magnetic field strength B is measured in Tesla and γ is the Lorentz factor. Therefore, adopting the local value of the magnetic field strength in the interplanetary medium $B \simeq 10^{-9}$ T, relativistic protons with $\gamma = 10^3$ (i.e. energies 10^{12} eV) have Larmor radius which are 3×10^{12} m $= 20$ AU, i.e. 20 times the distance from the Sun to the Earth. Thus particle with these energies and more are likely to preserve information about their arrival directions at the Solar system when they arrive at the top of the Earth's atmosphere.

Observations of the arrival directions of high-energy protons and nuclei can be undertaken using the Earth's atmosphere. As is shown in Fig. 2.1, cosmic ray particles create pions (π^0, π^+, π^-) in collisions with the nuclei of atoms and molecules in the upper layers of the atmosphere (above 15 km). The charged pions decay into muons, which have half-life such that they decay long before they reach

surface of the Earth, if their Lorentz factor $\gamma \geq 20$:

$$\pi^+ \rightarrow \mu^+ + \nu_\mu$$

$$\pi^- \rightarrow \mu^- + \bar{\nu_\mu} \tag{3.5}$$

with mean lifetime of 2.6×10^{-8} s and decay of muons

$$\mu^+ \rightarrow e^+ + \nu_e + \bar{\nu_\mu}$$

$$\mu^- \rightarrow e^- + \bar{\nu_e} + \nu_\mu \tag{3.6}$$

with mean lifetime of 2.2×10^{-6} s. Muons are the basis of studies of the isotropy of cosmic rays using underground muon detectors. These experiments are designed to be sensitive to primary particles entering the atmosphere with energies of 10^{12} eV and greater.

An apparently remarkable feature of the CR beam is that, at most energies, it is highly isotropic. Deviations from isotropy are generally less than 1%. This deviations are defined as

$$|\delta| = \frac{I_{max} - I_{min}}{I_{max} + I_{min}}, \tag{3.7}$$

where I_{min} and I_{max} are the minimum and maximum CR intensity as a function of arrival direction. For practical and historical reasons (Smith & Clay, 1997), the maxima and minima are derived from a Fourier analysis of measurements of the intensity along bands of declination viewed by the detector.

The strength and direction of the anisotropy in the arrival directions can be quantified by harmonic analysis (Evans et al., 2001). The number of events is proportional to N

$$N = \int d\delta \int d\alpha \cos\delta h(\delta) F(\alpha, \delta), \tag{3.8}$$

where the incoming flux of CR per unit solid angle F is function of right ascension α and declination δ. The measured flux is the incoming flux modulated by the response of the detector $h(\delta)$, which is the relative efficiency of the detection of events with direction. It depends only on the declination and not on the right ascension, because if the detector is run with reasonable efficiency, there will be almost uniform exposure in right ascension after a year.

Let us define

$$a = \frac{2}{N} \int d\delta \int d\alpha \cos\delta \cos\alpha h(\delta) F(\alpha, \delta),$$

$$b = \frac{2}{N} \int d\delta \int d\alpha \cos\delta \sin\alpha h(\delta) F(\alpha, \delta), \tag{3.9}$$

so that the amplitude R and phase ψ of the first harmonic is

$$\mathcal{R} = (a^2 + b^2)^{1/2}, \qquad \psi = \arctan\left(\frac{b}{a}\right). \tag{3.10}$$

Analysis of data by SMITH & CLAY (1997) says that the amplitude of the first harmonic sidereal variations is small and consistent with noise (for energy below PeV energy range). Since the anisotropies are low, it is necessary to consider the effect on the measurements of counting statistics for a finite data set and the effect of small count rate variations associating them with meteorological conditions. (Meteorological conditions have a strong effect when Fourier analysis is used in solar time but have a much more reduced effect in sidereal time or right ascension).

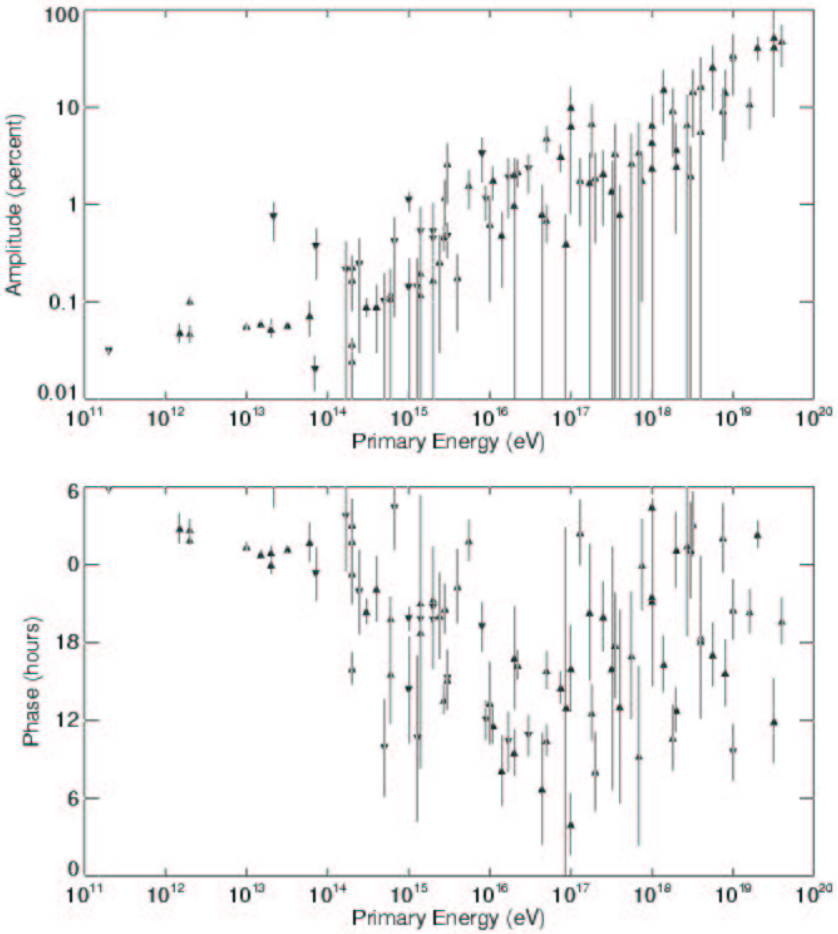

Figure 3.5: The compilation of anisotropy measurements (first harmonic Fourier amplitude and phase). Northern and southern hemisphere results are denoted by upward-pointing and downward-pointing triangles respectively. From SMITH & CLAY (1997).

If cosmic rays have origin associating with nearby astrophysical objects, we may expect cosmic ray anisotropy correlated with the galactic or supergalactic plane. In order to examine any preference for arrival directions along the galactic and supergalactic planes, the plane enhancement parameter f_E is used (TAKEDA ET AL., 1999). The value f_E is expressed by

$$I_{obs}(b)/I_{exp}(b) = (1 - f_E) + 1.402 f_E \exp(-b^2), \tag{3.11}$$

where b is the Galactic and supergalactic latitude in radians, $I_{obs}(b)$ and $I_{exp}(b)$ are the observed and expected intensities at latitude b. A positive f_E value suggests the Galactic or supergalactic plane enhancement, $f_E = 0$ indicates that the arrival direction distribution is isotropic, and a negative f_E shows depression around the plane. Figure 3.6 shows the dependence of f_E on the primary energy for the Galactic and supergalactic coordinates. Some excess can be seen around the supergalactic plane in the energy range $10^{19.1} - 10^{19.2}$ eV, where $f_E^{SG} = 0.36 \pm 0.15$. In other energies, the arrival direction distribution is consistent with the isotropic distribution.

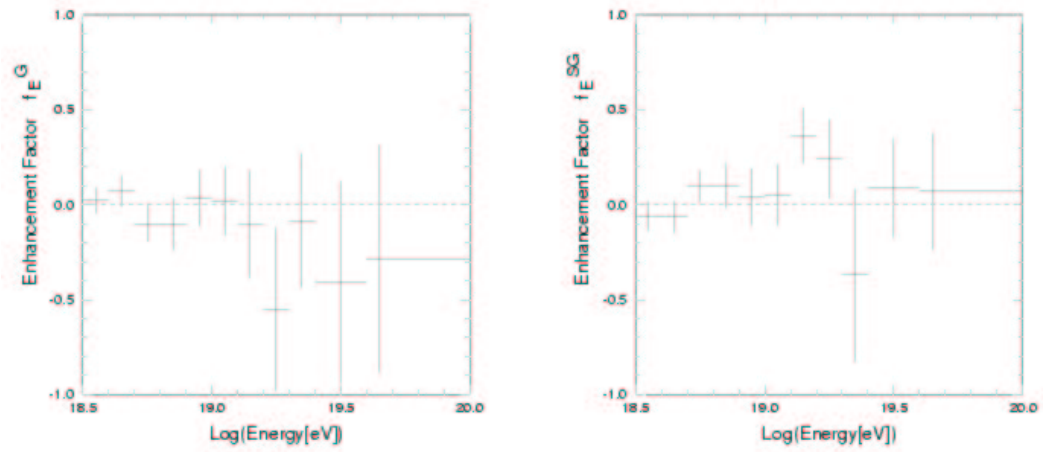

Figure 3.6: The dependence of the plane enhancement factor on the energy for the Galactic (left) and supergalactic (right) coordinates. From TAKEDA ET AL. (1999).

For extremely high-energies, there is a problem with the lack of data. Results from the Fly's Eye (BIRD ET AL., 1999) and the AGASA (HAYASHIDA ET AL., 1999) experiments report a small but statistically significant anisotropy of the order 4% in terms of Eq. 3.7 toward the Galactic plane at energies around 10^{18} eV. These analyses did not reveal a significant correlation with the Supergalactic Plane. The recent data seem to indicate that the events above 10^{20} eV are consistent with an isotropic distribution on large scales, as far as it is possible to conclude from less than 30 events in the world data set. At the same time, TAKEDA ET AL. (1999) find the significant small-scale clustering, particularly one triplet and three doublets within a separation angle of 2.5°, and the probability of observing these clusters by a chance coincidence under an isotropic distribution is smaller than 1%.

3.4 The abundances of the elements

As we hope the general elemental abundances of Universe (BURBIDGE ET AL., 1957) are made up of the primordial H and He, including heavier nuclei formed by H, He and by other processes. The cosmic rays should include naturally the products of the star life. And really, in the primary cosmic rays all stable nuclei of

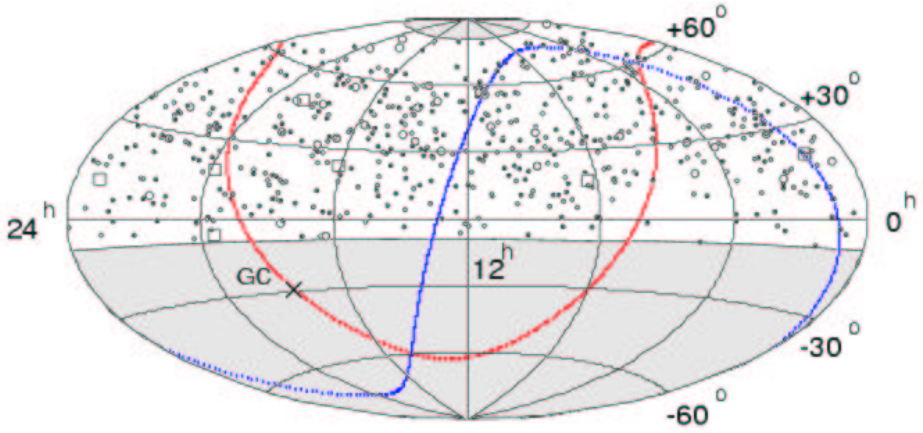

Figure 3.7: The arrival directions of cosmic rays with energies above 10^{19} eV on the equatorial coordinates (TAKEDA ET AL., 1999). Dots, open circles, and open squares represent cosmic rays with energies $(1 \div 4) \times 10^{19}$ eV, $(4 \div 10) \times 10^{19}$ eV, and $\geq 10^{20}$ eV, respectively. The Galactic and supergalactic planes are shown by the red and blue curves, respectively. GC designates the Galactic center.

the periodic table were detected. Other components of cosmic rays are electrons with positrons ($< 1\%$), photons ($< 0.1\%$) and antiprotons. In the same way as in the stars the most common elements of cosmic flux are hydrogen and helium (in the each energy range, where the abundances were precisely measured, i.e. approximately up to 10^{15} eV). The differences between abundant and rare elements achieve more than ten orders. Notice, that the abundances can not be constant, because of changes due to interactions between particles and ambient environment.

Summary of the abundances of the elements in the cosmic ray is shown in Fig. (3.8) . The Local galactic abundances were obtained from spectral measurements and analyses of meteorites. The following features are immediately apparent (LONGAIR, 1992):

(i) The abundance peaks of carbon, nitrogen and oxygen and of the iron group are present both in the cosmic ray and Local galactic abundances.

(ii) It can be seen that the odd-even effect in the relative stabilities of the nuclei according to atomic number known to be present in the Local galactic abundances of the elements is also present in the cosmic rays but to a somewhat lesser degree.

(iii) The light elements (lithium, beryllium and boron) are much overabundant in the cosmic rays relative to their Local galactic abundances.

(iv) There is an excess abundance in the cosmic rays of elements with atomic and mass numbers just less than those of iron, i.e. elements with atomic numbers between about calcium and iron.

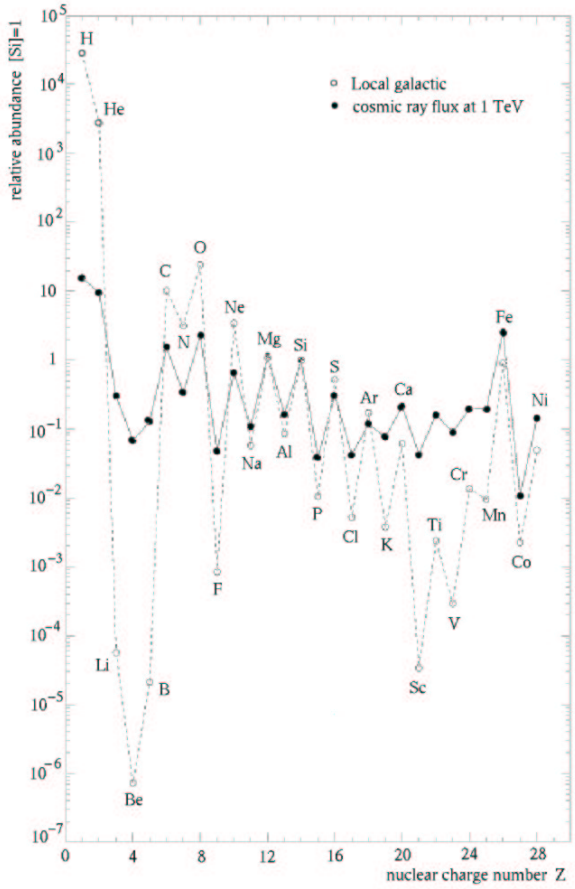

Figure 3.8: The cosmic abundances of the elements H to Ni in the cosmic rays found at the top of the Earth's atmosphere compared with the Local galactic abundances. The data of abundances are normalized to $[Si] = 1$. From WIEBEL (1994).

(v) There is an deficit of hydrogen and helium in the cosmic rays relative to the heavy elements.

Although there are differences, the distribution of element abundances in the cosmic rays is not so different from the Local galactic composition. Two of the differences, points (iii) and (iv), can be explained as a result of spallation. The primary cosmic rays accelerated in their sources have to propagate through the interstellar matter and there collisions occur between the cosmic particles and the ambient interstellar gas. The result is that the heavy nuclei are fragmented to nuclei with less atomic number. (Most of Li, Be and B is derived from C and O.)

Nuclei with $Z > 1$ are much more abundant relative to protons in the cosmic rays than they are in Local galactic material. This is not really understood, but it could have something to do with the fact that hydrogen is relatively hard to ionize for injection into the acceleration process[5], or it could reflect a difference in

[5]Acceleration by Fermi's process could occur only for the charged particles.

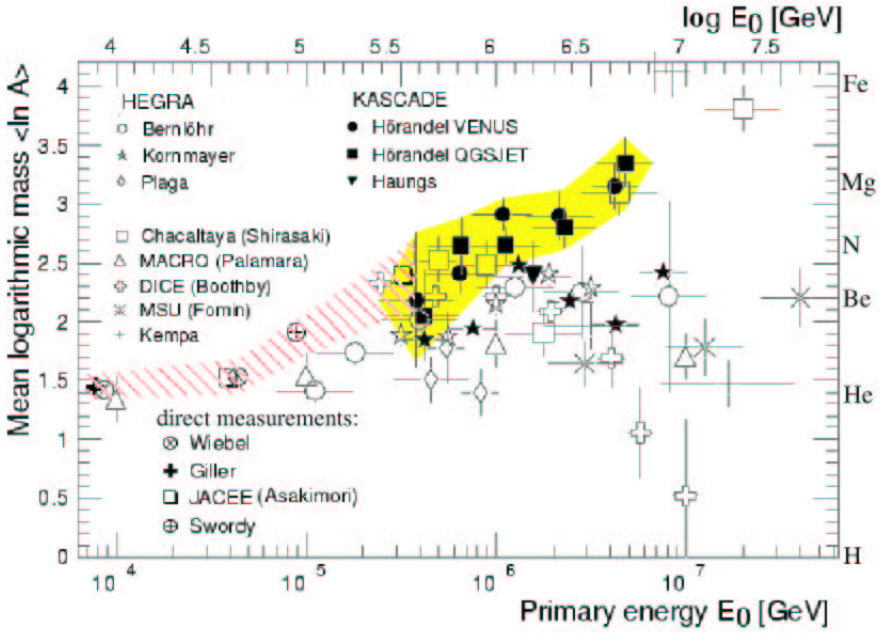

Figure 3.9: The measured mean logarithmic mass of primary cosmic rays versus primary energy for several experiments. Results from direct measurements are summarized in the hatched area. Yellow area, indicating an increase of the mean mass with energy, are data from KASCADE experiment (HÖRANDEL, 1999).

composition of the source.

The elements have been usually divided into four groups according to their mass and charge: low $(H + He)$, medium (C, N, O), high $(Ne - S)$ and very high $(Cl - Fe)$. The contributions of these four groups to the all-particle spectrum are shown in Tab. 3.1.

The comparison between abundances in Fig. (3.8) excludes some hypothesis about origin of cosmic rays. For example it is impossible that cosmic rays come from the Big Bang. Hydrogen and light elements are the only product of Big Bang, but in cosmic rays we observe also the heavy elements. In the same way we know, that cosmic-ray particles can not come from the old stars, because of a small abundance of heavy nuclei.

The abundances of elements in the knee region are very important for our work. Present data on cosmic-ray elemental and isotopic relative abundances are shown to be unable to distinguish between various models of cosmic-ray sources and therefore about origin of the knee. Current results of some experiments are shown in Fig. (3.9) . A strong scattering of the data is visible, from a pure proton to a very heavy composition. This may originate from different detection techniques and experimental methods. In addition there are also problems with interpretation of measured data, because of uncertainties in the simulation of interactions at such high energies (see Fig. 2.2).

Element	**Z**	**%**	**Group**	**Spectral index**	**Flux** $[\mathrm{m}^2\,\mathrm{s}\,\mathrm{sr}\,\mathrm{TeV/nucleous}]^{-1}$
H	1	42.26	low 42 %	2.75 ± 0.02	$(10.91 \pm 0.32) \times 10^{-2}$
He	2	25.57	26 %	2.62 ± 0.02	$(6.60 \pm 0.15) \times 10^{-2}$
Li	3	0.82		2.54 ± 0.09	$(2.08 \pm 0.51) \times 10^{-3}$
Be	4	0.19		2.75 ± 0.04	$(4.74 \pm 0.48) \times 10^{-4}$
B	5	0.34		2.95 ± 0.05	$(8.59 \pm 0.79) \times 10^{-4}$
C	6	4.18	medium	2.66 ± 0.02	$(1.06 \pm 0.01) \times 10^{-2}$
N	7	0.93		2.72 ± 0.05	$(2.35 \pm 0.08) \times 10^{-3}$
O	8	6.19	13 %	2.68 ± 0.03	$(1.57 \pm 0.04) \times 10^{-2}$
F	9	0.13		2.69 ± 0.08	$(3.28 \pm 0.48) \times 10^{-4}$
Ne	10	1.81		2.64 ± 0.03	$(4.60 \pm 0.10) \times 10^{-3}$
Na	11	0.30		2.66 ± 0.04	$(7.54 \pm 0.33) \times 10^{-4}$
Mg	12	3.16	high	2.64 ± 0.04	$(8.01 \pm 0.26) \times 10^{-3}$
Al	13	0.45		2.66 ± 0.04	$(1.15 \pm 0.15) \times 10^{-3}$
Si	14	2.76	9 %	2.68 ± 0.03	$(6.99 \pm 0.14) \times 10^{-3}$
P	15	0.11		2.69 ± 0.06	$(2.70 \pm 0.20) \times 10^{-4}$
S	16	0.86		2.46 ± 0.08	$(2.18 \pm 0.08) \times 10^{-3}$
Cl	17	0.12		2.68 ± 0.05	$(2.94 \pm 0.19) \times 10^{-4}$
Ar	18	0.32		2.69 ± 0.04	$(8.17 \pm 0.35) \times 10^{-4}$
K	19	0.21		2.65 ± 0.04	$(5.36 \pm 0.15) \times 10^{-4}$
Ca	20	0.57		2.72 ± 0.09	$(1.45 \pm 0.09) \times 10^{-3}$
Sc	21	0.12		2.64 ± 0.06	$(3.04 \pm 0.19) \times 10^{-4}$
Ti	22	0.45		2.61 ± 0.06	$(1.13 \pm 0.14) \times 10^{-3}$
V	23	0.25		2.63 ± 0.05	$(6.31 \pm 0.28) \times 10^{-4}$
Cr	24	0.54	very high	2.67 ± 0.06	$(1.36 \pm 0.12) \times 10^{-3}$
Mn	25	0.53		2.46 ± 0.22	$(1.35 \pm 0.14) \times 10^{-3}$
Fe	26	7.02	10 %	2.60 ± 0.09	$(1.78 \pm 0.18) \times 10^{-2}$
Co	27	0.03		2.72 ± 0.09	$(7.51 \pm 0.37) \times 10^{-5}$
Ni	28	0.39		2.51 ± 0.18	$(9.96 \pm 0.43) \times 10^{-4}$

Table 3.1: The abundances of elements with $Z < 29$ in the cosmic rays, their spectral index and differential flux at 10^{12} eV. From WIEBEL (1994).

Chapter 4

Acceleration mechanisms

4.1 Fermi's Original Theory

Diffusion of the charged particles in the turbulent magnetic fields carried along with the moving plasma is the mechanism for energy gains. The macroscopic kinetic energy of moving magnetized plasma is transferred to individual charged particles due to scattering on irregularities in the magnetic field, thereby increasing the energy per particle to many times its original value and achieving the nonthermal energy distribution characteristic of particle acceleration.

In the simplest version of statistical or diffusive shock acceleration mechanism (other names for Fermi acceleration[1]) there are given following presumptions: particle approach (neglecting effects of cosmic ray pressure on the shock profile), a plane geometry, the structure is given apriori and is not affected by the particles being accelerated and finally only non-relativistic shocks. The inhomogenities of magnetic field are assumed to scatter particles efficiently so as to result in a nearly isotropic distribution of the particles.

Let us consider a fast moving particle (with energy E_1) entering the slowly moving magnetic cloud (Fig. 4.1). Assuming the particle to be relativistic, i.e. $E \simeq pc$, one can obtain

$$E_1' = \gamma E_1(1 - \beta\cos\theta_1), \tag{4.1}$$

where $\beta = V/c$ and $\gamma = 1/\sqrt{1-\beta^2}$, V is speed of the cloud and the primes denote quantities measured in the cloud rest frame. Going back to the laboratory frame, one can obtain

$$E_2 = \gamma E_2'(1 + \beta\cos\theta_2'). \tag{4.2}$$

We assume that there is no collisions with the matter but only elastic scattering on the magnetic field irregularities, therefore, the total energy of the particle should be conserved in the rest frame of the moving cloud, $E_1' = E_2'$. Then we obtain

$$E_2 = \gamma^2 E_1(1 - \beta\cos\theta_1)(1 + \beta\cos\theta_2') \tag{4.3}$$

[1]The mechanism was first proposed by Fermi (1949).

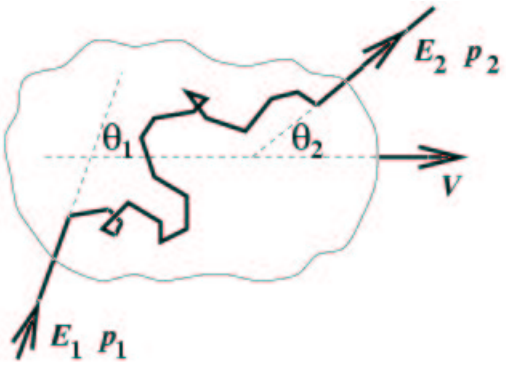

Figure 4.1: The sketch of the collision of the charged particle with magnetic cloud moving with velocity V. From PROTHEROE (1998).

which can be rewritten as the fractional change in energy $(E_2 - E_1)/E_1$

$$\frac{\Delta E}{E} = \frac{1 - \beta\cos\theta_1 + \beta\cos\theta_2' - \beta^2\cos\theta_1\cos\theta_2'}{1-\beta^2} - 1. \tag{4.4}$$

Since the particle motion inside the cloud is random, all θ_2' have equal probability, resulting to

$$< \cos\theta_2' >= 0. \tag{4.5}$$

The average value of $\cos\beta_1$ depends on the rate at which cosmic rays collide with clouds at different angles. The rate of collision is proportional to the relative velocity between the cloud and the particle so that the probability per unit solid angle of having the collision at angle θ_1 is proportional to $(v - V\cos\beta_1)$ (PROTHEROE, 1998) and for ultrarelativistic particles ($v \simeq c$) thus leads to

$$< \cos\theta_1 >= -\frac{\beta}{3}. \tag{4.6}$$

Averaging Eq. 4.4 over angles, one can obtain that

$$\frac{\Delta E}{E_1} = \frac{1+\beta^2/3}{1-\beta^2} - 1 \approx \frac{4}{3}\beta^2. \tag{4.7}$$

since $\beta \ll 1$.

We see that $\frac{\Delta E}{E_1} \propto \beta^2$ is positive (energy gain), but is 2nd order in β and because $\beta \ll 1$ the average energy gain is very small. This is because there are almost as many overtaking collisions (energy lost) as there are headon collisions (energy gain).

4.2 First Order Fermi Acceleration

Fermi's original theory was modified[2] to describe more efficient acceleration (first order in β) taking place at supernova shocks, but is generally applicable to strong shocks in other astrophysical contexts.

[2]BELL (1978), BLANDFORD & OSTRIKER (1978)

Several solar masses of material are ejected during a supernova explosion at a speed of $\sim 10^4$ km/s, which is much faster than the speed of sound in the interstellar medium which is ~ 10 km/s. The strong wave propagates radially out with velocity $-u_1$. The shocked gas flows away from the shock with the velocity u_2 relative to the shock front, and $|u_2| < |u_1|$. Thus in the laboratory frame the gas behind the shock moves to the left with velocity $V = -u_1 + u_2$, which can be interpreted as the velocity of the shocked gas ("downstream") relative to the unshocked gas ("upstream"), see Fig. 4.2.

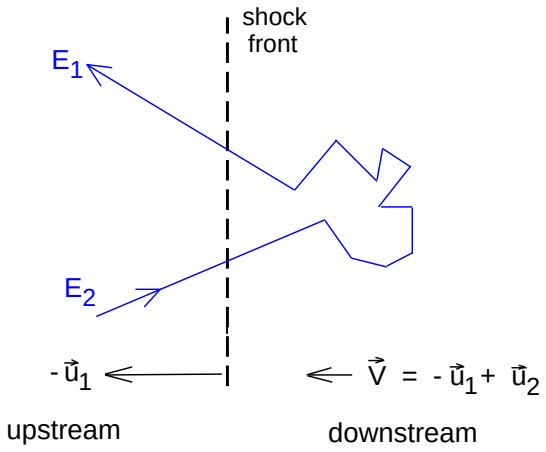

Figure 4.2: The interaction of cosmic ray of energy E_1 with the shock wave moving with speed $-u_1$ (GAISSER, 1990). The charged particle ahead of the shock front can pass through the shock and then be scattered by magnetic inhomogenities behind the shock. The encounter is one pair of in and out crossing the shock.

The crucial differences between both cases come when we take the angular averages to obtain the average fractional energy gain per encounter (GAISSER, 1990). For the planar shock

$$< \cos\theta_2' >= -\frac{2}{3} \tag{4.8}$$

and therefore

$$\frac{\Delta E}{E_1} = \frac{1 + 4\beta/3 + 4\beta^2/9}{1 - \beta^2} - 1 \approx \frac{4}{3}\beta. \tag{4.9}$$

Here $\beta = V/c \ll 1$ refers to the relative velocity of the plasma flow, not to the cosmic rays. The approximate forms of Eq. 4.9 and also Eq. 4.7 hold when the shock (cloud) velocities are non-relativistic.

The acceleration in this case is more efficient because the motions are not random. The geometry of the plane shock is such, that the encounter always result in the energy gain (because $\cos\theta_2'$ is always positive and $\cos\theta_1$ always negative).

This mechanism can be used with some modification for the relativistic shock wave (for example ELLISON ET AL. (1990) and ACHTERBERG (2000)).

4.3 Spectral index

The result of Fermi acceleration is the universal power-law spectrum of the accelerated particles. It can be written in differential form

$$\frac{dN(E)}{dE} \propto E^{-q}, \tag{4.10}$$

or in integral form

$$N \propto E^{-(q-1)}. \tag{4.11}$$

Here we define differential spectral index

$$q = \frac{R+2}{R-1}, \tag{4.12}$$

where

$$R = \frac{u_1}{u_2} \tag{4.13}$$

is the shock compression ratio, u_1 and u_2 being the upstream and downstream velocities of the fluid in the rest frame of the shock. For typical situation is $R < 4$ and hence $q > 2$ ($q = 2$ for the strong shocks).

The effectively continuous gain of energy can be characterized as

$$\frac{dE}{dt} = \frac{< \Delta E >}{t_{cycle}}, \tag{4.14}$$

where t_{cycle} is the time for one complete cycle (i.e. from crossing the shock from upstream to downstream, diffusing back towards the shock and crossing from downstream to upstream, and finally returning to the shock), and $< \Delta E >$ is the average energy gain per cycle.

The time of accelerating cycle t_{cycle} competes in Fermi process with mean escape time t_{esc}, i.e. possibility that the particle escapes from the cycle. The slope q of resulting power-law energy spectrum of the particle is related with these times by equation

$$q = 1 + \frac{t_{cycle}}{t_{esc}}. \tag{4.15}$$

Spectral shape for special cases as the finite acceleration volume and energy losses can be found, for example, in work Protheroe (1998). Spectral shape will be also changed by the influence of the propagation, the resulting value of the spectral shape will be bigger.

4.4 Acceleration in SNRs

An important task is to find the upper cut-off to the accelerated particle spectrum. Following the works Lagage & Cesarsky (1983) and Drury (2000) we adopt

the idea to calculate maximum particle particle momentum p_{max} by taking planar shock estimate for the mean acceleration rate

$$\dot{p} = \frac{p_{max}}{t_{cycle}}, \tag{4.16}$$

where

$$t_{cycle} = \frac{3}{u_1 - u_2}(L_1 + L_2) \tag{4.17}$$

giving the acceleration time scale t_{cycle} in terms of the upstream velocity into the shock, u_1, the downstream velocity away from the shock, u_2, and the mean penetration distances upstream and downstream of the accelerated particles, l_1 and L_2. Integrating over the evolution of the remnant

$$p_{max} = \int_0^{t_{max}} \dot{p} dt. \tag{4.18}$$

If one assumes that the diffusion of the particles can be characterized by a spatially constant diffusion coefficient κ_1 upstream and κ_2 downstream then

$$L_1 = \frac{\kappa_1}{u_1}, \quad L_2 = \frac{\kappa_2}{u_2} \tag{4.19}$$

giving the expression for the acceleration time scale

$$t_{cycle} = \frac{3}{u_1 - u_2}\left(\frac{\kappa_1}{u_1} + \frac{\kappa_2}{u_2}\right) = \frac{\kappa_1}{u_1^2}\frac{3R}{R-1}\left(1 + R\frac{\kappa_2}{\kappa_1}\right), \tag{4.20}$$

where $R = u_1/u_2$ is compression ratio of the shock. In general one excepts

$$1 < \frac{\kappa_1}{\kappa_2} < R \tag{4.21}$$

and $R \simeq 4$ so that the acceleration time scale can be simply

$$t_{cycle} = 10\frac{\kappa_1}{u_1^2}. \tag{4.22}$$

The problem is to estimate κ. It is usually parametrized by Bohm diffusion coefficient

$$\kappa_B = \frac{1}{3} r_g v = \frac{pv}{3ZeB} \tag{4.23}$$

which is formally diffusion coefficient corresponding to the mean free path equal to the gyroradius (v is particle speed, Z the charge in units of the electronic charge e and B the magnetic field strength). With the assumption that κ_B is the smallest possible value we get the estimate

$$t_{cycle} = \frac{10pv}{3ZeBu^2} \tag{4.24}$$

and hence

$$\dot{T} = v\dot{p} = 0.3ZeBu^2, \tag{4.25}$$

where T is particle kinetic energy and u is the shock velocity.

For simple models of expanding supernova remnants one obtain the energy cut-off

$$E_{max} = 0.3\, \rho_0^{-1/3}\, M_{ej}^{-1/6}\, E_{SN}^{1/2}\, B\, Ze \tag{4.26}$$

in the terms of explosion energy E_{SN}, ejecta mass M_{ej} and ambient density ρ_0 of supernovae explosion. For generally values of one solar mass ejecta, the explosion energy of 10^{44} J, the ambient medium of hydrogen number density 1 cm^{-3} and 3 μG magnetic field this leads to $(1 \div 6) \times 10^{14}\, Z$ eV. It is worth noting the very weak dependence on the ejecta mass, as well as the relatively weak dependence on ambient density and explosion energy. The strongest dependence is that on the magnetic field.

4.5 Direct acceleration

Particles may be accelerated directly by an extended electric field (arising in rapidly rotating magnetized conductors, such as neutron stars or supermassive objects). Such a mechanism has the advantage of being fast, but it suffers from the circumstance that the acceleration occurs in an environment of very high density, where energy loss exist. In addition, the complexity of such an analysis is daunting (Hillas, 1984): it is usually not obvious how to get a power-law spectrum to emerge.

If a rotating neutron star has a surface field $\sim 10^{12}$ G, a radius $r \sim 10$ km, and a rotational frequency $\omega/2\pi \sim 30$ s^{-1}, a circuit connected between pole and equator would see an electromagnetic field $\omega B r^2/c \sim 10^{18}$ V for a aligned or oblique dipole (Hillas, 1984).

In a case, when the magnetic field is strictly dipolar and when negligible binding of the charges in the solid surface is assumed, Scharlemann et al. (1978) obtained large acceleration at high altitudes, with electron energy $\Gamma_e m_e c^2$, with

$$\Gamma_e \approx 1.4 \times 10^5 \left(\frac{B_*}{10^{12}\,\mathrm{G}}\right) P^{-5/2} \left(\frac{\theta_c}{\theta_d}\right)^3 \left[\left(\frac{r}{R_*}\right)^{1/2} - 1\right] \left(\frac{\theta_*}{\theta_c}\right) \left(1 - \frac{\theta_*^2}{\theta_c^2}\right) |\cos\phi_*| \,. \tag{4.27}$$

Here θ_c is the opening angle of the polar field lines at the stellar surface, $\theta_d = (2\pi R_*/cP)^{1/2}$, R_* is the stellar radius, B_* is the magnetic field at the magnetic poles of the star, P is the stellar rotation period, and θ_* and ϕ_* are the magnetic colatitude[3] and the azimuth, respectively, where a field lines cuts the stellar surface.

4.6 Hillas condition

In any statistical acceleration mechanism and also direct acceleration scenarios (in which the electric field arises due to the moving magnetic field) there must be the magnetic field B to keep the particles confined within acceleration region.

[3]Colatitude is defined as follows: colatitude = 90° - latitude

Thus the size of acceleration region L containing the magnetic field, where the particle makes many irregular loops while gaining energy, must be much greater than $2r_g \sim 2\left(\frac{E}{10^{15}\,\mathrm{eV}}\right)\left(\frac{B}{\mu\mathrm{G}}\right)^{-1}$, where r_g is Larmor radius of the relativistic particle of charge Ze in the magnetic field B (strictly the component of magnetic field normal to the particle's velocity) and E is particle's energy. Including the effect of the characteristic velocity βc of scattering centers (it turns out that L has to be larger than $2r_g/\beta$) one gets the general condition (Hillas, 1984):

$$\left(\frac{B}{\mu\mathrm{G}}\right)\left(\frac{L}{\mathrm{pc}}\right) > 2\left(\frac{E}{10^{15}\,\mathrm{eV}}\right)\frac{1}{Z\beta}. \tag{4.28}$$

The dimensional argument expressed by Eq. (4.28) is often presented in the form of the Hillas diagram shown in Fig. 4.3, which shows that to achieve a given maximum energy, one must have acceleration sites that have either the large magnetic field or the large size of the acceleration region.

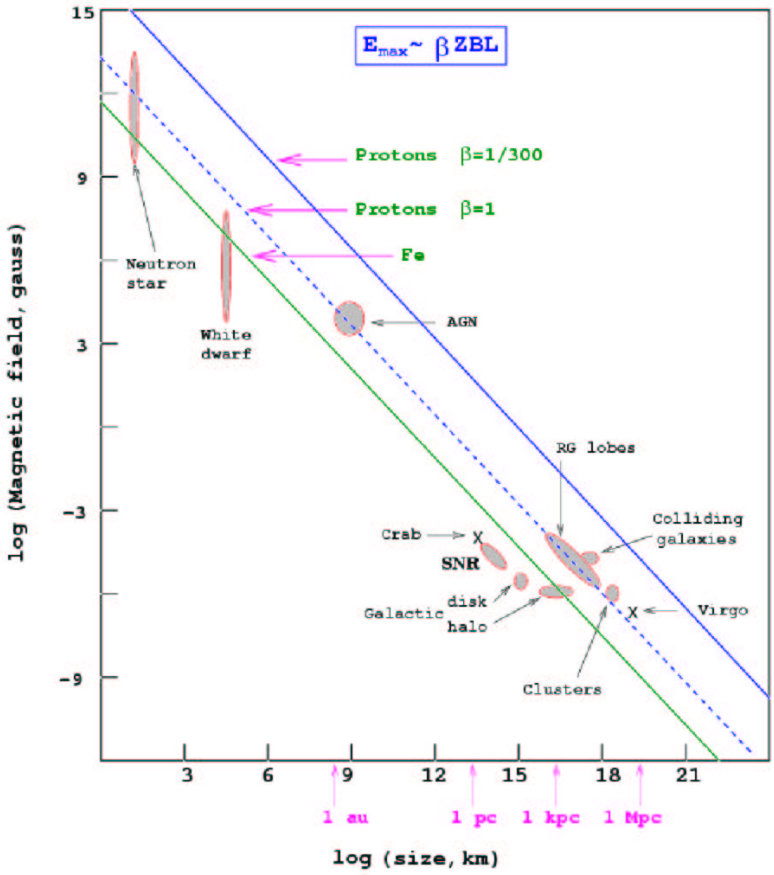

Figure 4.3: The Hillas diagram showing size and magnetic field strengths of possible sites of particle acceleration. Objects below the corresponding diagonal lines cannot accelerate protons (iron nuclei) to 10^{20} eV. βc is the characteristic velocity of the magnetic scattering centers. This picture was taken from Bhattacharjee & Sigl (1999).

Chapter 5

Galactic and extragalactic CRs

5.1 Origin of Galactic cosmic rays

While solar cosmic rays are identified by their association with solar flares or spatial association with interplanetary shocks, or by the compositional and spectral signatures of anomalous cosmic rays, the steady, nearly isotropic flux of high-energy particles comes from sources far outside the heliosphere (Gaisser, 2000). These sources still lack definitive identification. The fundamental difficulty is that diffusive propagation in the turbulent interstellar medium smooths out spatial and temporal variations that may characterize the sources.

It is generally believed that the bulk of CRs with energy below the knee are Galactic in origin and that their main production mechanism is acceleration by supernova shocks. It is known (from meteorite records) that the Galactic CR flux has been steady within a factor 2 for the past Gyr, the observed variations being compatible with solar activity changes and the motion of the Sun in the Galaxy (Dar&De Rújula, 2001). If the CRs are mainly of Galactic origin, their accelerators must compensate for the escape of CR from the Galaxy. The luminosity in CRs must therefore satisfy (Bhattacharjee & Sigl, 1999)

$$L_{CR} = \frac{4\pi}{c} \int \frac{Ej(E)}{\tau_{esc}(E)}\, dEdV, \tag{5.1}$$

where $\tau_{esc}(E)$ is the average time spent by CRs with energy E in the Galaxy. It can be estimated from the mean column density $X(E)$ of gas in the ISM that Galactic CR with energy E have traversed. Interaction of the primary CR particles with the gas in the Interstellar Matter (ISM) leads to production of various secondary species. From the secondary to primary abundances ratios of Galactic CR it were inferred that

$$X(E) = \rho_{gas}\tau_{esc}(E) \simeq 6.9 \left(\frac{E_9}{20Z}\right)^{-0.6} \text{g/cm}^2, \tag{5.2}$$

where ρ_{gas} is the average density of interstellar gas and Z is the mean charge number of the CR particles and $E_9 = E/(10^9 \text{ eV})$. The mean energy density u_{CR} of CR u_{CR} in the local interstellar medium and the total mass of gas in the Milky

Way that have been inferred from the diffuse Galactic gamma-ray, X-ray and radio emissions are (Bhattacharjee & Sigl, 1999)

$$u_{CR} = \frac{4\pi}{c} \int Ej(E)dE \simeq 1\,\mathrm{eV/cm^3} = 10^{-12}\,\mathrm{erg/cm^3} \tag{5.3}$$

and

$$M_{gas} \sim \rho_{gas} V \sim 4.8 \times 10^9 M_\odot, \tag{5.4}$$

respectively.

The median energy in the local ISM is about 6×10^9 eV, and more than 90% of the energy is carried by particles with $E < 5 \times 10^{10}$ eV. The average time for this energy is $\sim 10^{14}$ s. Then, simple integration yields

$$L_{CR} \sim M_{gas} \int \frac{Ej(E)}{X(E)}\bigg|_{6\times10^9\,\mathrm{eV}} = \frac{M_{gas}}{\rho_{gas}} \int \frac{Ej(E)}{\tau_{esc}}\bigg|_{6\times10^9\,\mathrm{eV}} \sim 10^{41}\,\mathrm{erg/s}. \tag{5.5}$$

This is about 10% of the estimated total power output in the form of kinetic energy of the ejected material in Galactic supernovae

$$L_{SNkinetic} \sim \frac{10^{51}\,\mathrm{erg}}{30\,\mathrm{yrs}} \sim 10^{42}\,\mathrm{erg/s}, \tag{5.6}$$

which, from the energetic point of view, could therefore account for most of the CR. This is one of the principal argument for supernova explosions as the source of CRs.

The characteristic time τ_{esc} is an effective parameter that emerges from a range of more relativistic models for diffusion and propagation of cosmic rays (Gaisser, 2000). In general τ_{esc} depends on energy. The relation between the source spectrum $Q_{sour}(E)$ and the observed spectrum is

$$\tau_{esc} Q_{sour}(E) \propto \frac{dN}{dE}\bigg|_{obs} \propto E^{-\alpha}. \tag{5.7}$$

The observed differential spectra index is $\alpha \approx 2.7$ for protons and primary nuclei such as carbon, oxygen, etc., with small differences among the various nuclei (Swordy et al. (1993) and Wiebel (1994)).

The energy dependence τ_{esc} can be measured by comparing the spectrum of a secondary nucleus to that of a parent primary nucleus. Primary nuclei are those accelerated in the sources. Secondary nuclei are those essentially absent in the source but which can be produced by spallation of primary nuclei of larger mass number. As a consequence, their spectral index at production is known. To the extent that spallation cross sections are approximately constant in energy, the spectral index at production for a secondary nucleus is the observed spectral index of its parent. Thus the analog of (5.7) for a secondary nucleus is

$$\tau_{esc} \frac{dN}{dE}\bigg|_{obs} \propto \frac{dN}{dE}\bigg|_{sec}. \tag{5.8}$$

The data on the secondary to primary ratio up to $2 - 5 \times 10^{10}$ eV may be fitted as a power law with the result

$$\tau_{esc} \propto E^{-\delta}, \tag{5.9}$$

with $\delta \sim 0.6$ (GARCIA-MUNOZ ET AL., 1987)[1]. The energy dependence of τ_{esc} must be taken into account in estimating the power requirement for cosmic rays. Since $\tau_{esc} \propto E^{-\delta}$, it follows from (5.7) that

$$Q_{sour}(E) \propto E^{-q} \tag{5.10}$$

with $q = \alpha - \delta \propto 2.1$. Thus the source spectrum is harder than the observed spectrum, and a more correct version of (5.3) is

$$P_{CR} = \frac{4\pi}{c} \int EQ(E)dE = \frac{4\pi}{c} \int E \left.\frac{dN}{dE}\right|_{obs} \frac{1}{\tau_{esc}(E)} dE. \tag{5.11}$$

This relation between observed flux and source power is true in general for other components of the cosmic radiation.

5.2 Acceleration of GCRs in supernova remnants

The implications of the shock acceleration process, assuming SNRs as the sources of the shocks, are as follows (AXFORD, 1994):

(i) The efficiency of energy transfer from the explosion energy to cosmic rays is in order to account for the power requirements of Galactic CRs on the basis of the observed properties and frequency of supernovae.

(ii) Shock-accelerated particles have a spectrum which is a power law in rigidity [2] with spectral index ~ 2 for strong shocks.

(iii) All species are treated in a roughly similar way so that the composition of the accelerated particles should, to a first approximation, reflect that of the ambient plasma. However, there can be variations as a consequence of the initial charge state of the plasma and the degree to which any nonthermal tail of the velocity distribution is affected by the charge state of the element.

(iv) The cosmic-ray source should mainly represent rather young material if the acceleration takes place mainly in the hot coronal component of the interstellar medium which originates from the debris of supernovae and intense stellar winds.

(v) As a consequence of the finite lifetime of the shock the cosmic-ray source spectrum produced in a SNR has a rigidity cutoff at $R \sim 10^{14}$ volts. This cutoff can be identified with the knee.

[1] See also page 38.

[2] Rigidity $R = \frac{pc}{Ze}$, [R]= 1 volt

(vi) CRs from SNR spend most of their life in the Galaxy outside their parent SNR and during this time produce secondaries by spallation. The ambient spectrum is steeper than that of the source since higher energy particles escape more readily from the Galaxy. This is reflected in the spectrum of the secondary component, the difference in spectral shapes providing a measure of the escape rate at each rigidity. One can deduce that, at least in the range $10^{10} - 10^{12}$ eV, the mean residence time varies approximately as $R^{-0.6}$ (SWORDY ET AL., 1990).

(vii) Reacceleration of cosmic rays following their escape from their source regions or their production as secondaries by spallation is always possible since there is a high probability of encountering other shocks. A power-law spectrum is not affected by interactions involving weak shocks but can be flattened by stronger shocks. Since the observed secondaries do not appear to have been affected in this way, this places a constraint on the probability of encountering additional shocks with strengths greater than ~ 2.5. This argument does not, however, excludes the shock-shock process described above since the secondaries are produced mainly outside the region concerned.

(viii) At lower rigidities, heavy primaries are lost by spallation rather than escape from the Galaxy. Since the spallation cross sections are energy independent to a first approximation, the spectrum in the region concerned tends to reflect the source spectrum and, in the case of Fe nuclei, is very close to expected spectrum for strong shock acceleration.

(ix) If SNR are sources of Galactic CRs it is easy to account for a lack of a significant anisotropy since the contributions from many nearby sources should overlap.

5.3 Two types of supernova explosions

A comparion of spectra of hydrogen and helium up to 10^{14} eV suggests that these two elements do not have the same spectrum of magnetic rigidity over this entire region[3] and that these two dominant elements therefore receive contributions from different sources. The basic premise of this theory (BIERMANN ET AL., 1995) is that galactic cosmic rays originate from two different sites: (1) supernova explosions into the interstellar medium[4], (2) supernova explosions of massive stars into their own stellar wind.

The supernovae of type Ia are likely explosions of white dwarfs, while the other supernova types are probably all from originally massive stars, above a zero-age main sequence mass of about 8 $M_\odot$. The supernovae of type Ia represent only 10% of all supernovae at present. The mass loss becomes important for zero-age main

[3]Heavy nuclei (including helium) have slopes flatter than the canonical 2.75 observed for protons up to 10^{12} eV (See Table (3.1)).

[4]BIERMANN ET AL. (1995) used phrase Sedov-type

sequence stars above 15 $M_\odot$. This mass loss arises in the form of strong winds, so we can identify the mass range above 15 $M_\odot$ with those supernova events that give rise to the wind component. The supernovae between 8 $M_\odot$ and 15 $M_\odot$ plus those of type Ia give the Sedov component.

The model accounts for the underabundance of hydrogen and helium relative to silicon at low energies. Hydrogen is underabundant because it comes from the Sedov-type explosions into the interstellar medium and silicon comes from wind explosions. Helium is underabundant because the winds of massive stars, i.e. blue and red supergiants as well as Wolf Rayet stars, are enriched in heavy elements. Biermann et al. (1995) use an escape probability with an energy dependence of $E^{-1/3}$. This theoretically motivated value is not in direct contradiction with the $E^{-0.6}$ energy dependence, derived from the measurements of the secondary-to-primary nuclei ratio in cosmic rays (Engelmann et al., 1990). The secondary-to-primary ratio measures the amount of matter traversed by cosmic rays, and could be strongly influenced by the matter distribution in galaxy and its temporal behavior.

5.4 Origin of the knee

Models explaining its origin can be divided into two distinct classes: astrophysical and interaction models. The astrophysical models attribute the change in the spectra of the observed extensive air shower (EAS) to the change in the energy spectra of the primary cosmic rays. The interaction models imply that the primary energy spectrum has no such sharp change and the observed steepening of EAS size spectra is due to the sudden change of the nature of the interactions between the high-energy particles of primary cosmic rays and the atmosphere. The astrophysical models are more numerous and developed. They might be also subdivided into two classes: the source models, with the change of the populations of the sources (Biermann et al. (1995) and Fichtel & Linsley (1986)) or their acceleration mechanisms, and the propagation models, with a change of the cosmic ray propagation between the source and the observer.

The basic idea of the latter class model, known as Galactic modulation or diffusion model, is that at low energies the particle gyroradius in the Galactic magnetic fields is small, their motion between the magnetic irregularities is like a slow diffusion and cosmic rays are trapped inside our Galaxy. However, Galactic magnetic fields are not strong enough to trap high-energy particles which begin to escape from the Galaxy (Ptuskin et al. , 1997). This rising leakage results in the steepening of the cosmic-ray energy spectrum (effectively an increase in δ). A problem for this interpretation is that the spectrum in the knee region may have more complicated structure than would be the case for a steepening of the rigidity spectrum of each elemental component of the cosmic radiation (see Figure 5.1).

Another problem is that simple extrapolation of $\tau_{esc}(E) \propto E^{-\delta}$ with $\delta \sim 0.6$ breaks down around 3×10^{15} eV since the effective escape length $c\tau_{esc} \sim 300$ pc at that energy (Gaisser, 2000). This corresponds to just one crossing of the

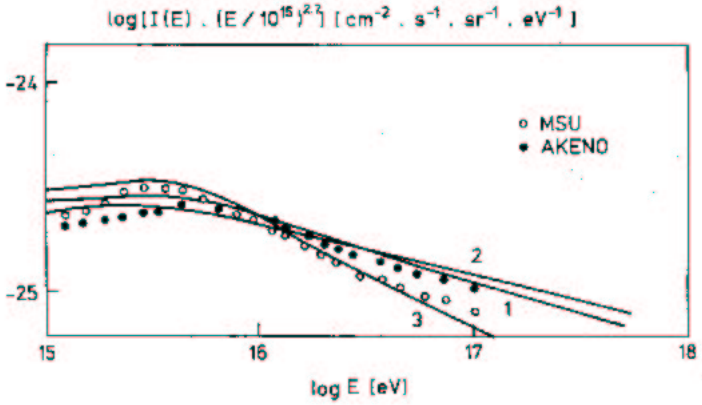

Figure 5.1: Cosmic ray spectra with mixed composition at the sources. The lines are results for different magnetic halo models (PTUSKIN ET AL. (1993)). Akeno and Moscow State University data are also shown.

disk and would tend to produce a large and increasing anisotropy approaching this energy. The measured anisotropy does increase around 10^{15} eV, but even at high energy the amplitude of the first harmonic is only a few percent (see Fig. 3.5).

The interaction models explore the fact that we still observe the knee indirectly, deep in the atmosphere, mostly by means of EAS. They argue that the slope of the EAS size spectrum steepens because interactions of high-energy particles suddenly change their character at the energy a few 10^{15} eV (NIKOLSKY, 1995).

ERLYKIN & WOLFENDALE (2000) discussed in detail the experimental study of the 10^{15} eV cosmic rays and its conclusion for proposed models. The spectra of all components have a sharp knee at the values corresponding to a primary energy of about 3×10^{15} eV. This is an important result because it does not leave room for the interaction models. If all the components of the shower show steepening of their spectra, then, in order to preserve the same slope of the primary spectrum in the wide energy range, it is necessary to assume that the primary particles transfer their energy into some unobservable component. The only known unobservable component which remains undetectable up to date is the neutrino. However, we know that the neutrino has only a weak interaction and is born in weak decays. The energy fraction carried away by it could not rise with the energy of the cascade, so neutrino cannot be the component which takes away the missing energy of the cascade. The alternative hypothesis is the production of a hypothetical heavy particle above a threshold energy $\sim 3 \times 10^{15}$ eV with a large and rising cross-section which escapes our detection due to exotic penetrating properties.

The primary mass composition in the knee region is still unknown, because the direct measurements do not reach yet the important 10^{15} eV region. All studies of the mass composition are indirect and based on the ratios between different shower components. The results of experiments are not definite as we can see in Fig. 3.9. There is also problem with the analysis, because of using the interaction models as was discussed in Section 2.1.

Erlykin & Wolfendale (1997) put forward a model in which the knee is formed by the explosion of just a single, nearby and recent supernova. The spectrum of cosmic rays from the shock caused by that explosion protrudes through the smooth background formed by many other sources (Figure 5.2). But there is still problem with identification of the source (Erlykin & Wolfendale, 2000).

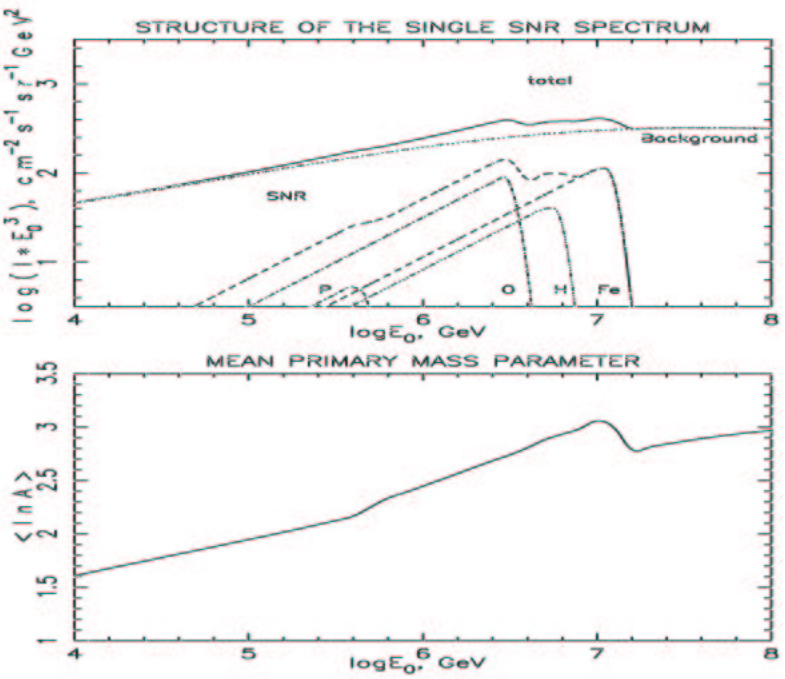

Figure 5.2: The Single Source Model of the primary energy spectrum. (a) Structure of the spectrum. SNR denotes the contribution from the single supernova and lines denotes as P, O, H, Fe - the contribution of the constituent spectra from protons, oxygen, heavy (Ne-S) and iron nuclei correspondingly. The background spectrum is assumed to be due to many (unspecified) sources. (b) Mean mass parameter in SSM, compare with Fig. 3.9. (from Erlykin & Wolfendale (2000)).

5.5 Beyond the knee

The origin of the cosmic ray particles with energies beyond the knee is still unknown. Protheroe & Szabo (1992) proposed that these cosmic ray particles have been originating in the extragalactic objects. However, cosmic rays in this energy regime may also be explained as of galactic origin, they may be produced due to the acceleration by a supernova shock racing through the stellar wind (Völk & Biermann (1988) and Biermann (1993)). Other theories put the origin of these particles in a galactic wind shock (Jokipii & Morfill, 1987), from reacceleration of existing energetic particles (Axford, 1994) and from neutron stars (Hillas, 1984).

A test would be an observation of the proton component only, since the extragalactic model predicts a large proton flux, while the galactic model requires a strong contribution of heavy nuclei. The galactic wind model would give normal, i.e. close to solar, abundances for these cosmic ray particles, as would be the reacceleration model except for the highest particle energies.

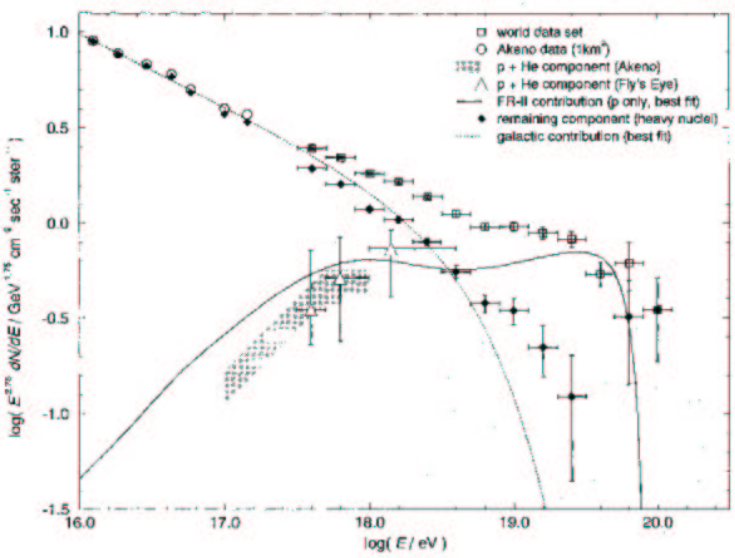

Figure 5.3: Data and model calculations for the different components of the EHE cosmic ray population observed near Earth (RACHEN ET AL., 1993). The best fit extragalactic proton composition is fitted to the Fly's Eye data for the proton/He component. The difference to the total cosmic ray spectrum gives an indication for the heavy nuclei contribution and can be fitted by an $E^{-3.1}$ spectrum with an exponential cutoff at 5×10^{18} eV.

5.6 Extragalactic cosmic rays

Since the Larmor radii of the particles with energy in 10^{18} eV region become larger than the thickness of the Galactic disk, it is likely that the origin of cosmic rays beyond several 10^{18} eV is extragalactic (AXFORD (1994) and RACHEN ET AL. (1993)). We can expect also that the extremely high-energy cosmic rays (EHECRs, cosmic rays above the ankle $E > 3 \times 10^{18}$ eV) are heavy nuclei. This suggestion is based on two simple arguments (NORMAN ET AL., 1995): the composition of shock-accelerated ions reflects the composition of the ambient medium, and the high-energy cutoff shock acceleration increases with the charge number, Z, of the nucleus. But the real situation remains still mysterious, because we have no clear experimental results.

Extremely high-energy cosmic rays show the flatter spectrum than cosmic rays just below the ankle. They have energies extending up to an observed maximum of $E_{max} = 3 \times 10^{20}$ eV (BIRD ET AL., 1995), and they are thought to be

predominantly protons[5] (Bird et al., 1994) and arrive from the directions without large scale anisotropy on the plane of the sky (Takeda et al., 1999). Since expected angular deflection by Galactic and extragalactic magnetic fields appears unable to alter the direction of such energetic particles by more than a few degrees (Sigl et al., 1994), this isotropy is thought to reflect the isotropic distribution of their sites of production.

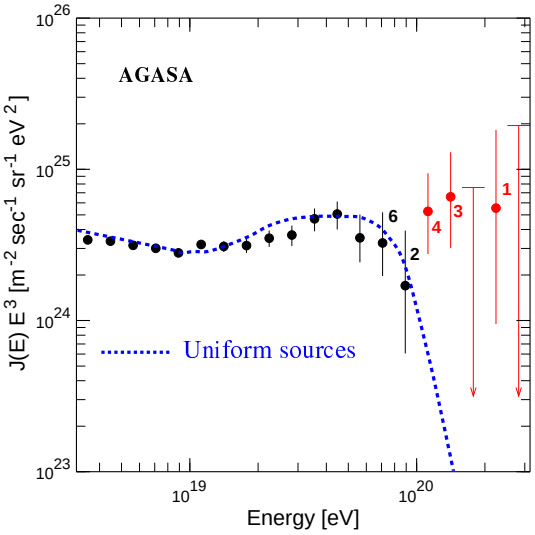

Figure 5.4: The energy spectrum observed with AGASA experiment (Hayashida et al., 2000). The vertical axis is multiplied by E^3. Numbers attached to points show the number of events in each energy bin. The dashed blue curve represents the spectrum expected for extragalactic sources distributed uniformly in the Universe.

5.7 Greisen-Zatsepin-Kuzmin cutoff

The interesting aspect of the extragalactic cosmic rays is that the highest energy particles are subject to the interactions with the omnipresent 2.7 K cosmic microwave background (CMB) radiation, which is a thermal relic of the Big Bang. This periodical energy losses cause the cutoff in the particle spectra of the distant extragalactic sources, known as the Greisen-Zatsepin-Kuzmin[6] (GZK) cutoff.

For a background photon of energy $\varepsilon \sim 10^{-3}$ eV in the cosmic rest frame (defined as the frame in which the CMB is isotropic), the threshold energy of

[5]While the analysis of the Fly's Eye group points to a likely change in mass composition from heavy to light at energies above 10^{18} eV, the Akeno analysis favors an unchanging composition. However, the two groups base their conclusions on simulations using quite different hadronic models. Dawson et al. (1998) presented a comparison of both experiments and argued that both measured a composition rich in iron around 10^{17} eV which becomes lighter at higher energies.

[6]Original theory was proposed independently by Greisen (1966) and Zatsepin & Kuzmin (1966) shortly after discovery the cosmic microwave background.

photo-pion productions ($N\gamma_b \rightarrow N(n\pi), n > 1$) for the nucleon is equal to (Bhattacharjee & Sigl, 1999):

$$E_{th} = \frac{m_\pi(m_N + m_\pi/2)}{\varepsilon} \simeq 6.8 \times 10^{16} \left(\frac{\varepsilon}{\mathrm{eV}}\right)^{-1} \mathrm{eV} \sim 6.8 \times 10^{19}\,\mathrm{eV}, \qquad (5.12)$$

where m_N (m_π) is the mass of the nucleon (pion).

Below this energy range, the dominant loss mechanism for protons is the production of electron-positron pairs on the CMB ($p\gamma_b \rightarrow pe^+e^-$), down to the corresponding threshold (Bhattacharjee & Sigl, 1999):

$$E_{th} = \frac{m_e(m_N + m_e)}{\varepsilon} \simeq 4.8 \times 10^{14} \left(\frac{\varepsilon}{\mathrm{eV}}\right)^{-1} \mathrm{eV} \sim 6.8 \times 10^{17}\,\mathrm{eV}. \qquad (5.13)$$

The next important loss mechanism which starts to dominate near and below the pair production threshold is redshifting due to the cosmic expansion. All other loss processes are negligible, possibly except in very dense regions of galaxies. Specifically, fewer than 20% of $10^{20.5}$ eV (10^{20} eV) protons can survive a trip of 18 Mpc (60 Mpc) (Stanev et al., 2000).

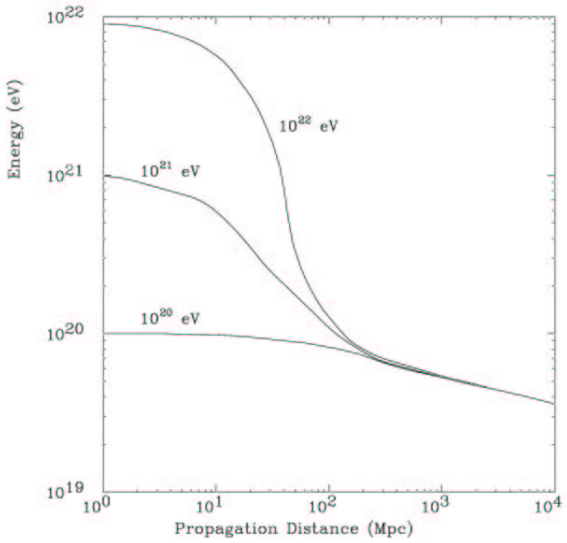

Figure 5.5: The energy of a proton as a function of the propagation distance through the 2.7 K cosmic microwave background for various initial energies. The energy loss is computed as due to the photo-pion production. From The Auger Collaboration (1997).

The β-decay ($n \rightarrow pe^-\bar{\nu}_e$) is the dominant loss process for neutrons with the range of the propagation (Bhattacharjee & Sigl, 1999):

$$R_n = \tau_n \frac{E}{m_n} \simeq 0.9 \left(\frac{E}{10^{20}\mathrm{eV}}\right) \mathrm{Mpc}, \qquad (5.14)$$

where the laboratory lifetime is $\tau_n \simeq 889$ s, m_n the neutron mass and E the neutron energy.

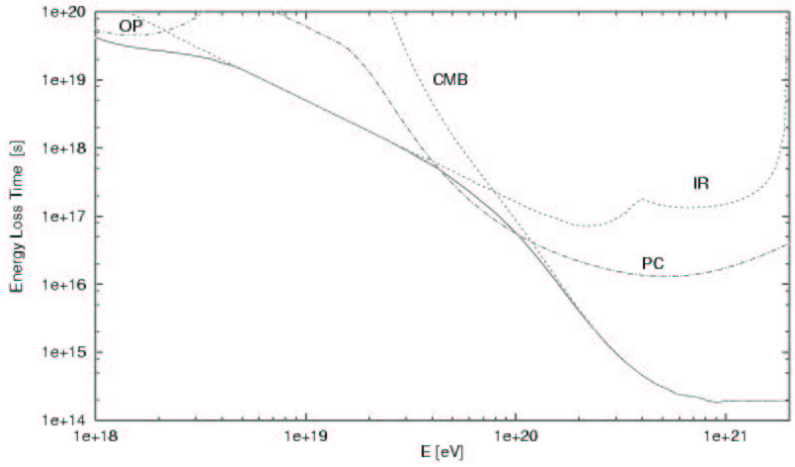

Figure 5.6: The effective energy loss time for Fe photodisintegration off microwave (CMB), infrared (IR) and optical (OP) photons, as well as the total one (solid line) and the pair creation (PC) energy loss time. From EPELE & ROULET (1998).

The dominant loss process for nuclei of energy $E \geq 10^{19}$ eV is the photodisintegration in the CMB and IR background. Apart from disintegration, nuclei are subject to the same loss processes as nucleons, where the respective threshold is given by substituting m_N by the mass of nucleus in the equations 5.12 and 5.13.

As in the case of the EHE nucleons and nuclei, the propagation of photons (and electrons/positrons) in this energy range is also governed by their interaction with CMB. The dominant interaction processes are the absorption of EHE photons due to pair-production, and inverse Compton scattering of the electrons/positrons on the background photons. Contrary to this the propagation of EHE neutrinos is governed mainly by their interaction with the relic neutrino background (with expected temperature T_ν=1.9 K at this time).

HILLAS (1968) has demonstrated the influence of the cosmological evolution on the GZK effect. For very distant sources the GZK cutoff appears at much lower energy, because of the higher density and temperature[7] of the CMB at earlier epochs.

Because the measured data do not confirm such cutoff (see Fig. 5.4), the astrophysical origin would require the sources within about 100 Mpc (see Fig. 5.5), but at the same time there is Hillas restriction on accelerators (Fig. 4.3), which excludes many objects as possible acceleration sites for cosmic ray up to energies above the GZK cutoff. The only way to avoid this conclusion without invoking an as yet unknown new physics is that the charged particles accelerated in sources at much larger distances give rise to the secondary neutrino beam that can propagate unattenuated.

[7]The density and temperature of CMB for redshift z are $\rho_\gamma(z) = \rho_{\gamma z=0}(1+z)^4$ and $T_\gamma(z) = T_{\gamma z=0}(1+z)$.

Chapter 6

Possible sources

6.1 Supernova remnants

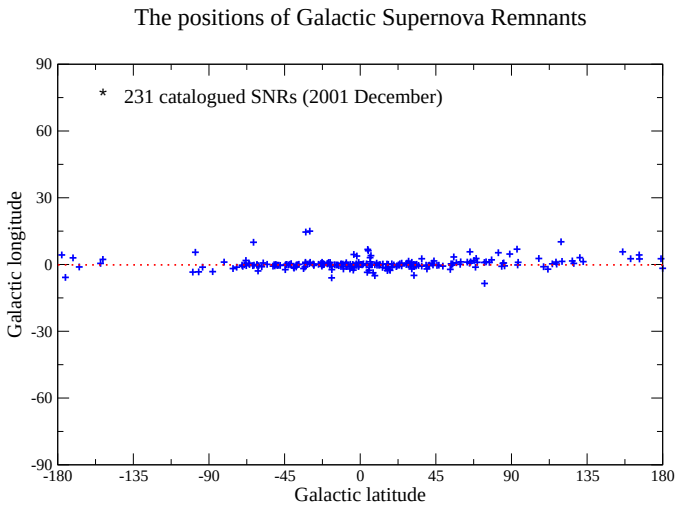

Figure 6.1: The positions of Galactic Supernova Remnants located by radio, UV, optical, infra-red or X-ray observations (GREEN, 2001). The dotted red line designates the Galactic equator.

In Chapter 5 we saw that there are some conditions to be satisfied by the theory of the origin of Galactic cosmic rays based on the shock acceleration in supernova remnants (SNRs). If supernova remnants are the sources capable of accelerating particles to $\sim 10^{15}$ eV or higher, then they should be also point sources of gamma-rays produced by interactions of the accelerated particles in or near the source (DRURY ET AL., 1994). The intensity depends, however, on the degree of mixing between the high energy particles and ambient material. Five sources are shown by ESPOSITO ET AL. (1996) to be coincident with SNRs in gamma-ray emission detected by the EGRET instrument. Theoretical estimates of the

gamma-ray luminosity of SNRs caused by the π^0-decay (Dorfi, 1991) have led to the conclusion that the expected TeV gamma-ray flux from nearby SNRs in high enough ambient densities should be just detectable by present instruments, but they have not to been detected by the TeV air Čerenkov telescopes (Gaisser, 2000).

There are several possibilities for explaining the absence of TeV gamma-rays at the level expected by using a hard spectrum to extrapolate the GeV observations of EGRET. It is possible (Gaisser et al., 1998) that the spectrum of accelerated particles in the source is significantly steeper than ~ 2.4, in which case the extrapolation to TeV of the fits in GeV range data can be consistent with the upper bounds from air Čerenkov telescopes. Alternatively, the observed photons in these sources may not to be associated with acceleration of cosmic rays or the maximum energy may be low in these particular remnants (Gaisser, 2000).

TeV gamma-rays have now been detected from the supernova remnants SN1006 (Tanimori et al., 1998) and Cassiopeia A (Aharonian et al., 2000).

6.2 Neutron stars

Blasi et al. (2000) find that neutron stars whose initial spin periods are shorter than ~ 10 ms and whose surface magnetic fields are in the $10^{12} - 10^{14}$ G range can accelerate iron from the surface of newborn neutron stars to EHE by a relativistic MHD wind. The typical energy was estimated as

$$E_{cr} \simeq 4 \times 10^{20} Z_{26} B_{13} \Omega_{3k}^2 \text{ eV}, \tag{6.1}$$

where $Z_{26} = Z/26$ the proton number, $B_s = 10^{13} B_{13}$ G the surface field $\Omega_{3k} = \Omega/3000$ rad s^{-1} the spin rate. The young neutron star is usually surrounded by the remnant of the presupernova star, the conditions when the column density of the envelope becomes transparent to EHE iron nuclei (≤ 100 g/cm^3) are shown in the Fig. 6.2. For plausible models of the Galactic and halo magnetic field, the Larmor radius of these EHECRs is less than the typical distance to a young neutron star. Therefore, the arrival direction distribution is approximately isotropic with a slight correlation with the Galactic center and disk.

de Gouveia Dal Pino & Lazarian (2000) and de Gouveia Dal Pino & Lazarian (2001) have pointed out that cosmic ray events above the GZK cutoff are mostly protons accelerated in the reconnection[1] site just above the magnetosphere of newborn pulsars Fig. 6.3. Pulsars with surface magnetic fields $10^{12}\,\text{G} < B_s \leq 10^{15}$ G and spin periods 1 ms $\leq P_s < 60$ ms are able to accelerate particles to energies above 10^{20} eV, the limit was summarized by the condition

$$B_s \geq 10^{13}\text{G} \left(\frac{P_s}{2.5\,\text{ms}} \right)^{4/3}. \tag{6.2}$$

[1]See in Section 6.7.

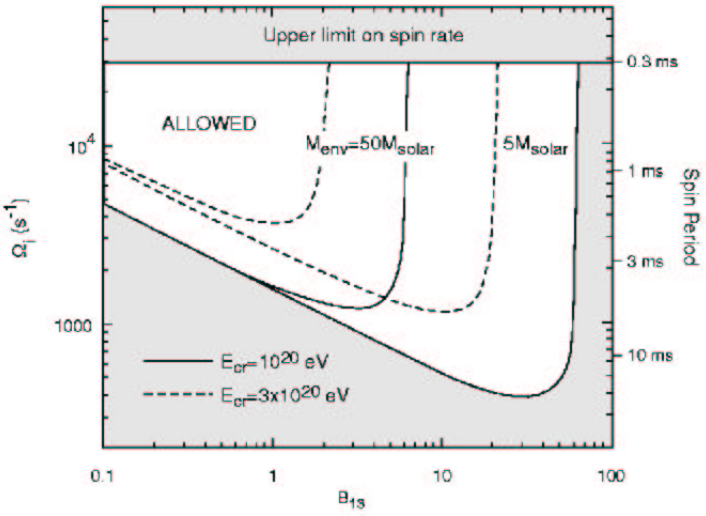

Figure 6.2: The parameter space for which acceleration and escape of the accelerated particles through the ejecta are allowed. The solid lines refer to particle energy $E_{cr} = 10^{20}$ eV and dashed lines to $E_{cr} = 3 \times 10^{20}$ eV for two values of the envelope mass. The horizontal line at spin period ~ 0.3 ms indicates the minimum period (maximum angular speed) allowed by neutron stars. From (Blasi et al., 2000).

The expected rate of suitable sources in our Galaxy is very small and the total flux is given by the integrated contribution from other galaxies within the volume that is unaffected by the GZK cutoff.

6.3 Radio galaxies

Since the hot spots[2] in Fanaroff-Riley class II (FR-II) radio galaxies are believed to be the largest and most powerful shock waves in the universe, it is natural to consider them as sources of high energy cosmic rays (Rachen & Biermann, 1993). The hot spots in FR-II galaxies are not expected to be the only extragalactic objects that can be accelerate particles to ultra-high energies. The reason for the restriction to the rare class of FR-II galaxies is, that highly energetic charged particles produced deeply inside galactic structures will suffer substantial adiabatic losses on their way out to the extragalactic medium. It is not the case of FR-II hot spots, because they are located at the edge of the extended radio lobe of the galaxy and the particles can immediately enter the extragalactic space.

It has been shown that the radio-to-optical spectra emitted by those hot spots can readily be explained as synchrotron radiation from particles accelerated at a strong shock wave by the first order Fermi mechanism (Meisenheimer et al., 1989). Obviously, the synchrotron emission of the relativistic particles is nothing else but the radio-to-optical spectra observed from the hot spots. For a power law

[2]The hot spots in strongly extended radio galaxies are identified as the endpoints of powerful jets ejected by the active nuclei of the galaxies deep into the extragalactic medium

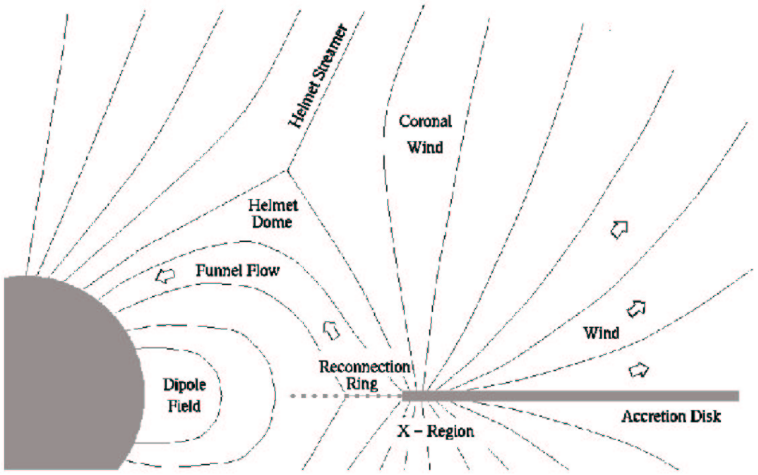

Figure 6.3: Two surfaces of null poloidal field lines, labeled as "helmet streamer" and "reconnection ring", are required to mediate the geometry of star's dipole-like with those opened by the wind and those trapped by the funnel flow emanating from R_x region (inner boundary of the accretion disk, where the equatorial flow divert into funnel inflow along the closed lines toward the star and centrifugally driven wind outflow). Across each null surface, the poloidal field suffers a sharp reversal of direction. Dissipation of the large electric currents that develop along the null surfaces will lead to reconnection of the oppositely directed field lines. From DE GOUVEIA DAL PINO & LAZARIAN (2000).

particle spectrum the synchrotron emission spectrum is also described by a power law with a spectral index $\alpha_s = (\alpha_p - 1)/2$. In five out of six observed hot spots, MEISENHEIMER ET AL. (1989) found radio spectral indices as $\alpha_s \simeq 0.5$ within the error estimates, which leads to $\alpha_p \simeq 2.0$ in agreement with the predictions of the first order Fermi acceleration at strong, non- or mildly relativistic parallel shock waves in a nonrelativistic gas. The only exception, Pictor A west, shows $\alpha_s \simeq 0.39$ and therefore requires flatter particle spectra ($\alpha_s \simeq 1.78$). MEISENHEIMER ET AL. (1989) found sub-mili-Gauss magnetic field strengths ($0.20 - 0.54$ mG) in the spot region.

The shock, which produces the acceleration, is due to the violent interaction of a jet emanating from an active nucleus with the medium in intergalactic space, and thus is expected to have chemical abundances between those typical for the inner parts of big elliptical galaxies (normal abundances, with heavy elements enriched by a factor up to 3 over solar) and those typical for intercluster gas (heavy element enrichment weakened to 1/3 solar) as has been pointed by RACHEN ET AL. (1993). This means, that protons dominate, and helium is of order 10% in number density relative to hydrogen; the elements carbon, nitrogen, oxygen, to iron should be between a maximum of 3 times solar, and negligible. Obviously, the propagation of nuclei heavier than hydrogen in the intergalactic space can lead to the spallation by photonuclear interactions with both the infrared and the microwave background, and thus lower the observed abundances of these nuclei.

We see in Fig. 6.5, which shows total contribution of three prominent FR-II

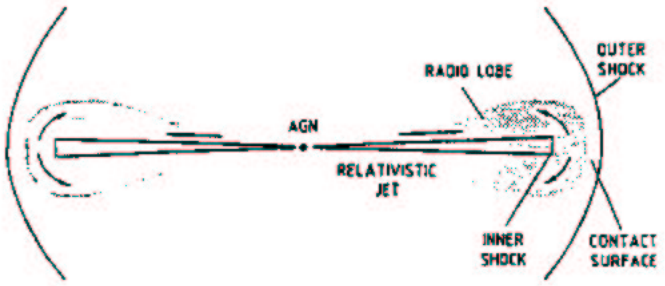

Figure 6.4: A schematic representation of an extended radio jet system showing the system of shock waves and contact surfaces. It is presumed that acceleration of particles possibly to 10^{20} eV takes place at the inner shocks and that the most intense radio-emitting regions are in the vicinity of the contact surfaces (AXFORD, 1994).

galaxies in our neighborhood, that Pic A is expected to produce the main part of all observed CR particles at about 8×10^{19} eV. But this is strongly connected to its flatter particle spectrum. If the power law index of Pic A is really as flat as was deduced from the synchrotron spectrum, can we expect that the cosmic ray events at this energy are peaked at about the position of Pic A? In the case of nano-Gauss extragalactic fields, most particles from Pic A with energies above 3×10^{19} eV will reach us from within one steradian about the position of the source (RACHEN & BIERMANN, 1993). Hence, if Pic A is really the dominant source of particles of highest energies, there should be an anisotropy connected with its position, which was not observed.

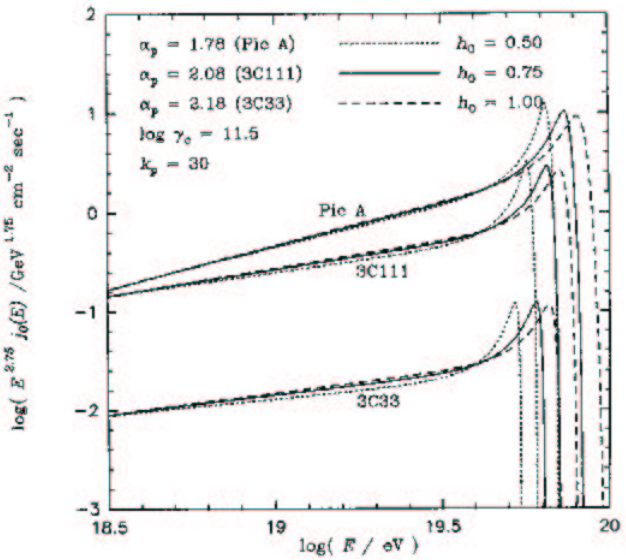

Figure 6.5: The total flux of the nearby FR-II galaxies, the spectral indices are deduced from their synchrotron spectra. From RACHEN & BIERMANN (1993).

6.4 Active Galactic Nuclei and Quasars

PROTHEROE & SZABO (1992) adopt a model in which protons are accelerated by first-order Fermi acceleration at a shock in an accretion flow onto a **supermassive black hole**. The main problem of such acceleration scenario is the lack of knowledge about the key parameters involved, such as magnetic field strength, plasma density, velocity and the configuration of the region around the black hole (AXFORD, 1994).

A reasonable limit on the **maximum energy as a function of the luminosity** for particles accelerated by Fermi's mechanism in AGNs can be calculated as follows (from NORMAN ET AL. (1995)). Assuming equipartition between the energy density in radiation and the magnetic field density in a source of radius R and with luminosity L implies

$$\frac{L}{4\pi R^2 c} = \frac{B^2}{8\pi}. \tag{6.3}$$

The maximum energy achievable due to Fermi's acceleration in a shock with velocity $V_s = \beta_s c$ and size R_s is

$$E_{max} \sim Ze\beta_s B R_s. \tag{6.4}$$

Assuming $R_s \simeq R$, this can be reformulated using equations above as

$$E_{max} = Ze\beta_s \left(\frac{2L}{c}\right)^{1/2}, \tag{6.5}$$

which gives

$$E_{max} = 2.5 \times 10^{19} \beta_{-1} Z L_{46}^{1/2} \text{ eV}, \tag{6.6}$$

with $L_{46} = L/10^{46}$ erg/s and $\beta_{-1} = \beta_s/0.1$.

If one interprets the proton-dominated component from $10^{18.5}$ to $10^{19.5}$ eV in the Fly's Eye data (BIRD ET AL., 1993) as coming from AGNs, then only fast shocks in luminous AGNs, with L$\geq 10^{44} - 10^{46}$ erg/s and $\beta_s \geq 0.1$, can account for this component. In the hard photon spectra associated with AGNs, escaping hadrons are degraded by photo-pion production. NORMAN ET AL. (1995) showed that neutrons above $10^{15} - 10^{16}$ eV cannot escape from the central region of AGNs due to photo-pion production and proton does not escape unless the source luminosities are lower than 10^{46} erg/s.

The maximum energy to which cosmic rays can be accelerated in the absence of losses is given by equation 6.4. Close to the black hole powering AGNs, losses can limit the maximum energy to a much lower value. The effect of losses near the black hole effectively rules out the acceleration of EHECRs in AGN (NORMAN ET AL., 1995). There can be possibility, as was investigated by PROTHEROE & SZABO (1992), that protons escape via spinflip from the centers of AGN. The idea is that these particles make a transition to a neutron in a proton-photon collision, and then escape unbound by magnetic fields. Finally outside the parent galaxy, these neutrinos decay back to the proton. As a consequence, this theory predicts that the

cosmic rays beyond the knee should be mostly protons. This work was intended to account only for cosmic particles with energies less than 10^{19} eV.

A quite different approach has been made by HASWELL ET AL. (1992) who have considered acceleration as a result of **magnetic reconnection**[3] in the accretion disk surrounding the nucleus (Fig. 6.6). In this way some of above objections are avoided.

Since the magnetic field is continually strengthened by being wound up as a result of the nonuniform rotation of the plasma in the disk, it is inevitable that reconnection and flaring must occur. The particle can achieve the maximum energy in a flare which is given by (HASWELL ET AL., 1992)

$$E_{max} \sim 3 \left(\frac{M}{M_\odot}\right) \left(\frac{n}{10^{16}}\right)^{1/2} \text{TeV}. \tag{6.7}$$

If we consider the case of a disk of density $n \sim 10^{16}$ cm^{-3} around a 10^8 M$_\odot$ black hole, we find that particles may be accelerated to $\sim 10^{21}$ eV. In the stellar case ($n \sim 10^{16}$ cm^{-3}, 10 M$_\odot$) the maximum energy is 4×10^{14} eV. HASWELL ET AL. (1992) showed that the electric fields involved in the flare are short-lived ($\sim$ 44 s) but enormous ($\sim 6 \times 10^6$ V/cm^2), which enables acceleration to occur in rather dense medium ($n \sim 10^{16}$ cm^{-3}).

The mechanism for the production of ultrarelativistic cosmic rays with energies greater than 10^{17} eV due to particle acceleration from AGN is consistent with some observed features: the extragalactic origin, apparent isotropy due to the many extragalactic AGN sources available in space and this mechanism can produce the energies well in excess of the GZK cutoff. Many questions in HASWELL ET AL. (1992) model are left open. The mechanism produces sporadic bursts of the emission of charged high-energy particles rather than a continuous stream of them so the theory says nothing about the spectrum of the accelerated particles. In addition there is not a complete solution for the topology of disk/boundary region magnetic field including turbulence and 3-dim behavior.

BOLDT & GLOSH (1999) have suggested that EHECR particles may be accelerated near the event horizons of spinning supermassive black holes associated with presently **inactive quasar remnants**. The required electromotive force is generated by the black hole induced rotation of externally supplied magnetic field lines threading the horizon. This suggestion avoids the problem of the lack of currently AGN and quasars within acceptable distances ($\leq$ 50 Mpc) to serve as possible sources of EHECR events. BOLDT & GLOSH (1999) estimate the number of supermassive black holes of required $\geq 10^9$ M$_\odot$ associated with dead quasars within a volume of radius $\sim$ 50 Mpc to be sufficient to explain the observed EHECR flux.

Several arguments support the possibility, that AGNs and radio galaxies could be the main contributors to extragalactic CR. First, at least two BL Lacertae[4]

[3]Once the magnetic field strength becomes strong enough to compress the disk plasma sufficiently that regions of reversed magnetic field are brought into contact, then reconnection will occur. Detailed discussion in Section 6.7.

[4]This type of quasar has many extreme properties: They are highly variable in radio, optical

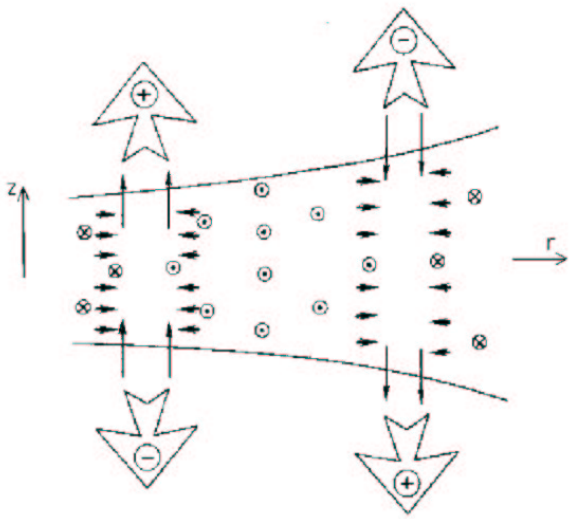

Figure 6.6: The picture illustrates the magnetic collapse process explored in HASWELL ET AL. (1992). The magnetic field direction is indicated with the standard symbols. The small, dark arrows show the direction of the bulk magnetohydrodynamic (MHD) fluid flow; the long thin arrows show the electric field vectors, and the larger, unfilled arrows indicate the direction of ejection of charged particles which decouple from MHD flow.

objects have been observed in gamma-rays above $\simeq 10^{13}$ eV, namely Markarian 421 (ZWEERINK ET AL., 1997) and Markarian 501 (AHARONIAN ET AL., 1997). Photons of such high energies may be produced by the decay of pions produced in interactions of the accelerated protons with the ambient matter in these sources (MANNHEIM, 1993) rather than by inverse Compton scattering of low-energy photons by accelerated electrons in these sources (BHATTACHARJEE & SIGL, 1999). Second, the energy content in the diffuse gamma-ray background is comparable to the one required for an extragalactic proton injection spectrum proportional to E^{-2} up to 10^{20} eV if it is to explain the observed cosmic rays spectrum above the ankle. This is expected if the diffuse photons again result from the decay of pions produced by the accelerated protons and the subsequent propagation of these photons (MANNHEIM, 1998).

Numerical simulations presented by ISOLA ET AL. (2001) showed that Centaurus A (the nearest radio galaxy, type FR-I at a distance 3.4 Mpc) can not be the only one source of all observed data.

6.5 Other astrophysical sources

ANCHORDOQUI ET AL. (2001) examine the hypothesis that the highest energy particles are the heavy nuclei from the nearby metally rich **starburst galaxies**

and X-ray spectral regions. No broad optical emission-lines. Optical polarization can be strong and variable. BL Lac objects appear to be associated with elliptical galaxies.

(M82 and NGC 253) and can produce all the events observed above ankle, if a two-step process is involved. The crucial point is that acceleration occurs in the terminal shock of the starburst superwind for energies above 10^{15} eV, well outside the problematic central region. Below 10^{19} eV, the distribution of the CR arrival directions is expected to be completely isotropic of Kolmogorov diffusion in ordered extragalactic magnetic fields $10 < B[\mathrm{nG}] < 15$. Within this model almost all CRs above GZK energy would be rather heavy nuclei. In addition, the model predicts a slight anisotropy above $10^{20.4}$ eV produced by non-diffuse iron debris.

Based on the assumption, that the galaxy distribution in the Universe and the matter distribution in numerically simulated universe show sheet-like and filamentary structures (Fig. 6.7), KANG ET AL. (1997) and KANG ET AL. (1996) have computed the contribution of the expected particle flux from the accretion shocks formed by the infalling flows toward **clusters of galaxies**. Their calculations show that the expected spectrum of high energy protons could match the observed cosmic ray spectrum up to GZK cutoff energy near 6×10^{19} eV. Concerning the events above 10^{20} eV, the model gives an explanation of the highest energy events detected by the Haverah Park at high northern galactic latitudes, since the Virgo and coma clusters are in that direction. Some aspects of this model need further consideration: whether one can prove observationally the existence of large-scale shocks, questions arise about the general and turbulent nature of the large-scale magnetic field and so on.

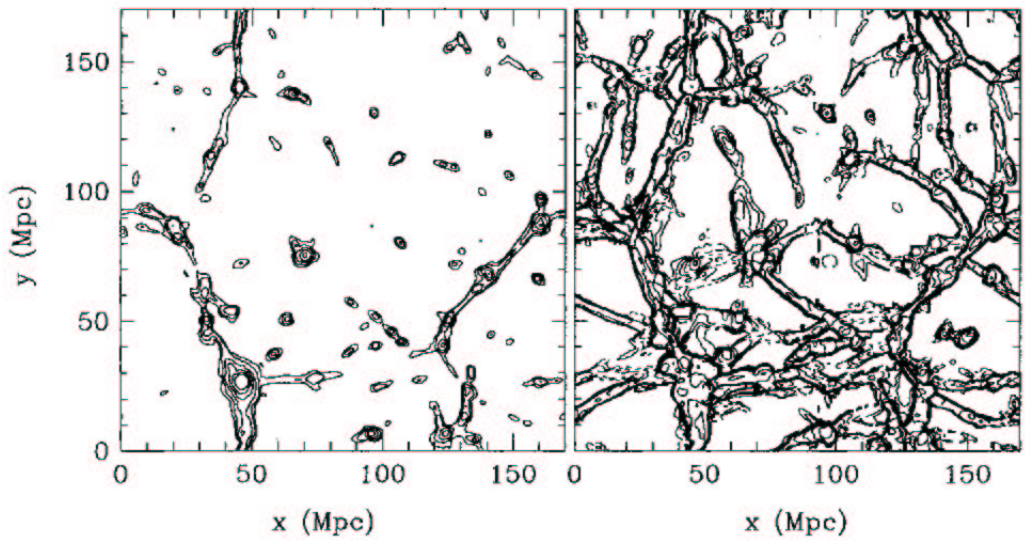

Figure 6.7: A representative slice cut of a simulated universe in a standard cold dark matter model. The left panel shows the X-ray luminosity distribution while the right panel shows the gas temperature distribution. The shocks can be seen clearly as strong gradients in the temperature distribution. From KANG ET AL. (1997).

6.6 Gamma ray bursts

Cosmological gamma ray bursts (GRBs) most likely contribute to a negligible fraction to the CR flux below the knee (Shemi & Piran, 1990), as compared to SNRs, the favorite CR source below this energy range.

On the contrary, in the EHE range the average rate of energy emission required to explain the observed flux is comparable to the average rate of energy emitted by GRBs in gamma-rays within the GZK radius (Vietri, 1995). In addition, the predicted spectrum seems to be consistent with the observed spectrum above 10^{19} eV for proton injection spectra $\propto E^{-2.3\pm0.5}$ (Waxman, 1995a), typical for the Fermi acceleration mechanism which is supposed to operate in dissipative wind models of GRBs.

Vietri (1995) noted that the isotropy of the EHECRs could be explained through the first-order Fermi acceleration by a relativistic blast wave with Lorentz factor Γ. At each shock crossing, a particle would increase its energy by a factor $\sim 4\Gamma^2 \sim 4 \times 10^5(\Gamma/300)^2$, so that only a few such cycles would suffice to produce EHECRs starting from low-energy particles. The efficiency to accelerate low-energy particles to extremely-high energies through relativistic shock acceleration has been shown to be infeasible (Gallant et al., 1999). They have distinguished between the initial shock crossing cycle, in which the particles can gain a large factor in energy, and subsequent crossing cycles, where the energy typically only doubles. Second-order Fermi acceleration, for example due to magnetohydrodynamic turbulence generated by charged dust or irregularities in the external medium or by first-order Fermi acceleration involving alleged shocks in a relativistic wind (Waxman, 1995b), could, however, accelerate EHECRs in GRB blast waves. So, we can summarize that that theoretical problems with accelerating particles to extremely high energies still remain.

The condition on the blast wave parameters that are required to accelerate protons to energies E beyond 10^{20} eV is (Bhattacharjee & Sigl, 1999):

$$\Gamma \geq 40 \left(\frac{E}{10^{20}\,\mathrm{eV}}\right)^{3/4} \left(\frac{t_{GRB}}{\mathrm{s}}\right)^{-1/4}, \tag{6.8}$$

where Γ is Lorentz factor of the blast wave and t_{GRB} is the timescale variability of the GRB.

As seen in Figure 6.8, the flux above 5×10^{19} eV is dominated by sources at distances greater than 100 Mpc and is therefore not expected to be sensitive to inhomogenities distribution of cosmological sources, i.e. no anisotropy related to large-scale source clustering is expected in the angular distribution of cosmic-ray events with energies up to $\sim 5 \times 10^{19}$ eV. The flux above 10^{20} eV is dominated by sources at distances less than 30 Mpc and is therefore likely to be sensitive to source inhomogenities (Waxman, 1995a).

Scully & Piran (2001) have shown that, if GRBs density distribution follows the star formation rate, the photo-meson production energy losses suffered by extremely high energy CRs coming from GRBs would produce too sharp cutoff of the energy spectra to be consistent with the air shower data. Furthermore, they

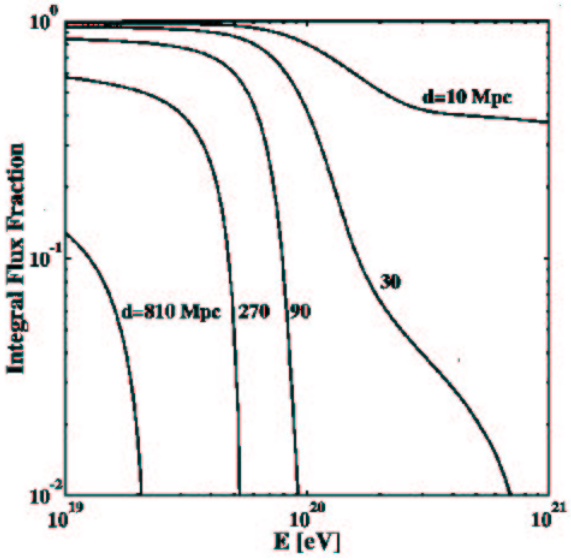

Figure 6.8: The fraction of the integral flux contributed by sources more distant than d, as was presented by Waxman (1995a).

show that cosmological GRBs fail to supply the energy input required to account the cosmic ray flux above 10^{19} eV by two or three orders of magnitude, contradicting the hypothesis advocated in Waxman (1995a).

The main energy losses in the GRB scenario are synchrotron radiation and pion production (Waxman & Bahcall, 1997). Both processes give rise to secondaries, they are photons in the synchrotron radiation, and photons with neutrinos from pion decays. The correlation of a fraction of all EHE neutrinos with GRBs would be a strong test of the GRB scenario of EHECR origin.

The synchrotron emission associated with proton acceleration to EHE in the cosmological GRBs has been found to carry away a fraction of about a percent of the total burst energy. At energies around 10 MeV, above a few hundred GeV and in the TeV range the experiments (proposed satellites and ground based air Čerenkov telescopes) should be sensitive enough to detect this particle's flux (Bhattacharjee & Sigl, 1999).

Since the EHECR's speed v_{CR} differs from c by a slight amount

$$v_{CR} = c\,\sqrt{1 - 1/\gamma_{CR}} \quad , \tag{6.9}$$

where $\gamma_{CR} \geq 10^9$, EHECR's should trail gamma-ray photons from GRBs by less than 10^{-3} s, even if they arrive from about 100 Mpc away. They should lead to the expectation that every time we see an EHECR, gamma-ray satellites should observe a GRB. However, EHECRs are bent along their path by the intergalactic magnetic field by approximately 10° (Sigl et al., 1994), leading to a path longer by $\simeq 10^{15}$ s (Vietri, 1995), thus washing away any correlation with GRBs.

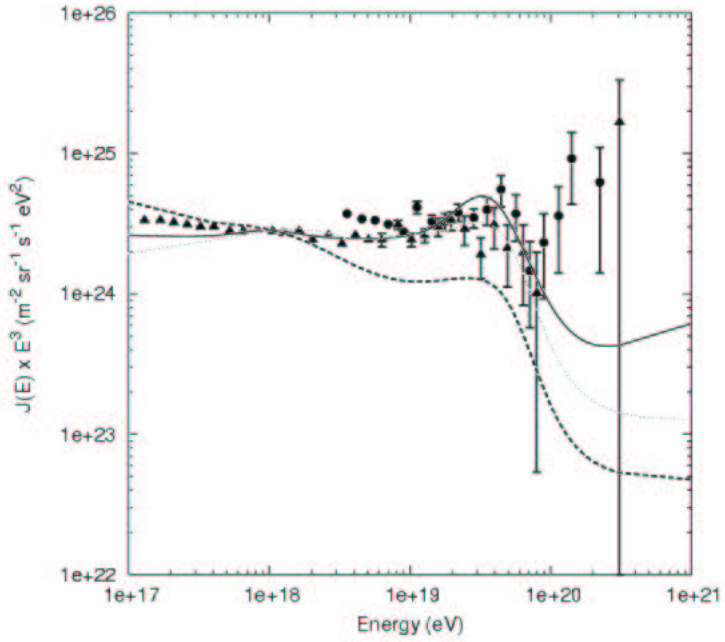

Figure 6.9: The highest energy region of the cosmic ray spectrum as observed by the Fly's Eye (triangles) and AGASA (filled dots) experiments. The solid line is the expected spectrum from sources whose density distribution follows the strong redshift dependence of GRBs. Also plotted are the expected spectra from sources whose density distribution evolves as the star formation rate (thick dashed line) and sources whose distribution is independent on redshift (dotted line). Taken from Scully & Piran (2001).

6.7 The Reconnection Theory of Acceleration

Colgate & Li (2001) are trying to find for the one mechanism to accelerate cosmic rays universally over the full energy spectrum, isotropically, and space filling. They presented three primary reasons for adopting the way of acceleration different from collisionless shock presented in sections above[5]:

1. The energy source is space filling and isotropic, thereby avoiding any anisotropy due to the single sources.

2. The Galactic and particularly the extragalactic energy source is sufficient to supply the full energy of the universal Galactic and extragalactic spectrum of 10^{60} to 10^{61} ergs sufficient to avoid the GZK cutoff.

3. The required small loss or high reversibility per scattering for shock acceleration is unlikely unless proven in the laboratory.

[5]The widely accepted mechanism of collisionless shock acceleration is most substantiated by the prediction of the power-law function not much different from that observed.

4. Efficient $E_{parallel}$ acceleration from reconnection[6] of force-free fields is well observed in the laboratory whereas collisionless shock acceleration still eludes laboratory confirmation and space observations have failed to observe the expected strong hydromagnetic turbulence of collisionless shock.

Accretion onto galactic black holes, neutron stars, cataclysmic variables, and T-Tauri stars[7] will all lead to reconnection associated with twisted fields by all condensations. The energy of these condensations is far more than required to maintain the cosmic rays in our Galaxy. The additional location to accelerate particles is in the force-free field helix next to the black hole of nearly every galaxy, where the predicted upper limit is 10^{23} eV.

6.8 Top-down models

The difficulties of bottom-up acceleration scenarios with production of ultrahigh-energy cosmic rays motivated proposal of the top-down, where EHECRs, instead of being accelerated, are the result of decay of massive particles (X particles)[8].

The particle accelerator experiments and the mathematical structure of the standard model of the weak, electromagnetic, and strong interactions suggest that these forces should be unified at energies about 2×10^{25} eV (SIGL, 2001), five orders of magnitude above the highest energies observed in CRs. The relevant grand unified theories (GUTs) predict the existence of X particles with mass m_X around the GUT scale of $\sim 2 \times 10^{25}$ eV. If their lifetime is comparable to or larger than the age of universe, they would be dark-matter candidates, and their decays could contribute to UHECRs fluxes today, with an anisotropy pattern that reflects the expected dark-matter distribution. These models avoid GZK cutoff because the EHECR flux is dominated by particle decays in the halo of our Galaxy.

However, in many GUTs, supermassive particles are expected to have lifetimes not much longer than their inverse mass (SIGL, 2001):

$$\tau \sim 6.6 \times 10^{-41} \left(\frac{10^{25}\,\mathrm{eV}}{m_X} \right) \mathrm{s}, \tag{6.10}$$

[6]Magnetic reconnection (henceforth called "reconnection") refers to the breaking and reconnecting of oppositely directed magnetic field lines in plasma. In the process, the magnetic field energy is converted to the plasma kinetic and thermal energy.

[7]Class of very young stars (pre-main sequence) having a mass and temperature similar to that of the Sun, are active and variable, very fast rotators, seen near many molecular clouds. They represent an early stage in stellar evolution, hydrogen burning has not started yet. The model for them has an expected magnetic field with a strength of about 1 kG

[8]Two classes of massive X particles have been proposed (BHATTACHARJEE & SIGL, 1999):

- X particles produced by collapse of cosmic topological defects produced in the early Universe, the X particle mass can be as large as a typical GUT scale $\sim 10^{25}$ eV;
- long-lived with mass $\geq 10^{20}$ eV, produced in the early Universe in processes associated with inflation and they are also good candidate for the cold dark matter.

and thus have to be produced continuously if their decays are to give rise to EHECRs. This can only occur by emission from topological defects that are relics of cosmological phase transitions that could have occurred in the inflationary early Universe at temperature close to the GUT scale. Phase transitions in general are associated with a breakdown of a group of symmetries. Topological defects occur between regions that are casually disconnected, such that the orientation of the order parameter cannot be communicated between these regions and thus will adopt different values. Examples of the topological defects are **cosmic strings** [9], **magnetic monopoles**[10] and **domain walls**[11].

In the modern version (BHATTACHARJEE & SIGL, 1999) of the top-down scenario of cosmic ray origin, the X particles typically decay to quarks and leptons. The quarks hadronizes, i.e. produces jets (jet is a shower of particles is confined in a narrow cone whose axis lies along the direction of propagation of the original quark) of hadrons containing mainly light mesons (pions) with a small percentage of baryons (mainly nucleons). The pions decay to photons, neutrinos and charged leptons, together with a small fraction of nucleons, are produced directly with energies up to $\sim m_X$ without any acceleration mechanism.

In order to observe the decay products of the X particles as EHECR particles today, three basic conditions must be satisfied:

1. The X particles must decay in recent cosmological epoch, or equivalently at non-cosmological distances ($\leq$100 Mpc) from Earth. Otherwise the decay products of the X particles lose all energy by interacting with the background radiation, and hence do not survive as EHECR particles[12].

2. The X particles must be sufficiently massive with mass $m_X \gg 10^{20}$ eV.

3. The number density and rate of decay of the X particles must be large enough to produce detectable flux of EHECR particles[13].

Topological Defects There are different mechanisms of production of EHE particles by Topological Defects (TD). In some cases TD become unstable and decompose to constituent fields (superheavy Higgs and gauge bosons), which then

[9]Strings correspond to the breakdown of a rotational symmetry U(1) around a certain direction; a laboratory example are vortices in superfluid helium.

[10]Magnetic monopoles correspond to the breakdown of arbitrary three-dimensional rotations SO(3) to rotations U(1) around a specific direction.

[11]Domain walls correspond to the breakdown of a discrete symmetry where the order parameter is only allowed to take several discrete values; a laboratory example is the Bloch walls separating regions of different magnetization along the principal axis of a ferromagnet.

[12]A possible exception is the case where neutrinos of sufficiently high energy originating from X particle decay at large cosmological distances $\gg 100 Mpc$ give rise to EHE nucleons and/or photons within 100 Mpc from Earth through the decay of Z bosons resonantly produced through the interaction of original EHE with the thermal relic background (anti)neutrinos[B+s,p.21], if neutrinos have a small mass of order $\sim$ eV

[13]To explain the measured flux about 10 X particles must decay within every solar size volume 1AU per year. This scenario has to be full filled over a volume of radius 10 Mpc in the present epoch (BHATTACHARJEE & SIGL, 1999).

decay to ordinary particles. In case of monopoles and antimonopoles connected by strings, high energy particles are produced by annihilation of monopole-antimonopole pairs. EHECR from TD has spectrum with a soft GZK cutoff which does not contradict observations.

Cosmic strings The flux of EHECRs from gauge cosmic strings is smaller than the observed fluxes by about 10 orders of magnitude, too small to be detectable with current technology (Gill & Kibble, 1994). Thus any CRs observed above 10^{19} eV are not due to such cosmic strings.

Two types of assumptions have led previous authors to the conclusion that cosmic strings could be responsible for EHECRs. Firstly, the absolute amplitudes of the predicted spectra were found matching to experiment, thus assuming that strings are responsible for EHECRs, rather than from any knowledge of the evolution of a cosmic string network. If this is done then there is a tendency for the scenario, to predict too large photon flux at around a few hundered MeV, although it is possible to resolve this crisis (Chi et al., 1992). Secondly, the energy yielded by each event was sometimes expressed as a fraction of a physical length, such as the length of a loop. This scaling of the energy per event vastly overestimates the flux.

6.9 Primordial black holes

As first shown by Hawking (1975), quantum theory predicts that a black hole emits thermal radiation. The possibility of observing this radiation is small: the entire black hole would emit only a few hundred quanta per second, and this is too small flux to be observed at astronomical distances (Heckler, 1996). However, since temperature of the black hole, and hence flux radiation, is inversely proportional to the black hole mass (see Eg. 6.13), the possibility of detecting Hawking radiation from much smaller mass black holes becomes observationally feasible. We should note that since there are no known astrophysical processes that can produce these small mass black holes, we assume that they were produced in the early Universe[14], hence they are called primordial black holes (PBHs).

The mass loss rate of a PBH is (Barrau, 2000):

$$\frac{dM}{dt} \approx -7.9 \times 10^{26} \frac{1}{M^2}. \tag{6.11}$$

From equation 6.11 it follows (Maki et al., 1996) that

$$M_* \approx 5.3 \times 10^{14} \left(\frac{t_u}{16\,\mathrm{Gyr}}\right)^{1/3} \mathrm{g} \approx 3^{-19} \left(\frac{t_u}{16\,\mathrm{Gyr}}\right)^{1/3} \mathrm{M}_\odot, \tag{6.12}$$

where M_* is the initial mass of a PBH expiring today, i.e., its initial lifetime equals the present age of the Universe t_u equals to 16 Gyr (Maki et al., 1996). PBHs

[14] PBHs may have been formed via initial density fluctuations, phase transitions or the collapse of cosmic strings

with initial mass $M_i < M_*$ should have completely evaporated by now, while those with M_i slightly larger than M_* have at present an extremely high temperature

$$T_{BH} \approx \frac{\hbar c^3}{8\pi G M} \approx 1.1 \times 10^{13} \left(\frac{M}{\mathrm{g}}\right)^{-1} \mathrm{GeV} \tag{6.13}$$

and will expire by explosion soon. The total number of emitted particles by a single PBH above a 10^{20} eV threshold is 8.5×10^{14} particles over the lifetime of the PBH (Barrau, 2000).

The detection of low-energy cosmic ray antiprotons ($< 5 \times 10^8$ eV) put a much more severe limit on the density of exploding PBHs near the Earth than the theory[15] and this result exclude PBHs as serious candidates for EHECR.

In addition Heckler (1996) shows that once a black hole surpasses the critical temperature, the emitted Hawking radiation interacts with itself and forms a nearly thermal photosphere. Because the photosphere decreases the energy of the emitted particles, the possibility that black holes are the source of ultra-high energy background photons or other cosmic rays seems remote. Even when including quantum chromodynamics (QCD) and electro-weak theory, it would be difficult to produce extremely high energy $e^{\pm}$ or photons that would not be affected in the photosphere. Of course, the black hole could emit other high energy particles such as neutrinos, but even in this case the neutrino photosphere will eventually form, for hot enough black holes.

6.10 New physics

Neutrinos Weakly interacting particles such as neutrinos will have no difficulty in propagating through the intergalactic medium, namely the corresponding mean free path $l_\nu \approx 4 \times 10^{28}$ cm is just above the present size of the horizon, $H_0^{-1} \approx 10^{28}$ cm (Anchordoqui, 1998). Many sources of extremely high energy neutrinos are known, they can be produced in astrophysical objects by the decay of pions or kaons generated as subproducts of proton-photon interactions during the acceleration process or else by top-down mechanisms (Bhattacharjee & Sigl, 1999). In the latter, the neutrino flux might extend even up to $10^{25} - 10^{28}$ eV. However, at these energies the atmosphere is still transparent to neutrinos, and the point of first interaction should be equally likely at all atmospheric depths (Elbert & Sommers, 1995), whereas the showers certainly started high in the atmosphere. On the other hand, the interaction cross section for extremely-high energy neutrinos is not experimentally confirmed. Expected cross sections are calculated within the standard model, and it is conceivable that new physics at extremely high energies might enhance neutrino cross sections.

Cosmic ray neutrino annihilation with relic neutrinos in the galactic halo was suggested as an alternative source of EHECRs(Waxman, 1998). Annihilation of high energy, $\sim 10^{21}$ eV, neutrinos on big bang relic neutrinos of ~ 1 eV mass,

[15] The required density of exploding PBHs was determined from the particle flux above 10^{20} eV.

clustered in the Galactic halo or in a nearby galaxy cluster halo, has been suggested to generate high energy nucleons and photons which may account for the detected flux of $> 10^{20}$ eV cosmic rays. Very large flux of primary neutrinos with superhigh energies is needed for this hypothesis.

EHE neutrinos may be detected by their EAS. This is important for two reasons (Bertou et al., 2000). The first is that the detection of neutrinos (together with an important component of photons) in the higher energy range of the spectrum is a solid signature of the top-down mechanisms. The second is that the projected high energy neutrino telescopes (under-water or under-ice km^3 scale detectors) are ineffective at energies above 10^{16} eV at which the Earth becomes opaque to upward going neutrinos. Therefore large ground arrays for which the interaction medium is not the earth but the atmosphere, and which could become efficient enough at 10^{17} eV and above, would be complementary to the neutrino telescopes in the exploration of the whole spectrum. The neutrino cross-sections at these EHEs become non-negligible. The main difficulty for an observer is to identify the EAS as coming from a neutrino flux. A clear neutrino signature would be to see a shower starting deep in the atmosphere (it is impossible in a case of hadronic shower).

Lorentz invariance breaking An alternative explanation for the EHECRs requires the breakdown of Lorentz invariance, too small to have been detected otherwise, which might affect elementary particle kinematics in such a way that some hadronic resonances which are instable at low energies would become stable at very high energies. Therefore the GZK cutoff can be relaxed or removed.

Breaking of Lorentz invariance leads to existence of the absolute Lorentz frame (Berezinsky, 2001). Lorentz invariance is a basic principle for building a Lagrangian for any interaction. Equation of motion remains Lorentz invariant and the violation occurs spontaneously in the solutions. Lagrangians for all interactions are constructed as Lorentz scalars and spontaneous Lorentz invariance breaking occurs due to non-zero values of field components in vacuum states. Breaking of Lorentz invariance can be made arbitrarily small, and all physical effects accompanied by Lorentz invariance breaking are small too. The absolute Lorentz frame exists, but all physical effects, which distinguish it from other frames, are small, and thus all frames are nearly equivalent, similar to the Lorentz invariant theory.

Wormholes Even something more exotic could be found: The highest energetic particles may have shortcut their journey traversing a wormhole. The wormhole is a tunnel in the topology of the space-time from where in-coming causal curves can pass through and become out-going on the other side (Morris et al., 1988). Whether such wormholes are actually allowed by the laws of physics is currently unknown.

Chapter 7

Propagation in magnetic field

My project consists of modelling the trajectories of cosmic rays as they traverse the Galaxy. I am interested in behaviour of UHECRs under the influence of the Galactic magnetic field (GMF). More specifically, I wish to study how atomic number Z and mass number A can influence the escape of nuclei from the Galaxy.

7.1 Lorentz force

The first step is to model the trajectories of charged particles through any magnetic field. We know that charged particles moving through the magnetic field are subject to the Lorentz force, which is of the form:

$$\vec{F} = q(\vec{E} + \vec{v} \times \vec{B}). \tag{7.1}$$

Where q and $\vec{v}$ are the particle charge and velocity[1], respectively, $\vec{E}$ is the electric field and $\vec{B}$ is the magnetic field. The Galaxy has no net electric field, so the equation of motion reduces to:

$$\vec{F} = q(\vec{v} \times \vec{B}). \tag{7.2}$$

Which we will modify into

$$\vec{a} = \frac{q}{m}(\vec{v} \times \vec{B}) = \frac{Zc^2}{E[\mathrm{eV}]}(\vec{v} \times \vec{B}), \tag{7.3}$$

where $\vec{a}$ is acceleration of particle with mass $m = \gamma m_0$ and atomic number Z, c is the velocity of light in the vacuum.

7.2 Numerical solution

For the complicated magnetic field, this ordinary differential equation must be solved by numerical methods. I developed a fourth-order Runge-Kutta routine with

[1] Almost equal to the velocity of light in the vacuum, because UHECRs are reaching the highest known relativistic γ factors: from 10^4 at 10^{13} eV to 10^{11} at 10^{20} eV, the highest ever detected.

adaptive step size control to integrate this equation and output the trajectories. Simply put, this method reduces the Lorentz force equation to six first-order differential equations (two for each spatial dimension):

$$\begin{aligned}
\vec{K}_1 &= \vec{v}_n, & \vec{L}_1 &= \vec{v}_n \times \vec{B}_0; \\
\vec{K}_2 &= \vec{v}_n + \vec{L}_1 dt/2, & \vec{L}_2 &= \vec{K}_2 \times \vec{B}_0; \\
\vec{K}_3 &= \vec{v}_n + \vec{L}_2 dt/2, & \vec{L}_3 &= \vec{K}_3 \times \vec{B}_0; \\
\vec{K}_4 &= \vec{v}_n + \vec{L}_3 dt, & \vec{L}_4 &= \vec{K}_4 \times \vec{B}_0; \\
\vec{x}_{n+1} &= \vec{x}_n + (\vec{K}_1 + 2\vec{K}_2 + 2\vec{K}_3 + \vec{K}_4) dt/6, \\
\vec{v}_{n+1} &= \vec{v}_n + (\vec{L}_1 + 2\vec{L}_2 + 2\vec{L}_3 + \vec{L}_4) dt/6
\end{aligned} \tag{7.4}$$

where we defined $\vec{B}_0 = \frac{q}{m}\vec{B}$. To be abble to model the motion of the particle through any magnetic field, we need to choose the appropriate magnetic field for the Galaxy.

7.3 Galactic magnetic field

The first evidence for the existence of the Galactic magnetic field was inferred from the observation of linear polarization of starlight (Hiltner, 1949). The Galactic magnetic field appears to have an ordered structure, at least in the region within 3 kpc from our Solar system. This is the region where the strength and direction of magnetic field can be determined by observations of Faraday rotation[2] in the radio continuum emission of pulsars.

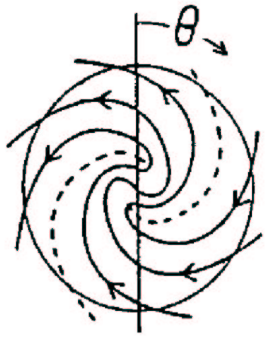

Figure 7.1: A sketch of the bisymmetric spiral model.

Through analyses of the Faraday rotation measurements of pulsars, it was found that the Galaxy has the global field[3] of the bisymmetric spiral (BSS) configuration,

[2]Magnetic fields directed along the path of an electromagnetic wave will change the index of refraction slightly between the left and the right-hand polarized radiation. This effect is known as Faraday rotation.

[3]The global models omit the presence of random component and try to model just regular component.

rather than others. BSS model consists of the two-arm logarithmic spiral model with the constant pitch angle and shows π-symmetry. More exactly, it has also a dipole character (it has field reversals and odd-parity with respect to the Galactic plane), so it is referred to as the BSS-A model. The field strength at the point (r, θ) in the Galactic plane for BSS-A model is (Han & Qiao, 1994):

$$B(r, \theta) = B_0(r) \ln\left(\theta - \beta \frac{r}{r_0}\right), \tag{7.5}$$

where $r_0 = 10.55$ kpc is the Galactocentric distance of the location with maximum field at $l = 90°$ and $\beta = 1/\tan p = -5.67$ for the constant pitch angle $p = -10°$ (see Fiq. (7.2)). $B_0(r)$ is taken to be $B_0(r) = 3\frac{R}{r}\,\mu$G for $r >$ 4kpc and constant in the central region of the Galaxy with value equal for $r = 4$ kpc, i.e. $6.4\,\mu$G. The radial and azimuthal components of the field are

$$\begin{aligned} B_\theta &= B(r, \theta) \sin p \\ B_r &= B(r, \theta) \cos p. \end{aligned} \tag{7.6}$$

The configuration of the BSS-A model of GMF is shown in Fig. 7.2.

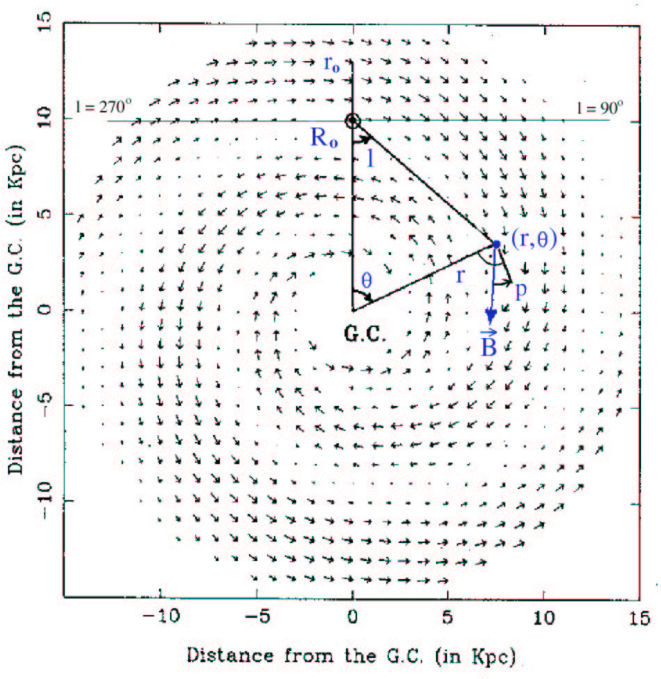

Figure 7.2: The bisymmetric logarithmic open-spiral configuration of the magnetic field in the Galactic plane. The geometrical meanings: r_0 and θ are galactocentric distance and azimuthal angle around the Galactic center (G.C.), θ is defined as increasing clockwise; p is the pitch angle of the field spiral. At the point $(r_0, \theta = 0)$ the field strength $\vec{B}$ reaches the maximum. The field directions are indicated by arrows and the size of arrows is proportional to the field strengths. From Han & Qiao (1994).

The fields strength above and below the Galactic plane is (STANEV, 1997):

$$|B(r,\theta,z)| = |B(r,\theta)|\, exp(-|z|/z_0) \tag{7.7}$$

with $z_0 = 1$ kpc for $|z| < 0.5$ kpc and $z_0 = 4$ kpc for $|z| > 0.5$ kpc.

It follows from the measurements that the Galactic magnetic field has two components - regular and random (non-ordered). The total magnetic field B_{tot} that a cosmic ray experiences is represented by the vector sum of the regular and random components:

$$\vec{B}_{tot} = \vec{B}_{reg} + \vec{B}_{ran} \tag{7.8}$$

For the simulations presented here, B_{reg} is obtained from the BSS-A model of HAN & QIAO (1994).

The random magnetic fields appear to have the length in the range $10 \div 100$ pc (BECK, 2000) and their strengths are $1 \div 3$ times greater than the regular component (LEE & CLAY, 1995). The driving force for these random magnetic fields are provided by supernovae which occur incidentally in time and space thorough the Galaxy (LEE & CLAY, 1995). Experience from external galaxies shows that the regular field is weaker and the random field is stronger in the spiral arms, probably due to field tangling by star-forming processes and the expansion of supernova remnants (BECK, 2000).

Chapter 8

Results of computer modelling

In this chapter the results of the modelling the motion of protons and four atomic nuclei (helium, oxygen, magnesium and iron) in the Galactic magnetic field will be presented. The simulation program was written in C programming language and the graphical results were plotted in GRACE, GNUPLOT and IDL.

The equation of motion was integrated by the fourth-order Runge-Kutta routine with adaptive step size control as was discussed in Section 7.2. The position error of the integration was equal to 10^8 metres.

The geometrical boundaries of the Galactic disk and its shape are displayed in Figure 8.1. The bulge is a symmetric ellipsoid with a semi-major axis in the Galactic plane 3 kpc and a semi-minor axis of 2 kpc. Around the bulge there is a thin cylinder with a radius 15 kpc and half-height of 300 pc.

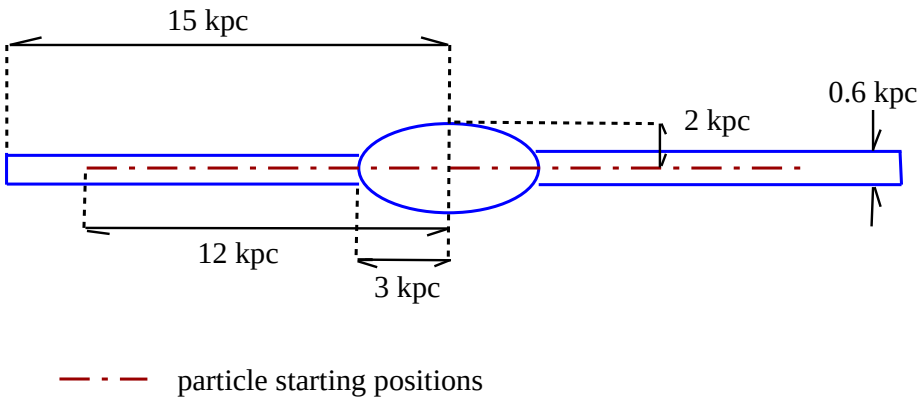

Figure 8.1: The boundary of the Galaxy.

For the purpose of the simulations with random magnetic field the Galaxy was divided into the cubic cells of assumed size L_0. Two values of cell length were studied, particularly 10 and 50 pc. The random orientation and strength of the irregular magnetic field ($B_{ran} < \sqrt{3}\times 10^{-9}$ T) were generated randomly in a fraction of the cells.

The optimal value of travel time for particle motion in the Galaxy in this model was found as $T = 10^{12}$ s $\sim 3.2 \times 10^4$ yr. Gaisser (2000) has shown that the average time spent by cosmic rays with energy $\sim 10^9$ eV is $\tau_{esc} \sim 10^{14}$ s $\simeq 3 \times 10^6$ yr. The similar value 6.7×10^6 yr has been computed by Brunetti & Codino (2000) for protons in the energy range $(1 \div 100) \times 10^9$ eV. This average time of cosmic-ray protons was defined as the time interval elapsed between the birth and death in the Galactic disk via nuclear collision or extinction by ionization energy losses and between the birth and the crossing of the disk boundaries.

The influence of the half-thickness of the Galactic disk on the **escape of nuclei** was tested first for the regular component of GMF and for travel time equal to 10^{11} s. Three values (300, 400 and 500 pc) were used and no important effect of the half-thickness on the chemical composition was found (Fig. 8.2). The Galactic disk with half-thickness equal to 300 pc was used for the following modelling.

The dependence of nuclei escaping on the energy is similar for all configurations. At the lowest energies (from 10^{13} eV to 5×10^{14} eV) there are differences between nuclei escaping and from 5×10^{14} eV roughly to 10^{16} eV the numbers of escaping nuclei are similar. If the particles have energy higher than 10^{16} eV, then the particles with smaller charge will escape more rapidly than others, as in the case of the lowest energy range. The particles above 10^{16} eV are escaping independently of their charge (page 71 and 73) only from the regular magnetic field. So the result is that the different nuclei escaping for the highest energies is caused mainly by random component of Galactic magnetic field.

The particle escape depends also on the number of the cells with random magnetic field, for higher number of the cells the particle escape is slower for both tested size of the cells. More particles have escaped from the Galaxy when the size of the cells was 50 pc (page 78), than in the case of the Galaxy with the cells of the size 10 pc (page 75).

The **chemical composition** of cosmic rays can be easily computed from the values of the particle escapes. Our starting composition at 10^{12} eV was taken from Tab. 3.1 on page 26 (Wiebel, 1994). The representative element, which was the most abundant one, was chosen from each group in this table. The abundance of the element is then put equal to the sum of all elements in the given group. From the group named 'low' were chosen both two elements, because they represent more than two thirds of all cosmic particles. For purposes of our modelling we have therefore chosen protons and nuclei of helium, oxygen, magnesium and iron.

We take up the average value of the mean logarithm of mass number as the useful indicator of the composition

$$< \ln A >= \frac{\sum_i n_i (\ln A_i)}{\sum_i n_i}, \tag{8.1}$$

where n_i denotes the weight of element i with mass number A_i. The values of the

mean logarithmic mass <ln A> for the elements which were used in our modelling are presented in Tab. (8.1).

${}^{A}_{Z}$X	${}^{1}_{1}$H	${}^{4}_{2}$He	${}^{16}_{8}$O	${}^{24}_{12}$Mg	${}^{56}_{26}$Fe
<ln A>	0	1.39	2.77	3.18	4.03

Table 8.1: The mean logarithmic mass of five atomic nuclei used in our modelling.

Two increase of the mean logarithm of mass number <ln A> was found in the same energy intervals, where the lighter particles escape faster from the Galaxy. In the interval from 5×10^{14} eV to 10^{16} eV, there is a decrease almost to the original value <ln A> = 1.41. This is caused by the differences in the geometrical boundaries of the Galactic disk and the bulge, because they strongly influence the escape. The explanation of the constant values of the escape of all nuclei, and therefore the chemical composition close to that of the original, in the energy range from 5×10^{14} eV roughly to 10^{16} eV will be apparent from Figures on page 80. In the energy region above 5×10^{14} eV all particles escaped from the disk, contrary to the particles in the bulge. It is worth to note, that the magnetic field in the bulge region is also stronger than in the disk. Particles will not escape from the bulge until they attain the energy above 10^{16} eV. Then the escape will again behave as the function of particle charge and we can expect an increase of the heavy elements.

Therefore we can summarize that the escape from the Galactic disk has the main importance in the lowest energy range of our modelling. and contrary to this the escape from the Galactic bulge determines the behavior of nuclei in the highest energy range.

The cells with random magnetic field may influence also the chemical composition of cosmic rays. For the cell size of 10 pc the increase of the mean logarithmic mass depends mainly on the number of cells with random magnetic field. For higher values the increase in the low energy range is smaller, but on the other hand it is bigger in the high-energy range (Fig. 8.3). Contrary to this the increase of the mean logarithmic mass is higher for smaller number of cells with size 50 pc in both energy ranges (Fig. 8.4).

The final part of this work is the comparison of modelling with the **experimental results**, which were presented in Fig. 3.9. There is no change in the chemical composition for the energies below 5×10^{14} eV. The data from direct measurements indicate the increase of the mean logarithmic mass up to 5×10^{14} eV. The results from non-direct experiments are not clear because of large spread of measured values of their strong scattering, but the most favored is the scenario of increase of the mean logarithmic mass above 10^{15} eV.

The distinct different patterns of the mean logarithmic mass are influenced by the approximations and assumptions used in our modelling. Below 10^{15} eV the propagation of particles in the Galaxy must be solved by more realistic method, for example by diffusion models (Gaisser, 1990). The effects of particle energy

losses and gains, the interactions in the interstellar matter and different sources of cosmic rays have to be included in the computing in the higher energy range. We have used only one type of the source in the Galactic plane and they had constant chemical composition. However, there are indications that we can expect more types of sources in Galactic and extragalactic space resulting in more complicated composition of the cosmic ray flux.

We have also used only one model of regular Galactic magnetic field. However, it was improved by simple model of random components. The results indicate that these irregular components have significant influence on the propagation of cosmic particles, even for the highest energies used in our modelling. On the other hand the magnetic field of halo was ignored.

We can summarize that in our model we have tested influence of the Galactic magnetic field on the motion and chemical composition of cosmic rays. We have found that for the energies above 10^{16} eV, where our model is sufficient to describe the motion of nuclei, we can expect an increase of the mean logarithmic mass $<\ln A>$, under assumption that the Galactic sources will have the same characteristics which were used in our model.

(a)

log(E[eV])	$^{1}_{1}$H	$^{4}_{2}$He	$^{16}_{8}$O	$^{24}_{12}$Mg	$^{56}_{26}$Fe
13	61%	62%	61%	50%	27%
14	63%	61%	62%	51%	31%
14.7	64%	62%	64%	62%	60%
15	63%	59%	61%	60%	61%
16	62%	62%	62%	61%	60%
17	62%	62%	61%	62%	61%
18	62%	62%	61%	61%	61%
19	63%	63%	62%	61%	62%

(b)

log(E[eV])	$^{1}_{1}$H	$^{4}_{2}$He	$^{16}_{8}$O	$^{24}_{12}$Mg	$^{56}_{26}$Fe
13	52%	51%	36%	31%	12%
14	58%	57%	39%	35%	18%
14.7	57%	56%	54%	52%	56%
15	56%	58%	54%	55%	56%
16	56%	54%	56%	58%	56%
17	56%	56%	56%	56%	55%
18	57%	56%	56%	56%	56%
19	59%	58%	57%	55%	57%

(c)

log(E[eV])	$^{1}_{1}$H	$^{4}_{2}$He	$^{16}_{8}$O	$^{24}_{12}$Mg	$^{56}_{26}$Fe
13	51%	47%	38%	29%	12%
14	47%	47%	39%	33%	15%
14.7	50%	53%	46%	54%	45%
15	52%	52%	51%	52%	50%
16	51%	52%	52%	52%	52%
17	51%	51%	51%	51%	51%
18	51%	50%	51%	51%	51%
19	53%	52%	51%	51%	51%

Table 8.2: The fractions of escape for protons and nuclei from the Galaxy with only regular magnetic field after 10^{11} s. (a) The results for half-height of Galactic disk equal to 300 pc, (b) 400 pc, (c) 500 pc.

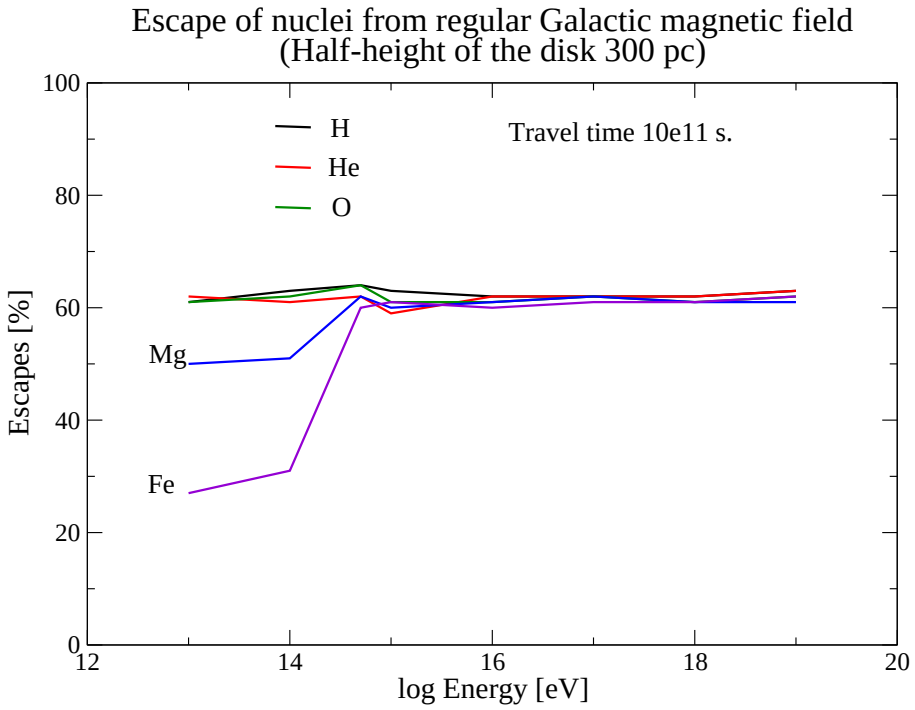
Escape of nuclei from regular Galactic magnetic field
(Half-height of the disk 300 pc)
Travel time 10e11 s.
H
He
O
Mg
Fe
Escapes [%]
log Energy [eV]
0
20
40
60
80
100
12
14
16
18
20

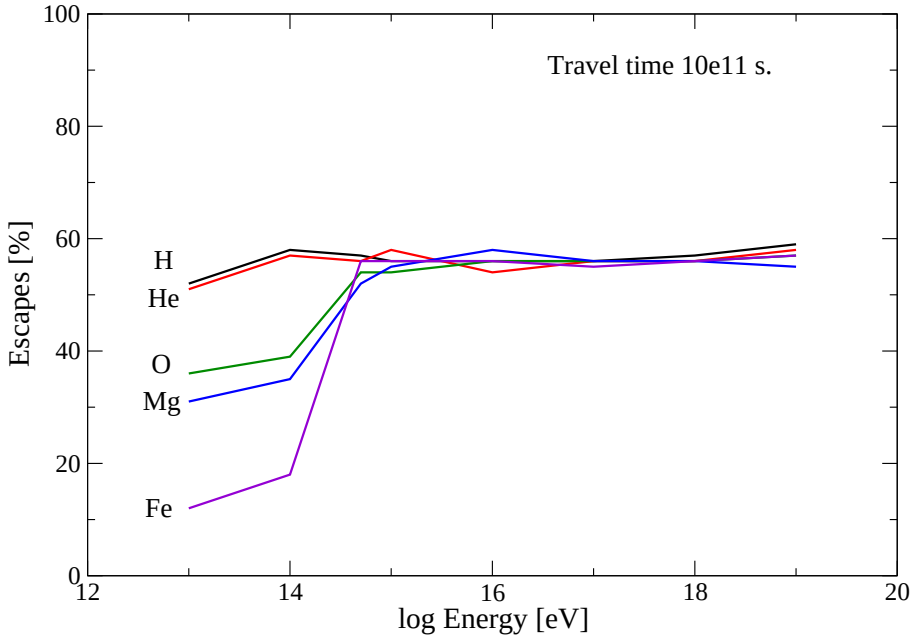
Escape of nuclei from regular Galactic magnetic field
(Half-height of the disk 400 pc)
Travel time 10e11 s.
H
He
O
Mg
Fe
Escapes [%]
log Energy [eV]
0
20
40
60
80
100
12
14
16
18
20

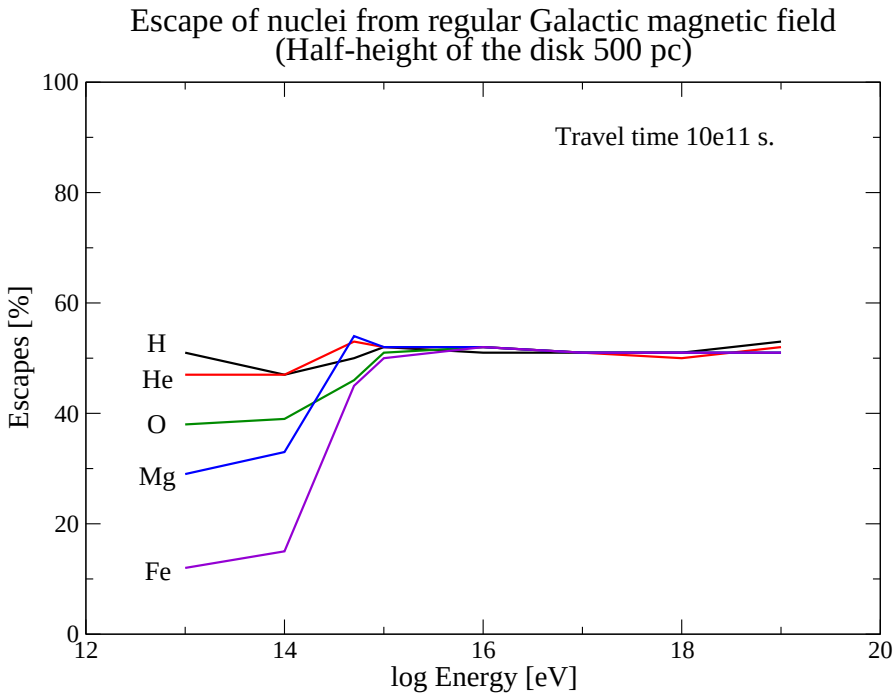

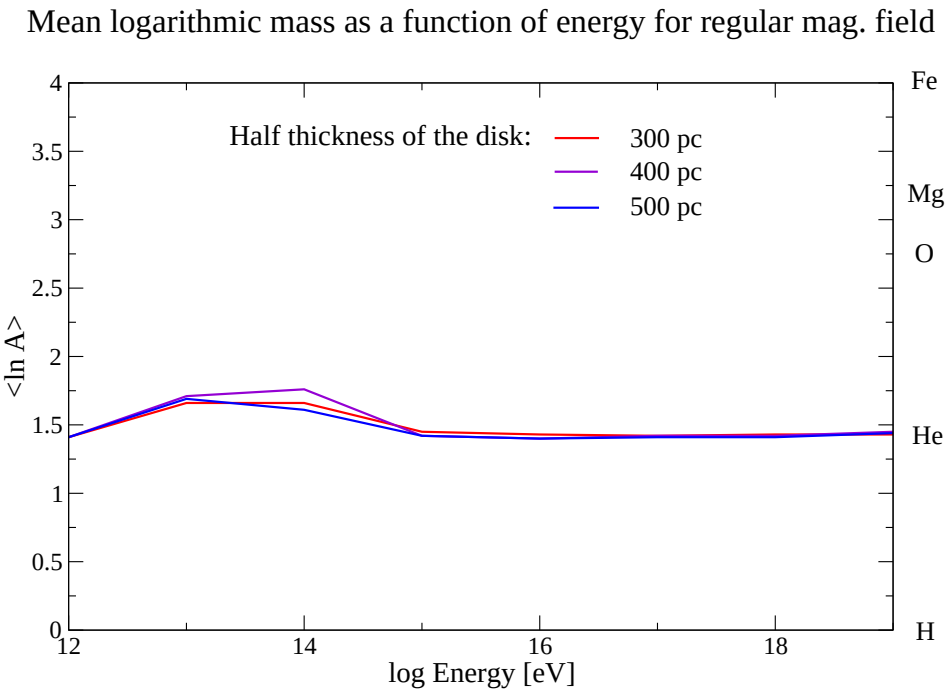

Figure 8.2: The influence of the half-height of Galactic disk on the chemical composition of cosmic rays. The travel time was equal to 10^{11} s.

log(E[eV])	$^{1}_{1}$H	$^{4}_{2}$He	$^{16}_{8}$O	$^{24}_{12}$Mg	$^{56}_{26}$Fe
13	87%	85%	76%	68%	30%
14	88%	88%	86%	85%	85%
14.7	89%	88%	88%	87%	87%
15	91%	89%	87%	88%	88%
16	90%	91%	91%	89%	89%
17	91%	90%	92%	92%	90%
18	96%	93%	92%	92%	89%
19	99%	99%	96%	95%	93%

Table 8.3: The fractions of escape for protons from the Galaxy with only regular magnetic field after 10^{12} s. The half-height of the Galactic disk was equal to 300 pc.

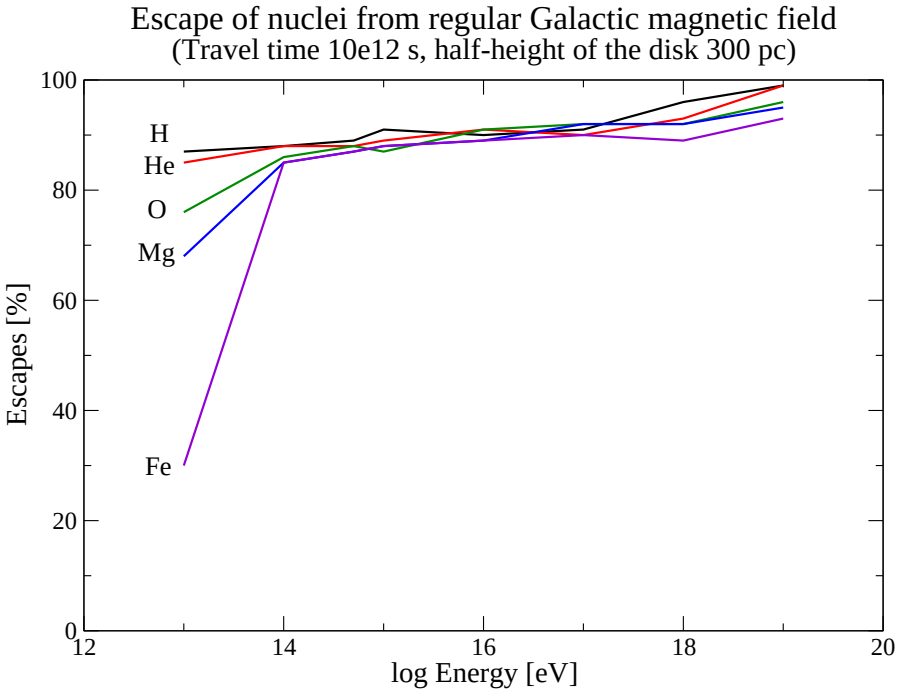

(a)

log(E[eV])	$^{1}_{1}$H	$^{4}_{2}$He	$^{16}_{8}$O	$^{24}_{12}$Mg	$^{56}_{26}$Fe
13	64%	62%	50%	33%	1%
14	71%	68%	52%	40%	11%
14.7	72%	70%	69%	67%	60%
15	73%	72%	72%	68%	63%
16	77%	74%	73%	72%	70%
17	89%	82%	76%	75%	71%
18	98%	97%	92%	88%	80%
19	99%	99%	98%	97%	96%

(b)

log(E[eV])	$^{1}_{1}$H	$^{4}_{2}$He	$^{16}_{8}$O	$^{24}_{12}$Mg	$^{56}_{26}$Fe
13	58%	51%	27%	18%	0%
14	59%	56%	31%	25%	3%
14.7	60%	59%	58%	57%	42%
15	62%	60%	59%	58%	56%
16	68%	65%	64%	61%	59%
17	82%	77%	67%	63%	60%
18	98%	98%	85%	79%	72%
19	99%	99%	98%	97%	94%

(c)

log(E[eV])	$^{1}_{1}$H	$^{4}_{2}$He	$^{16}_{8}$O	$^{24}_{12}$Mg	$^{56}_{26}$Fe
13	25%	22%	2%	0%	0%
14	36%	35%	8%	3%	0%
14.7	39%	39%	38%	35%	21%
15	42%	41%	39%	37%	35%
16	42%	41%	40%	39%	36%
17	80%	73%	43%	42%	41%
18	98%	97%	85%	82%	62%
19	99%	99%	98%	97%	95%

Table 8.4: The fractions of escape for protons and nuclei from the Galactic magnetic field with regular and random components after 10^{12} s. The size of the cells was equal to $L_0 = 10$ pc. (a) 10% of all cells with random magnetic field, (b) 20% of all cells with random magnetic field, (c) 40% of all cells with random magnetic field.

Escape of nuclei from Galaxy (L_0 = 10pc, 10%)

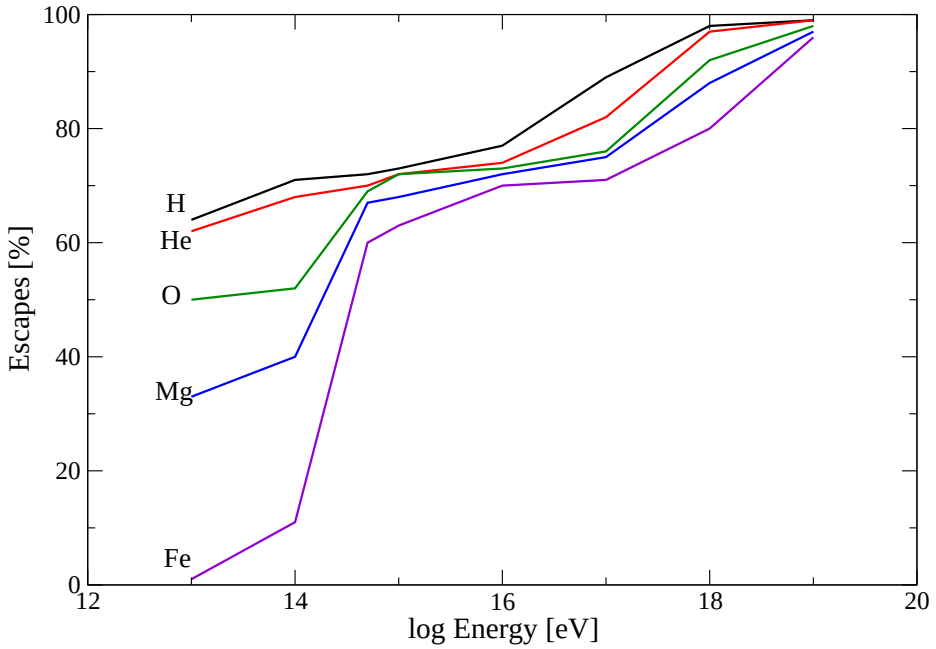

Escape of nuclei from Galaxy (L_0 = 10pc, 20%)

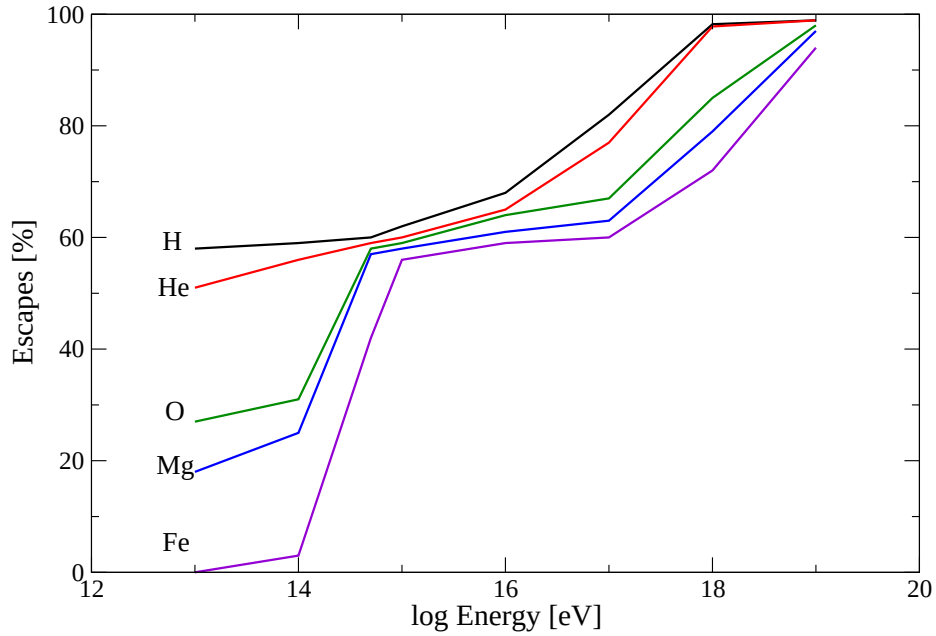

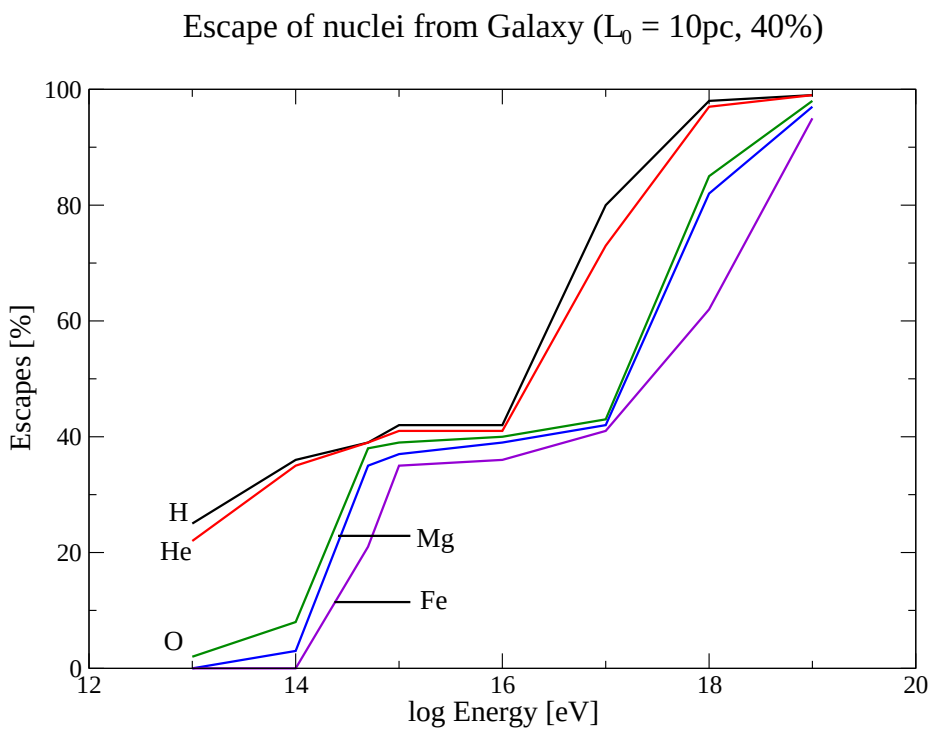

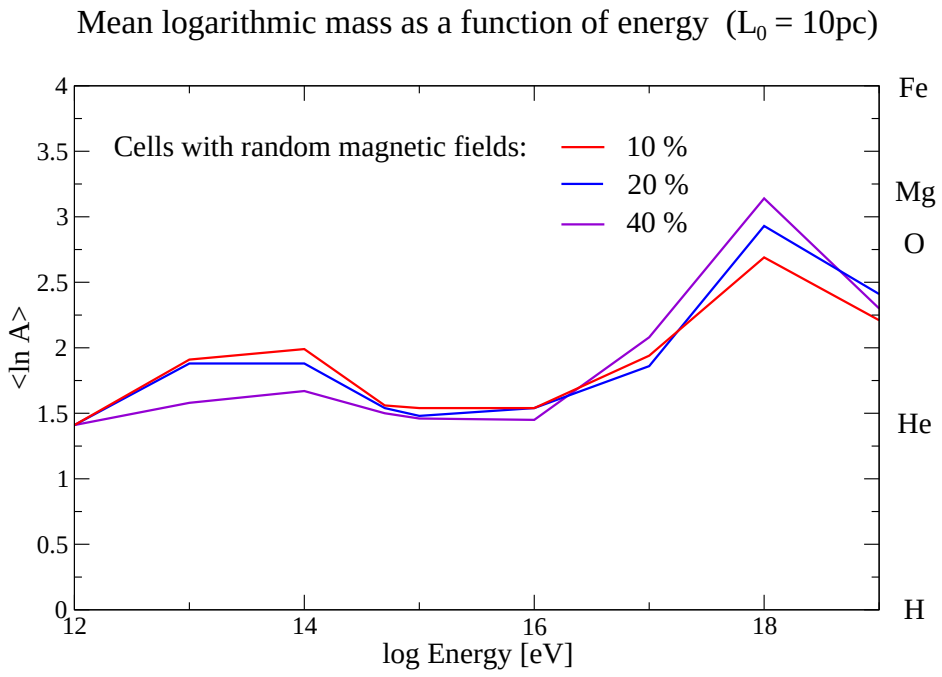

Figure 8.3: The mean logarithmic mass <ln A> as the function of the energy for the random magnetic fields in the cells of size L_0=10 pc.

(a)

log(E[eV])	$^{1}_{1}$H	$^{4}_{2}$He	$^{16}_{8}$O	$^{24}_{12}$Mg	$^{56}_{26}$Fe
13	77%	62%	48%	30%	10%
14	92%	91%	80%	75%	42%
14.7	94%	94%	92%	90%	73%
15	94%	94%	93%	92%	89%
16	95%	95%	94%	93%	93%
17	95%	95%	95%	93%	93%
18	100%	100%	97%	95%	95%
19	100%	100%	99%	99%	99%

(b)

log(E[eV])	$^{1}_{1}$H	$^{4}_{2}$He	$^{16}_{8}$O	$^{24}_{12}$Mg	$^{56}_{26}$Fe
13	65%	63%	38%	25%	2%
14	70%	68%	63%	60%	40%
14.7	68%	67%	66%	66%	65%
15	70%	70%	69%	68%	68%
16	71%	70%	69%	69%	70%
17	76%	72%	71%	70%	67%
18	97%	93%	77%	76%	72%
19	99%	99%	98%	96%	90%

Table 8.5: The fractions of escape for protons and nuclei from the Galactic magnetic field with regular and random components after 10^{12} s. The size of the cells was equal to $L_0 = 50$ pc. (a) 20% of all cells with random magnetic field, (b) 40% of all cells with random magnetic field.

Escape of nuclei from Galaxy (L_0 = 50pc, 20%)

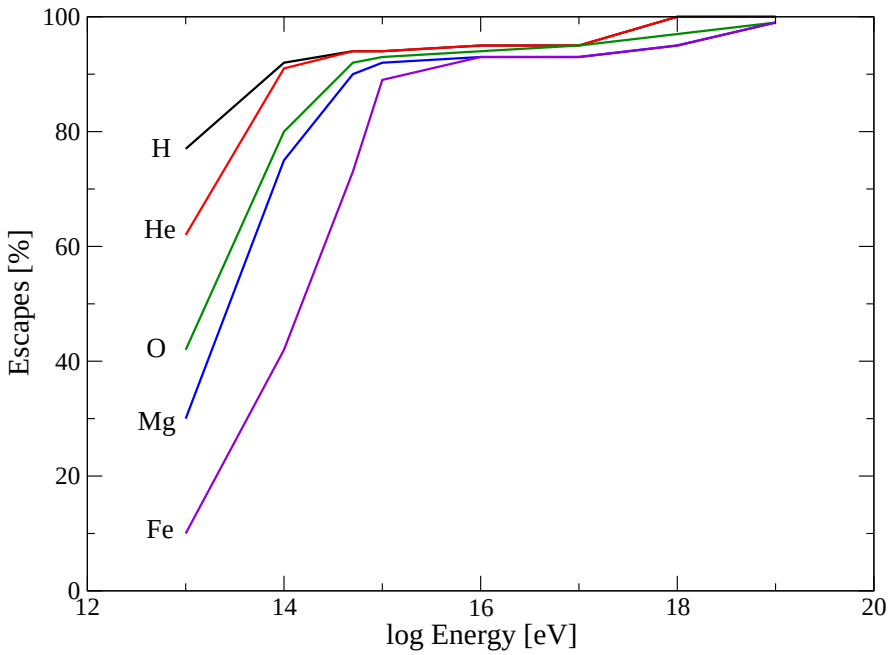

Escape of nuclei from Galaxy (L_0 = 50pc, 40%)

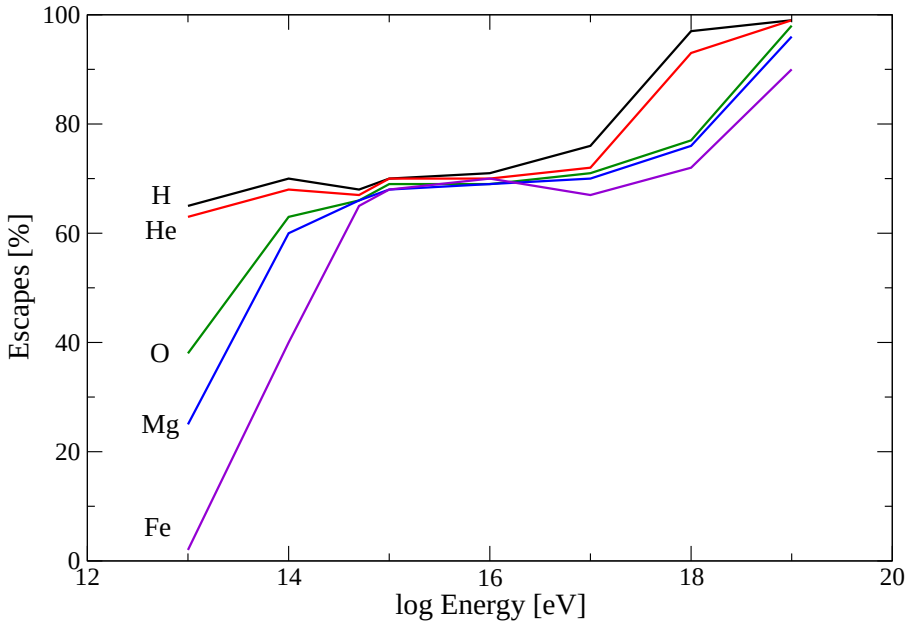

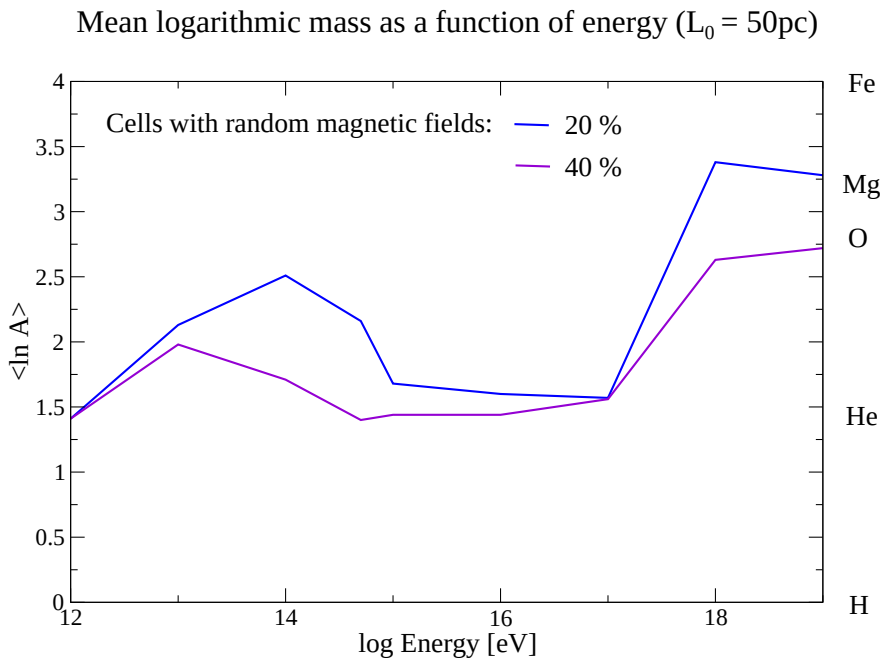

Figure 8.4: The mean logarithmic mass <ln A> as the function of the energy for the random magnetic fields in the cells of size L_0=50 pc.

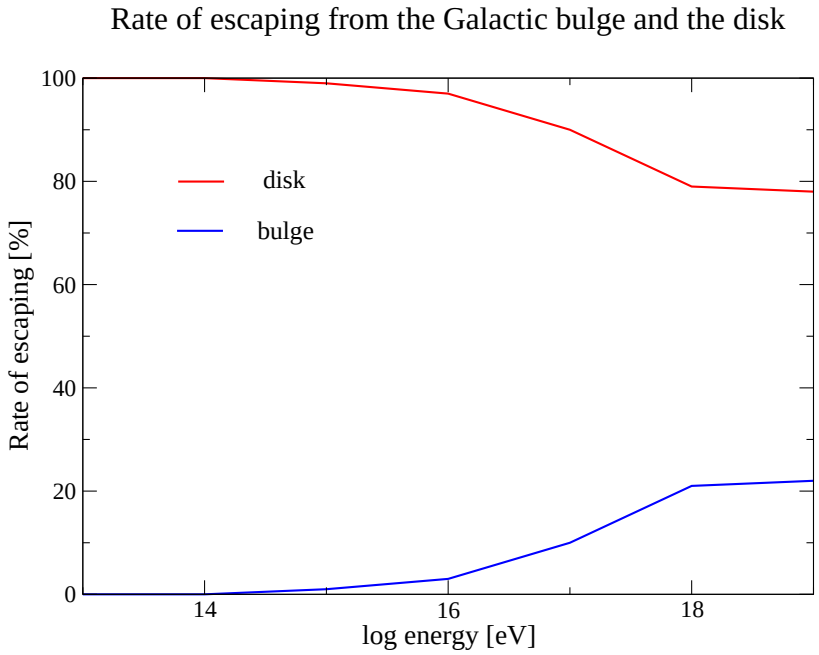

Figure 8.5: The rate of proton escape from the Galactic bulge and the disk as a function of the energy. The travel time was 10^{12} s. The half-height of the disk was 300 pc. The size of the cells was equal to 10 pc and 20% of cells were with random magnetic field.

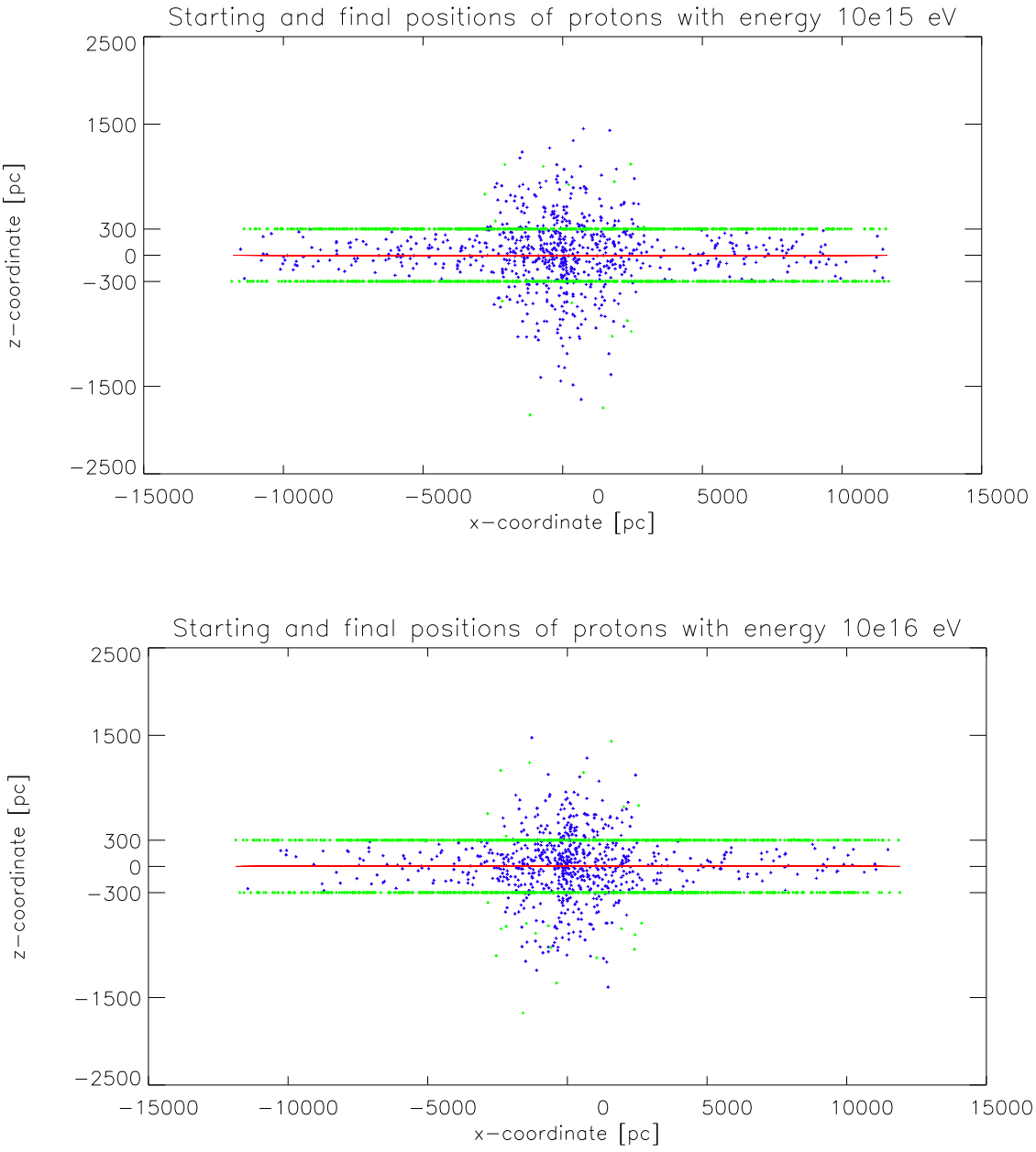

Figure 8.6: The comparison of proton escape for two energies, 10^{15} and 10^{16} eV. The red line indicates starting positions (2,000 particles were computed), green dots show exit points and blue dots the final position of non-escaping particles.

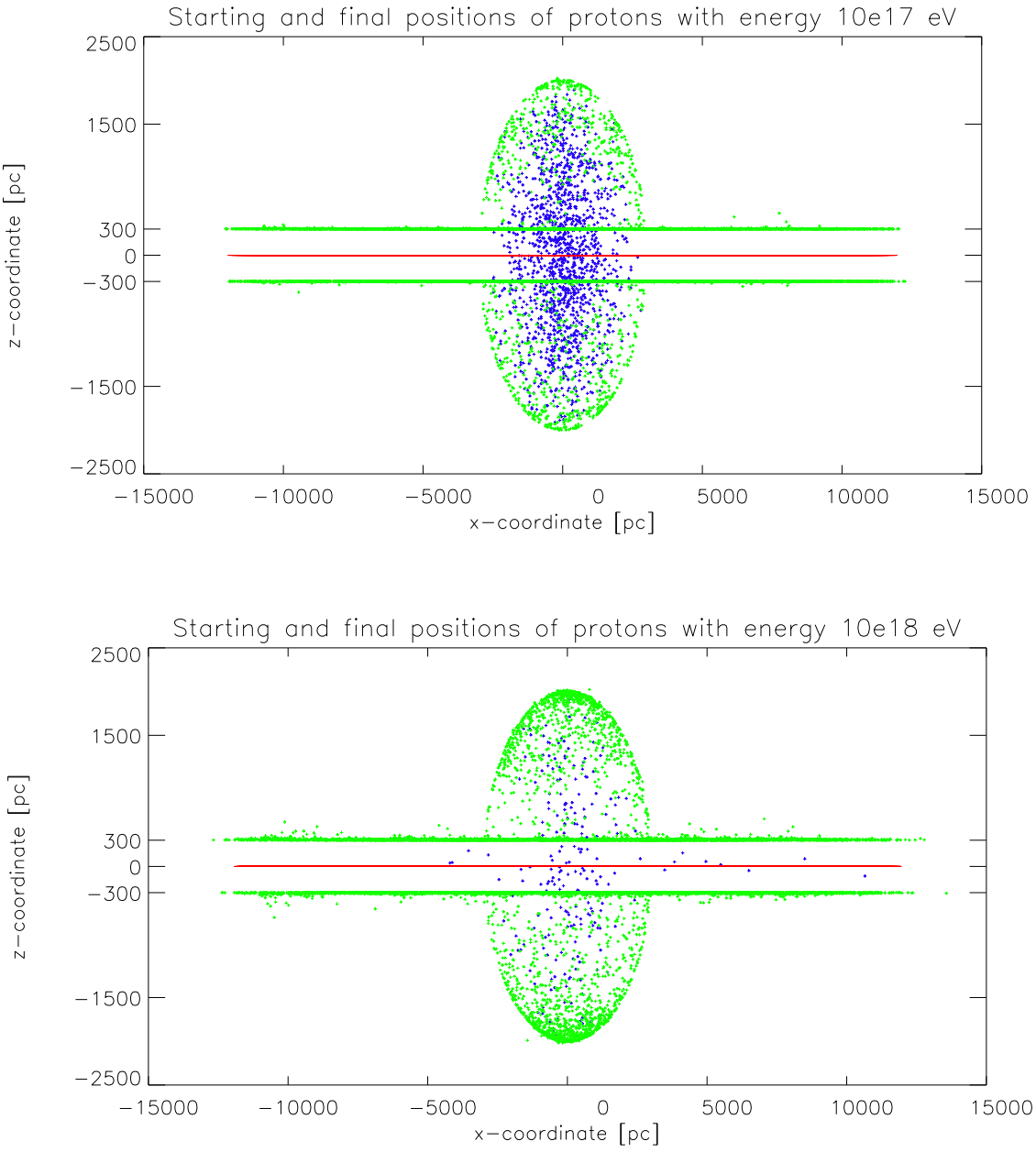

Figure 8.7: The comparison of proton escape for two energies, 10^{17} and 10^{18} eV. The red line indicates starting positions (10,000 particles were computed), green dots show exit points and blue dots the final position of non-escaping particles.

Chapter 9

Conclusions

The topic of very high-energy astrophysics was discussed in this work. Ground-based and orbiting observatories have led to a wealth of discoveries at the highest energy range of cosmic rays and their detection techniques together with their results were summarized as first. The review of possible acceleration mechanisms of cosmic rays in energy range from TeV to the end of the observed energy spectra was included into the work. Theoretical models of the astrophysical sources and some exotic theories about the origin of the most energetic cosmic rays in the Universe were addressed in detail in the last part of the general introduction.

My project consisted of modelling the trajectories of cosmic rays under the influence of the Galactic magnetic field. The importance of regular and irregular magnetic field on motion of charged particles was studied in the wide energy range. The results concerning the nuclei escape and chemical abundances of cosmic rays were presented as the function of energy and discussed in detail.

Bibliography

Achterberg, A. (2000): Particle Acceleration at Relativistic Shocks. *High Energy Gamma-ray Astronomy. International Symposium in Heidelberg.*, **Vol. 558**, 392

Aharonian, F.; Akhperjanian, A.G.; Barrio, J.A.; Bernloehr, K.; Beteta, J.J.G.; Bradbury, S.M.; Contreras, J.L.; Cortina, J.; Daum, A.; Deckers, T.; Feigl, E.; Fernandez, J.; Fonseca, V.; Frass, A.; Funk, B.; Gonzalez, J.C.; Haustein, V.; Heinzelmann, G.; Hemberger, M.; Hermann, G.; Hess, M.; Heusler, A.; Hofmann, W.; Holl, I.; Horns, D.; Kankanian, R.; Kirstein, O.; Koehler, C.; Konopelko, A.; Kornmayer, H.; Kranich, D.; Krawczynski, H.; Lampeitl, H.; Lindner, A.; Lorenz, E.; Magnussen, N.; Meyer, H.; Mirzoyan, R.; Moeller, H.; Moralejo, A.; Padilla, L.; Panter, M.; Petry, D.; Plaga, R.; Prahl, J.; Prosch, C.; Puehlhofer, G.; Rauterberg, G.; Rhode, W.; Rivero, R.; Roehring, A.; Sahakian, V.; Samorski, M.; Sanchez, J. A.; Schmele, D.; Schmidt, T.; Stamm, W.; Ulrich, M.; Völk, H.J.; Westerhoff, S.; Wiebel-Sooth, B.; Wiedner, C.A.; Willmer, M.; Wirth, H. (1997): Measurement of the flux, spectrum, and variability of TeV γ-rays from MKN 501 during a state of high activity. *Astronomy&Astrophysics*, **327**, 5

Aharonian, F.A.; Krawczynski, H.; Pühlhofer, G.; Rowell, G.P. (2000): Search for TeV Gamma Rays from Supernova Remnants Cas A and Tycho with the HEGRA Stereoscopic System of Atmospheric Cherenkov Telescopes. High Energy Astrophysics Division Meeting #32 - Honolulu, *3220*

Anchordoqui, L.A. (1998): From 3K to 10^{20} eV. `astro-ph/9812445`

Anchordoqui, L.A.; Goldberg, H.; Reucroft, S.; Swain, J. (2001): Extragalactic Sources for Ultra High Energy Cosmic Ray Nuclei `hep-ph/0107287`

The Auger Collaboration (1997): *Pierre Auger Observatory Design Report, Fermilab*

Axford, W. I. (1994): The origins of high-energy cosmic rays. *The Astrophysical Journal Supplement Series*, **90**, 937

Barrau, A. (2000): Primordial black holes as a source of extremely high energy cosmic rays. *Astroparticle Physics*, **12**, 269

Beck, R. (2000): Galactic and extragalactic magnetic fields. `astro-ph/0012402`

Bell, A.R. (1978): The acceleration of cosmic rays in shock fronts - I,II. *Monthly Notices of the Royal Astronomical Society*, **182**, 147,443

Berezinsky, V. (2001): Puzzles in astrophysics in the past and present. `astro-ph/0107306`

Bertou, X.; Boratav, M.; Letessier-Selvon, A. (2000): Physics of extremely high energy cosmic rays. `astro-ph/0001516`

Bhattacharjee, P.; Sigl, G. (1999): Origin and propagation of extremely high energy cosmic rays. `astro-ph/9811011`

Bird, D.J.; Corbató, S.C.; Dai, H.Y.; Dawson, B.R.; Elbert, J.W.; Gaisser, T.K.; Green, K.D.; Huang, M.A.; Kieda, D.B.; Ko, S.; Larsen, C.G.; Loh, E.C.; Luo, M.; Salamon, M.H.; Smith, D.; Sokolsky, P.; Sommers, P.; Stanev, T.; Tang, J.K.K.; Thomas, S.B.; Tilav, S. (1993): Evidence for correlated changes in the spectrum and composition of cosmic rays at extremely high energies. *Physical Review Letter*, **71**, 3401

Bird, D.J.; Corbato, S.C.; Dai, H.Y.; Dawson, B.R.; Elbert, J.W.; Emerson, B.L.; Green, K.D.; Huang, M.A.; Kieda, D.B.; Luo, M.; Ko, S.; Larsen, C.G.; Loh, E.C.; Salamon, M.H.; Smith, J.D.; Sokolsky, P.; Sommers, P.; Tang, J.K.K.; Thomas, S.B. (1994): *The Astrophysical Journal*, **424**, 491

Bird, D. J.; Corbato, S.C.; Dai, H.Y.; Elbert, J.W.; Green, K.D.; Huang, M.A.; Kieda, D.B.; Ko, S.; Larsen, C.G.; Loh, E.C.; Luo, M.Z.; Salamon, M.H.; Smith, J.D.; Sokolsky, P.; Sommers, P.; Tang, J.K.K.; Thomas, S.B. (1995): Detection of a cosmic ray with measured energy well beyond the expected spectral cutoff due to cosmic microwave radiation. *The Astrophysical Journal*, **441**, 144

Bird, D. J.; Dai, H. Y.; Dawson, B. R.; Elbert, J. W.; Huang, M. A.; Kieda, D. B.; Ko, S.; Loh, E. C.; Luo, M.; Smith, J. D.; Sokolsky, P.; Sommers, P.; Thomas, S. B. (1999): Study of Broad-Scale Anisotropy of Cosmic-Ray Arrival Directions from 2×10^{17} to 10^{20} Electron Volts from Fly's Eye Data. *The Astrophysical Journal*, **511**, 739

Biermann, P.L.; Gaisser, T.K.; Stanev, T. (1995): Origin of galactic cosmic rays. *Physical Review D*, **51**, 3450

Biermann, P.L. (1993): Cosmic rays: I. The cosmic ray spectrum between 10^4 GeV and 3 10^9 GeV. *Astronomy&Astrophysics*, **271**, 649

Blandford, R.D.; Ostriker, J.P. (1978): Particle acceleration by astrophysical shocks. *The Astrophysical Journal*, **221**, L29

Blasi, P; Epstein, R.I.; Olinto, A.V. (2000): Ultra-high-energy cosmic rays from young neutron star winds. *The Astrophysical Journal*, **533**, L123

Boldt, E.; Ghosh, P. (1999): Cosmic rays from remnants of quasars? *Monthly Notices of the Royal Astronomical Society*, **307**, 491

Brunetti, M. T.; Codino, A. (2000): Age of Cosmic-Ray Protons Computed Using Simple Configurations of the Galactic Magnetic Field. *The Astrophysical Journal*, **528**, 789

Bunner, A.N. (1967): Cosmic ray detection by atmospheric fluorescence. PH. D. THESIS, *Cornell University, New York*

Burbidge, E.,M.; Burbidge, G.R.; Fowler, W.A.; Hoyle, F. (1957): Synthesis of the Elements in Stars. *Reviews of Modern Physics*, **29**, 547

Chi, X.; Dahanayake, Ch.; Wdowczyk, J.; Wolfendale, A.W. (1992): Cosmic rays and cosmic strings. *Astroparticle Physics*, **1**, 129

Colgate, S.A.; Li, H. (2001): The Origin of All Cosmic Rays: A Space Filling Mechanism. THE ROLE OF NEUTRINOS, STRINGS, GRAVITY, AND VARIABLE COSMOLOGICAL CONSTANT IN ELEMENTARY PARTICLE PHYSICS, *Kluwer Academic/Plenum Publishers, New York*

Dar, A.; De Rújula, A. (2001): What is the cosmic-ray luminusity of our Galaxy? *The Astrophysical Journal*, **547**, 33

Dawson, B. R.; Meyhandan, R.; Simpson, K. M. (1998): A comparison of cosmic ray composition measurements at the highest energies. *Astroparticle Physics*, **9**, 331

de Gouveia Dal Pino, E.M.; Lazarian, A. (2000): Ultra-High-Energy Cosmic-Ray Acceleration by Magnetic Reconnection in Newborn Accretion-induced Collapse Pulsars. *The Astrophysical Journal*, **536**, L31

de Gouveia Dal Pino, E.M.; Lazarian, A. (2001): Constraints on the Acceleration of Ultra-High-Energy Cosmic Rays in Accretion-induced Collapse Pulsars. *The Astrophysical Journal*, **560**, 358

Dorfi, E.A. (1991): Gamma rays and cosmic rays in supernova remnants with radiative cooling. *Astronomy&Astrophysics*, **251**, 597

Drury, L.O'C. (2000): Particle acceleration in supernova remnants. *High Energy Gamma-ray Astronomy. International Symposium in Heidelberg.*, **Vol. 558**, 71

Drury, L.O'C.; Aharonian, F.A.; Völk, H.J. (1994): The gamma-ray visibility of supernova remnants. A test of cosmic ray origin. *Astronomy&Astrophysics*, **287**, 959

Elbert, J.,W.; Sommers, P. (1995): In search of a source for the 320 EeV Fly's Eye cosmic ray. *The Astrophysical Journal*, **441**, 151

Ellison, D.C.; Jones, F.C.; Reynolds, S.P. (1990): First-order Fermi particle acceleration by relativistic shocks. *The Astrophysical Journal*, **360**, 702

Engelmann, J. J.; Ferrando, P.; Soutoul, A.; Goret, P.; Juliusson, E. (1990): Charge composition and energy spectra of cosmic-ray nuclei for elements from Be to NI - Results from HEAO-3-C2. *Astronomy&Astrophysics*, **223**, 96

Epele, L.N.; Roulet, E. (1998): On the propagation of the highest energy cosmic ray nuclei. *The Journal of High Energy Physics*, **10**, 9

Erlykin, A.D.; Wolfendale, A.W. (1997): A Single Source of Cosmic Rays in the Range 10^{15}-10^{16} eV. *Journal of Physics G: Nuclear and Particle Physics*, **23**, 979

Erlykin, A.D.; Wolfendale, A.W. (2000): Models for the Origin of the Knee in the Cosmic-Ray Spectrum. `astro-ph/0011057`

Esposito, J.A.; Hunter, S.D.; Kanbach, G.; Sreekumar, P. (1996): EGRET Observations of Radio-bright Supernova Remnants. *The Astrophysical Journal*, **461**, 820

Evans, N.W.; Ferrer, F.; Sarkar, S. (2001): The Anisotropy of the ultra-High energy Cosmic Rays. `astro-ph/0103085`

Fermi, E. (1949): On the Origin of the Cosmic Radiation. *Physical Review*, **75**, 1169

Fichtel, C.E.; Linsley, J. (1986): High-energy and ultra-high-energy cosmic rays. *The Astrophysical Journal*, **300**, 474

Fowler, J.W.; Fortson, L.F.; Jui, C.C.H.; Kieda, D.B.; Ong, R.A.; Pryke, C.L.; Sommers, P. (2001): A measurement of the cosmic ray spectrum and composition at the knee. *Astroparticle Physics*, **15**, 49

Gaisser, T.K. (1990): Cosmic Rays and Particle Physics. *Cambridge University Press*

Gaisser, T.K.;Protheroe, R.J.; Stanev, T. (1998): Gamma-Ray Production in Supernova Remnants. *The Astrophysical Journal*, **492**, 219

Gaisser, T.K. (2000): Origin of Cosmic Radiation. *High Energy Gamma-ray Astronomy. International Symposium in Heidelberg.*, **Vol. 558**, 27

Gallant, Y. A.; Achterberg, A.; Kirk, J. G. (1999): Particle acceleration at ultra-relativistic shocks. Gamma-ray burst afterglow spectra and UHECRs. *Astronomy and Astrophysics Supplement*, **138**, 549

Garcia-Munoz, M.; Simpson, J.A.; Guzik, T.G.; Wefel, J.P.; Margolis, S.H. (1987): Cosmic-ray propagation in the galaxy and in the heliosphere: The path-length distribution at low energy. *The Astrophysical Journal Supplement*, **64**, 269

Gill, A.J.; Kibble, T.W.B. (1994): Cosmic rays from cosmic strings. *Physical Review D*, **50**, 3660

Gonzales-Mestres, L. (2000): Gamma and cosmic-ray tests of special relativity. `astro-ph/0011181`

Green, D.A. (2001): A Cataloque of Galactic Supernova Remnants (2001 December version) *Mullard Radio Astronomy Observatory, Cavendish Laboratory, Cambridge, UK* available on the World-Wide-Web at `http://www.mrao.cam.ac.uk/surveys/snrs/`

Greisen, K. (1966): End to the Cosmic-Ray Spectrum? *Physical Review Letters*, **16**, 748

Han, J.L.; Qiao, G.J. (1994): The magnetic field in the disk of our Galaxy. *Astronomy&Astrophysics*, **288**, 759

Haswell, C. A.; Tajima, T.; Sakai, J.I. (1992): High-energy particle acceleration by explosive electromagnetic interaction in an accretion disk. *The Astrophysical Journal*, **401**, 495

Hawking, S. W. (1975): Particle creation by black holes. *Communications in Mathematical Physics*, **43**, 199

Hayashida, N.; Nagano, M.; Nishikawa, D.; Ohoka, H.; Sakaki, N.; Sasaki, M.; Takeda, M.; Teshima, M.; Torii, R.; Yamamoto, T.; Yoshida, S.; Honda, K.; Kawasumi, N.; Tsushima, I.; Inoue, N.; Kusano, E.; Shinozaki, K.; Souma, N.; Kadota, K.; Kakimoto, F.; Kamata, K.; Kawaguchi, S.; Kawasaki, Y.; Kitamura, H.; Matsubara, Y.; Murakami, K.; Uchihori, Y.; Yoshii, H. (1999): The anisotropy of cosmic ray arrival directions around 10^{18} eV *Astroparticle Physics*, **10**, 303

Hayashida, N.; Honda, K.; Inoue, N.; Kadota, K.; Kakimoto, F.; Kakizawa, S.; Kamata, K.; Kawaguchi, S.; Kawasaki, Y.; Kawasumi, N.; Kusano, E.; Mahrous, A.M.; Mase, K.; Minagawa, T.; Nagano, M.; Nishikawa, D.; Ohoka, H.; Osone, S.; Sakaki, N.; Sasaki, M.; Shinozaki, K.; Takeda, M.; Teshima, M.; Torii, R.; Tsushima, I.; Uchihori, Y.; Yamamoto, T.; Yoshida, S.; Yoshii, H. (2000): Updated AGASA event list above 4×10^{19} eV. `astro-ph/0008102`

Heckler, A.F. (1996): On the formation of a Hawking-radiation photosphere around microscopic black holes. `astro-ph/9601029`

Hess, V.F. (1912): Über Beobachtungen der durchdringenden Strahlung bei sieben Freiballonfahrten. *Physikalische Zeitschrift*, **13**, 1084

Hillas, A.M. (1968): Cosmic rays in an evolving universe. *Canadian Journal of Physics*, **46**, 623

Hillas, A.M. (1984): The origin of ultra high energy cosmic rays. *Annual Review of Astronomy and Astrophysics*, **22**, 425

Hiltner, W.A. (1949): On the Presence of Polarization in the Continuous Radiation of Stars. II. *The Astrophysical Journal*, **109**, 471

Hörandel, J.R. (1999): Cosmic-ray mass composition in the PeV region estimated from the hadronic component of EAS. *26th Int. Cosmic Ray Conference*, , HE 8.3.

Isola, C.; Lemoine, M.; Sigl, G. (2001): Centaurus A as the Source of ultra-high energy cosmic rays? `astro-ph/0104289`

Jokipii, J.R.; Morfill, G. (1987): Ultra-high-energy cosmic rays in a galactic wind and its termination shock. *The Astrophysical Journal*, **312**, 170

Kang, H.; Ryu, D.; Jones, T. W. (1996): Cluster Accretion Shocks as Possible Acceleration Sites for Ultra-High-Energy Protons below the Greisen Cutoff. *The Astrophysical Journal*, **456**, 422

Kang, H.; Rachen, J.P.; Biermann, P.L. (1997): Contributions to the Cosmic Ray Flux above the Ankle: Clusters of Galaxies. *Monthly Notices of the Royal Astronomical Society*, **286**, 257

Köhler, C. (1998): Entwicklung einer Methode zur Bestimmung der Energie kosmischer TeV-Gamma-Quanten mit den Tscherenkow-Teleskopen der HEGRA-Kollaboration- Das Energiespektrum der aktiven Galaxie Mrk501. PH. D. THESIS, *Ruprecht-Karls-Universität Heidelberg*

Kroeger, R. (1986): Measurements of hydrogen and helium isotopes in Galactic cosmic rays from 1978 to 1984. *The Astrophysical Journal*, **303**, 816

Lagage, P.O.; Cesarsky, C.J. (1983): The maximum energy of cosmic rays accelerated by supernova shocks. *Astronomy&Astrophysics*, **125**, 249

Lampeitl, H. (2000): Untersuchun der ausgedehnten galaktischen Region im Längenbereich zwischen 37° und 43° auf diffuse γ-Strahlung und Punktquellen im Energiebereich oberhalb 1 TeV mit dem HEGRA-Tscherenkov-Teleskopsystem. PH. D. THESIS, *Ruprecht-Karls-Universität Heidelberg*

Landau, L. D.; Pomeranchuk, I.J. (1953): *Dokl. Akad. Nauk. SSSR*, **92**, 535 & 735

Lee, A.A.; Clay, R.W. (1995): The anisotropy of EHE cosmic rays. *Journal of Physics G: Nuclear and Particle Physics*, **21**, 1743

Longair, M.S. (1992): High Energy Astrophysics - Particles, photons and their detection. SECOND EDITION, *Cambridge University Press*

Maki, K.; Mitsui, T.; Orito, S. (1996): Local Flux of Low-Energy Antiprotons from Evaporating Primordial Black Holes. astro-ph/9601025

Mannheim, K. (1993): The proton blazar. *Astronomy&Astrophysics*, **269**, 67

Mannheim, K. (1998): Possible Production of High-Energy Gamma Rays from Proton Acceleration in the Extragalactic Radio Source Markarian 501. *Science*, **279**, 684

Marsella, G. (1998): High altitude atmospheric shower detection techniques for γ-ray Astronomy. PH. D. THESIS, *Università Degli Studi di Lecce*

Max-Planck Institut für Kernphysik: World wide web page of Institute http://www.mpi-hd.mpg.de/hfm/CosmicRay/ChLight/ChLat.html

Meisenheimer, K.; Roser, H.-J.; Hiltner, P. R.; Yates, M. G.; Longair, M. S.; Chini, R.; Perley, R. A. (1989): The synchrotron spectra of radio hot spots. *Astronomy&Astrophysics*, **219**, 63

Morris, M.S.; Thorne, K.S.; Yurtsever, U. (1988): Wormholes, Time Machines and the Weak Energy Condition. *Physical Review Letters*, **61**, 1446

Nagano, M.; Watson, A.A. (2000): Observations and implications of the ultrahigh-energy cosmic rays. *Reviews of Modern Physics*, **72**, 689

Nikolsky, S.I. (1995): Break in the cosmic ray spectrum or confinement violation near 10^6 TeV? *Nuclear Physics B - Proceedings Supplements*, **39A**, 228

Norman, C.A.; Melrose, D.B.; Achterberg, A. (1995): The origin of cosmic rays above $10^{18.5}$ eV. *The Astrophysical Journal*, **454**, 60

Pfotzer, G. (1936): *Zeitschrift für Physik*, **102**, 23

Protheroe, R.J. (1998): Acceleration and Interaction of Ultra High Energy Cosmic Rays. astro-ph/9812055

Protheroe, R.J.; Szabo, A.P. (1992): High energy cosmic rays from active galactic nuclei. *Physical Review Letter*, **69**, 2885

Ptuskin, V.S.; Rogovaya, S.I.; Zirakashvili, V.N.; Chuvilgin, L.G.; Khristiansen, G.B.; Klepach, E.G. and Kulikov, G.V. (1993): Diffusion and drift of very high eneergy cosmic rays in galactic magnetic fields. *Astronomy&Astrophysics*, **268**, 726

Ptuskin, V.S.; Völk, H.J.; Zirakashvili, V.N.; Breitschwerdt, D. (1997): Transport of relativistic nucleons in a galactic wind driven by cosmic rays. *Astronomy&Astrophysics*, **321**, 434

Rachen, J.P.; Biermann, P.L. (1993): Extragalactic ultra-high energy cosmic rays. I. Contribution from hot spots in FR-II radio galaxies. *Astronomy&Astrophysics*, **272**, 161

Rachen, J.P.; Stanev, T.; Biermann, P.L. (1993): Extragalactic ultra-high energy cosmic rays. II. Comparison with experimental data. *Astronomy&Astrophysics*, **273**, 377

Scully, S.T.; Stecker, F.W. (2001): On the Spectrum of Ultrahigh Energy Cosmic Rays and the Gamma Ray Burst Origin Hypothesis. `astr-ph/0006112`

Scharlemann, E.T.; Arons, J.; Fawley, W.M. (1978): Potential drops above pulsar polar caps - Ultrarelativistic particle acceleration along the curved magnetic field. *The Astrophysical Journal*, **222**, 297

Shemi, A.; Piran, T. (1990): The appearance of cosmic fireballs. *The Astrophysical Journal*, **365**, L55

Sigl, G.; Schramm, D. N.; Bhattacharjee, P. (1994): On the origin of highest energy cosmic rays. *Astroparticle Physics*, **2**, 401

Sigl, G. (2001): Ultrahigh-Energy Cosmic Rays: Physics and Astrophysics at Extreme Energies. *Science*, **291**, 73

Smith, .G.K.; Clay, R.W. (1997): Cosmic Ray Anisotropy Studies with a Small Air Shower Array. *Australian Journal of Physics*, **50**, 827

Stanev, T. (1997): Ultra-High-Energy Cosmic Rays and the Large-Scale Structure of the Galactic Magnetic Field. *The Astrophysical Journal*, **479**, 290

Stanev, T.; Engel, R.; Mücke, A.; Protheroe, R.J.; Rachen, J.P. (2000): Propagation of ultra-high energy protons in the nearby universe. `astro-ph/0003484`

Swordy, S.P; Müller, D.; Meyer, Peter; L'Heureux, J.; Grunsfeld, J.M. (1990): Relative abundances of secondary and primary cosmic rays at high energies. *The Astrophysical Journal*, **349**, 625

Swordy, S.P; L'Heureux, J.; Meyer, P.; Müller, D. (1993): Elemental abundances in the local cosmic ray at high energies. *The Astrophysical Journal*, **403**, 658

Takeda, M.; Hayashida, N.; Honda, K.; Inoue, N.; Kadota, K.; Kakimoto, F.; Kamata, K.; Kawaguchi, S.; Kawasaki, Y.; Kawasumi, N.; Kusano, E.; Matsubara, Y.; Murakami, K.; Nagano, M.; Nishikawa, D.; Ohoka, H.; Osone, S.; Sakaki, N.; Sasaki, M.; Shinozaki, K.; Souma, N.; Teshima, M.; Torii, R.; Tsushima, I.; Uchihori, Y.; Yamamoto, T.; Yoshida, S.; Yoshii, H. (1999): Small-Scale Anisotropy of Cosmic Rays above 10^19 eV Observed with the Akeno Giant Air Shower Array. *The Astrophysical Journal*, **522**, 225T and `astr-ph/9902239`

Tanimori, T.; Hayami, Y.; Kamei, S.; Dazeley, S.A.; Edwards, P.G.; Gunji, S.; Hara, S.; Hara, T.; Holder, J.; Kawachi, A.; Kifune, T.; Kita, R.; Konishi, T.; Masaike, A.; Matsubara, Y.; Matsuoka, T.; Mizumoto, Y.; Mori, M.; Moriya,

M.; Muraishi, H.; Muraki, Y.; Naito, T.; Nishijima, K.; Oda, S.; Ogio, S.; Patterson, J.R.; Roberts, M.D.; Rowell, G.P.; Sakurazawa, K.; Sako, T.; Sato, Y.; Susukita, R.; Suzuki, A.; Suzuki, R.; Tamura, T.; Thornton, G.J.; Yanagita, S.; Yoshida, T.; Yoshikoshi, T. (1998): Discovery of TeV Gamma Rays from SN 1006: Further Evidence for the Supernova Remnant Origin of Cosmic Rays. *The Astrophysical Journal*, **497**, L25

Vietri, M. (1995): The Acceleration of Ultra-High-Energy Cosmic Rays in Gamma-Ray Bursts *The Astrophysical Journal*, **453**, 883

Völk, H.J.; Biermann, P.L. (1988): Maximum energy of cosmic-ray particles accelerated by supernova remnant shocks in stellar wind cavities. *The Astrophysical Journal*, **333**, 65

Watson, A.A. (2000): Ultra-high-energy cosmic rays : the experimental situation. *Physics Reports*, **333**, 309

Waxman, E. (1995a): Cosmological Origin for Cosmic Rays above 10^{19} eV. *The Astrophysical Journal*, **452**, L1

Waxman, E. (1995b): Cosmological gamma-ray bursts and the highest energy cosmic rays. *Physical Review Letters*, **75**, 386

Waxman, E.; Bahcall, J. (1997): High Energy Neutrinos from Cosmological Gamma-Ray Burst Fireballs. *Physical Review Letters*, **78**, 2292

Waxman, E. (1998): Can high energy neutrino annihilation on relic neutrinos generate the observed highest energy cosmic-ray? `astro-ph/9804023`

Wiebel, B. (1994): Chemical composition in high energy cosmic rays. `http://wpos6.physik.uni-wuppertal.de:8080/Public/papers-public.html`

Zatsepin, G.T.; Kuzmin, V.A. (1966): *Journal of Experimental and Theoretical Physics Letters*, **4**, 78

Zweerink, J.A.; Akerlof, C.W.; Biller, S.D.; Boyle, P.; Buckley, J.H.; Burdett, A.; Bussons Gordo, J.; Carter-Lewis, D.A.; Catanese, M.; Cawley, M.F.; Fegan, D.J.; Finley, J.P.; Gaidos, J.A.; Hillas, A.M.; Krennrich, F.; Lamb, R.C.; Lessard, R.W.; McEnery, J.E.; Mohanty, G.; Quinn, J.; Rodgers, A.J.; Rose, H.J.; Samuelson, F.W.; Schubnell, M.S.; Sembroski, G.; Srinivasan, R.; Weekes, T.C.; Wilson, C. (1997): The TeV Gamma-Ray Spectrum of Markarian 421 during an Intense Flare. *The Astrophysical Journal*, **490**, 141

Appendix A

Shortcuts and constants

Shortcuts

AGN	active galactic nuclei	GRB	gamma ray burst
CMB	cosmic microwave background	GUT	grand unified theory
CR	cosmic ray	GZK	Greisen-Zatsepin-Kuzmin
EAS	extensive air shower	PBH	primordial black hole
FR	Fanaroff-Riley	SNR	supernova remnant
GMF	Galactic magnetic field	TD	topological defect

Origin of prefixes

Name		**Value**	**U.S. nomenclature**
Kilo	1000^1	10^3	
Mega	1000^2	10^6	
Giga	1000^3	10^9	one billion
Tera	1000^4	10^{12}	one trillion
Peta	1000^5	10^{15}	one quadrillion
Exa	1000^6	10^{18}	one quintillion
Zetta	1000^7	10^{21}	one sextillion
Yotta	1000^8	10^{24}	one septillion

- The prefix kilo is a modification of chilioi, the Greek word for a thousand.
- Mega comes from the Greek mega meaning "large, great".
- Giga comes from the Greek gigas meaning "giant"
- Tera comes from the Greek teras meaning "monster".

- But also, and apparently by coincidence, the prefix tera suggests the Greek tetra, meaning 4. This is significant because tera- is the fourth prefix (n = 4 in 10^{3n}) in the SI system of metric prefixes. This coincidence was exploited in defining the subsequent prefixes peta-, exa-, zetta-, and yotta-, corresponding to the cases n = 5 through 8 in 10^{3n}, so that they suggest the Greek numbers penta, hexa, hepta, and okta for 5, 6, 7, and 8, respectively.

Classification of energies

(There is no convention about the energy classification. We will follow the classification used by MARSELLA (1998).)

Name	shortcut	Energy range	in eV
Low Energy	LE	0.5 - 10 MeV	$5 \cdot 10^5 - 10^7$
Medium Energy	ME	10 - 30 MeV	$10^7 - 3 \cdot 10^7$
High-Energy	HE	30 MeV - 10 GeV	$3 \cdot 10^7 - 10^{10}$
Very High-Energy	VHE	10 GeV - 10 TeV	$10^{10} - 10^{13}$
Ultra High-Energy	UHE	10 TeV - 100 PeV	$10^{13} - 10^{17}$
Extremely High-Energy	EHE	100 PeV - 100 EeV	$10^{17} - 10^{20}$

Physical constants

Electron charge $e = 1.6022 \times 10^{-19}$ C
Mass of proton $m_p = 1.6726 \times 10^{-27}$ kg
parsec $pc = 3.0856 \times 10^{16}$ m
Solar mass $M_\odot = 1.989 \times 10^{30}$ kg
Speed of light in vacuum $c = 299792458$ m s^{-1}

Non-SI units:

electron-volt $1\ eV = 1.6022 \times 10^{-19}$ J $= 1.6022 \times 10^{-12}$ erg
Gauss $1\ G = 10^{-4}$ T